MARTIN MARIETTA ENERGY SYSTEMS LIBRARIES
3 4456 0250981 8

CENTRAL RESEARCH LIBRARY
DOCUMENT COLLECTION

[redacted]

ANP

AEC RESEARCH AND DEVELOPMENT REPORT

ORNL-2115
Vol. II
C-85–Propulsion Systems

4A

FIRST SEMIANNUAL ANP SHIELDING

INFORMATION MEETING

MAY 7-8, 1956

VOLUME II

NTRAL RESEARCH LIBRARY
DOCUMENT COLLECTION
RARY LOAN COPY
T TRANSFER TO ANOTHER PERSON
wish someone else to see this document,
name with document and the library will
a loan.

DECLASSIFIED
CLASSIFICATION CHANGED TO:
BY AUTHORITY OF: AEC 11-19-65
BY: C. Wells 6/17/66

[redacted]

OAK RIDGE NATIONAL LABORATORY
OPERATED BY
UNION CARBIDE NUCLEAR COMPANY
A Division of Union Carbide and Carbon Corporation
UCC
POST OFFICE BOX P · OAK RIDGE, TENNESSEE

[redacted]

[redacted]

LEGAL NOTICE

This report was prepared as an account of Government sponsored work. Neither the United States, nor the Commission, nor any person acting on behalf of the Commission:

A. Makes any warranty or representation, express or implied, with respect to the accuracy, completeness, or usefulness of the information contained in this report, or that the use of any information, apparatus, method, or process disclosed in this report may not infringe privately owned rights; or

B. Assumes any liabilities with respect to the use of, or for damages resulting from the use of any information, apparatus, method, or process disclosed in this report.

As used in the above, "person acting on behalf of the Commission" includes any employee or contractor of the Commission to the extent that such employee or contractor prepares, handles or distributes, or provides access to, any information pursuant to his employment or contract with the Commission.

[redacted]

C-85, Propulsion Systems

ORNL-2115 - Vol. II

This document consists of 158 pages. Copy 4 of 150 copies. Series A.

Papers Presented at the

FIRST SEMIANNUAL ANP SHIELDING INFORMATION MEETING, May 7-8, 1956,

VOLUME II

Date Issued

JUL 2 1956

Sponsored by
AIRCRAFT REACTORS BRANCH
Division of Reactor Development, USAEC

at

OAK RIDGE NATIONAL LABORATORY
Operated by
UNION CARBIDE NUCLEAR COMPANY
A Division of Union Carbide and Carbon Corporation
Post Office Box P
Oak Ridge, Tennessee

[redacted]

[redacted]

MARTIN MARIETTA ENERGY SYSTEMS LIBRARIES

3 4456 0250981 8

ORNL-2115
Reactors-Aircraft Nuclear
Propulsion Systems
M-3679 (18th ed.)

INTERNAL DISTRIBUTION

1. C. E. Center
2. Biology Library
3. Health Physics Library
4-5. Central Research Library
6. Reactor Experimental Engineering Library
7-31. Laboratory Records Department
32. Laboratory Records, ORNL R.C.
33. A. M. Weinberg
34. L. B. Emlet (K-25)
35. J. P. Murray (Y-12)
36. J. A. Swartout
37. E. H. Taylor
38. E. D. Shipley
39. A. H. Snell
40. M. L. Nelson
41. W. H. Jordan
42. S. J. Cromer
43. G. E. Boyd
44. R. A. Charpie
45. S. C. Lind
46. F. L. Culler
47. A. Hollaender
48. K. Z. Morgan
49. C. E. Winters
50. D. S. Billington
51. A. J. Miller
52. E. P. Blizard
53. D. D. Cowen
54. W. M. Breazeale (consultant)
55. M. J. Skinner
56. R. R. Dickison
57. A. Simon
58. F. C. Maienschein
59. A. D. Callihan
60. C. E. Clifford
61. F. L. Keller
62. R. W. Peelle
63-64. ORNL - Y-12 Technical Library, Document Reference Section

EXTERNAL DISTRIBUTION

65. AF Plant Representative, Baltimore
66-67. AF Plant Representative, Burbank
68. AF Plant Representative, Marietta
69-71. AF Plant Representative, Santa Monica
72-73. AF Plant Representative, Seattle
74. AF Plant Representative, Wood-Ridge
75. Air Research and Development Command (RDGN)
76. Air Research and Development Command (RDZPA)
77. Air Technical Intelligence Center
78. Air University Library
79-81. ANP Project Office, Fort Worth
82. Argonne National Laboratory
83. Armed Forces Special Weapons Project, Sandia
84. Armed Forces Special Weapons Project, Washington
85. Assistant Secretary of the Air Force, R&D
86-91. Atomic Energy Commission, Washington
92. Bureau of Aeronautics
93. Bureau of Aeronautics General Representative
94. Chicago Operations Office
95. Chicago Patent Group

96. Chief of Naval Research
97. Convair-General Dynamics Corporation
98-101. General Electric Company (ANPD)
102. Hartford Area Office
103. Headquarters, Air Force Special Weapons Center
104. Lockland Area Office
105. Los Alamos Scientific Laboratory
106. National Advisory Committee for Aeronautics, Cleveland
107. National Advisory Committee for Aeronautics, Washington
108. Naval Air Development and Material Center
109. Naval Research Laboratory
110. North American Aviation, Inc. (Aerophysics Division)
111. Nuclear Development Corporation of America
112. Office of the Chief of Naval Operations (OP-361)
113. Patent Branch, Washington
114-117. Pratt & Whitney Aircraft Division (Fox Project)
118. Sandia Corporation
119. School of Aviation Medicine
120. USAF Project Rand
121. University of California Radiation Laboratory, Livermore
122-139. Wright Air Development Center (WCOSI-3)
140-149. Technical Information Service Extension, Oak Ridge
150. Division of Research and Development, AEC, ORO

[redacted]

PREFACE

The papers presented at the First Semiannual ANP Shielding Information Meeting are published in three volumes. Volumes I and III are also identified as ORNL-2115.

[redacted]

[redacted]

TABLE OF CONTENTS

Volume II

	Paper No.
Scintillation Response of LiI(Eu) Crystals to Monoenergetic Fast Neutrons ..... R. B. Murray, J. Schenck, Oak Ridge National Laboratory	II-A
Investigation of the Hornyak Button as a Fast Neutron Dosimeter ..... F. J. Muckenthaler, Oak Ridge National Laboratory	II-B
Nuclear Radiation Heating ..... B. L. Byrum, J. A. Biggerstaff, Martin, Baltimore	II-C
Gamma-Ray Heating in a 300-Mw CFR Shield ..... C. A. Goetz, Pratt and Whitney, R. M. Davis, Martin: at Oak Ridge National Laboratory	II-D
Neutron Induced Gamma Radiation ..... T. S. Webb, Convair, Ft. Worth	II-E
Modification of Albert-Welton Point Kernel ..... F. A. Aschenbrenner, General Electric Company, ANP Dept., Evendale	II-F
A Neutron Air Scattering Model ..... J. W. Haffner, General Electric Company, ANP Dept., Cincinnati	II-G
Energy Absorption Resulting from Gamma Radiation Incident on a Multiregion Shield with Slab Geometry ..... S. Auslender, Pratt and Whitney, at Oak Ridge National Laboratory	II-H
The Effect of Angular Distribution at the Shield Surface on the Gamma-Ray Air Scattering Probabilities ..... D. R. Otis, Convair, San Diego, H. C. Woodsum, Pratt and Whitney: at Oak Ridge National Laboratory	II-I
Monte Carlo Study of Multiple Scattering of Gamma Rays in Air ..... G. Abel, Convair, Ft. Worth	II-J

[redacted]

Paper II-A

SCINTILLATION RESPONSE OF LiI(Eu) CRYSTALS TO MONOENERGETIC FAST NEUTRONS

R. B. Murray J. Schenck
Oak Ridge National Laboratory

UNCLASSIFIED

SCINTILLATION RESPONSE OF LiI(Eu) CRYSTALS TO MONOENERGETIC FAST NEUTRONS

by

R. B. Murray J. Schenck
Oak Ridge National Laboratory
Oak Ridge, Tennessee

The scintillation response of LiI(Eu) crystals to monoenergetic fast neutrons has been investigated in the course of a study directed toward the development of a more versatile and efficient fast-neutron spectrometer. The scintillation response has been determined as a function of neutron energy (in the range 0.63 to 14.9 Mev), Eu concentration, Li isotope concentration, and crystal temperature. The pulse height spectra of those crystals containing Li^6 demonstrate a peak from the fast neutron induced Li^6 $(n,\alpha)t$ reaction. At room temperature the peak from fast neutrons of energies less than 6 Mev is broad and roughly rectangular in shape. A substantial improvement in the shape and resolution of the fast-neutron peak is found, however, on cooling the crystals to about -140°C.

The investigation which is reported here is a part of the program at this laboratory directed toward the development of a more efficient and versatile fast-neutron spectrometer which would be suitable for the measurement of fission neutron spectra, i.e., continuous spectra in the energy region 1-12 Mev. Previous measurements of this type have been carried out with proton recoil spectrometers which have the twofold disadvantage of extremely low sensitivity and the requirement of a neutron collimation. The scintillation response of LiI(Eu) crystals to neutrons is due to the $Li^6(n,\alpha)t$ reaction ($Q = 4.78$ Mev); the reaction products in slowing down and stopping excite the crystal to radiate light which can be detected by a conventional photomultiplier arrangement. Analysis of the photomultiplier pulse height spectrum provides a measure of the total energy released in the crystal, hence the energy of the incoming neutron.

The advantages offered by a LiI(Eu) crystal as the detecting element in a fast-neutron spectrometer are several: (1) the crystal is an isotropic detector, so that a neutron collimator need not be used to define the direction of the incident neutron; (2) the crystal is small (e.g., 1 in. in diameter, 1/8-in.-thick), making possible spectral measurements at a "point;" (3) the detection efficiency is orders of magnitude greater than that afforded by proton recoil spectrometers; and (4) pulses from gamma rays below about 4.8 Mev fall below the thermal peak, and can thus be biased out. The difficulties which may be

encountered are: (1) response to high energy gammas; (2) the energy resolution for fast neutrons is rather broad; and (3) the crystals are hygroscopic and must be maintained in a moisture-free environment.

The detection efficiency for crystals of Li^6I as a function of neutron energy is shown in Fig. 1. The shape of the curve is determined entirely by the energy dependence of the $Li^6(n,\alpha)t$ cross section. The pulse height spectra shown in this paper (except the Li^7I spectrum) are from crystals of 2 mm thickness; the spectra obtained from 10 mm crystals are quite similar.

Monoenergetic fast neutrons in the energy region 0.63 to 14.9 Mev were obtained from the (p,t), (d,d), and (d,t) reactions using gas targets. The incident particle was accelerated by the ORNL 2.5 Mev Van de Graaff generator. The pulse height spectra shown in Figs. 2, 3, and 4 are from 2 mm crystals of Li^6I with 0.025 mole percent europium activator, with incident neutrons of energies 0.63, 1.57, and 5.79 Mev, respectively. These spectra were obtained at room temperature. In each case the large thermal peak arises from neutrons degraded in energy by scattering from the walls, floor, etc. The magnitude of this peak is due to the very large cross section for the (n,α) reaction at thermal energies. In these spectra it is seen that the fast-neutron peak appears as a broad and "rectangular" band, rather than the sharp Gaussian shape of the thermal-neutron peak. This behavior is tentatively ascribed to a difference in the scintillation efficiency of LiI(Eu) for the alpha and triton at room temperature. For the fast neutron induced reaction both the alpha and triton have a range of energies available to them, since the energy division between the reaction products depends upon their angular distribution. For very slow (thermal) neutrons, however, the energy distribution between the alpha and triton is uniquely specified.

Figure 5 shows the pulse height spectrum from 5.79 Mev neutrons on an 8 mm thick crystal of $Li^7I(Eu)$. This may be compared with Fig. 4, 5.79 Mev neutrons on $Li^6I(Eu)$, in which a large fast-neutron peak occurs. No evidence of a fast-neutron peak was observed in the Li^7 crystal. The small thermal peak in Fig. 5 is due to a trace of Li^6 impurity; the continuous background is presumably due to gamma rays produced by inelastic scattering or radiative capture of neutrons either in the crystal or in the laboratory.

The pulse height spectrum from 14.9 Mev neutrons on $Li^6I(Eu)$ is shown in Fig. 6. Two qualitative differences between this spectrum and those at lower energies are observed. First, the fast-neutron peak has a nearly Gaussian shape with a full width at half maximum of about 9%. Second, the continuum is quite large compared to the 14.9 Mev neutron peak, and rises sharply to a plateau just below the (n,α) peak. In the

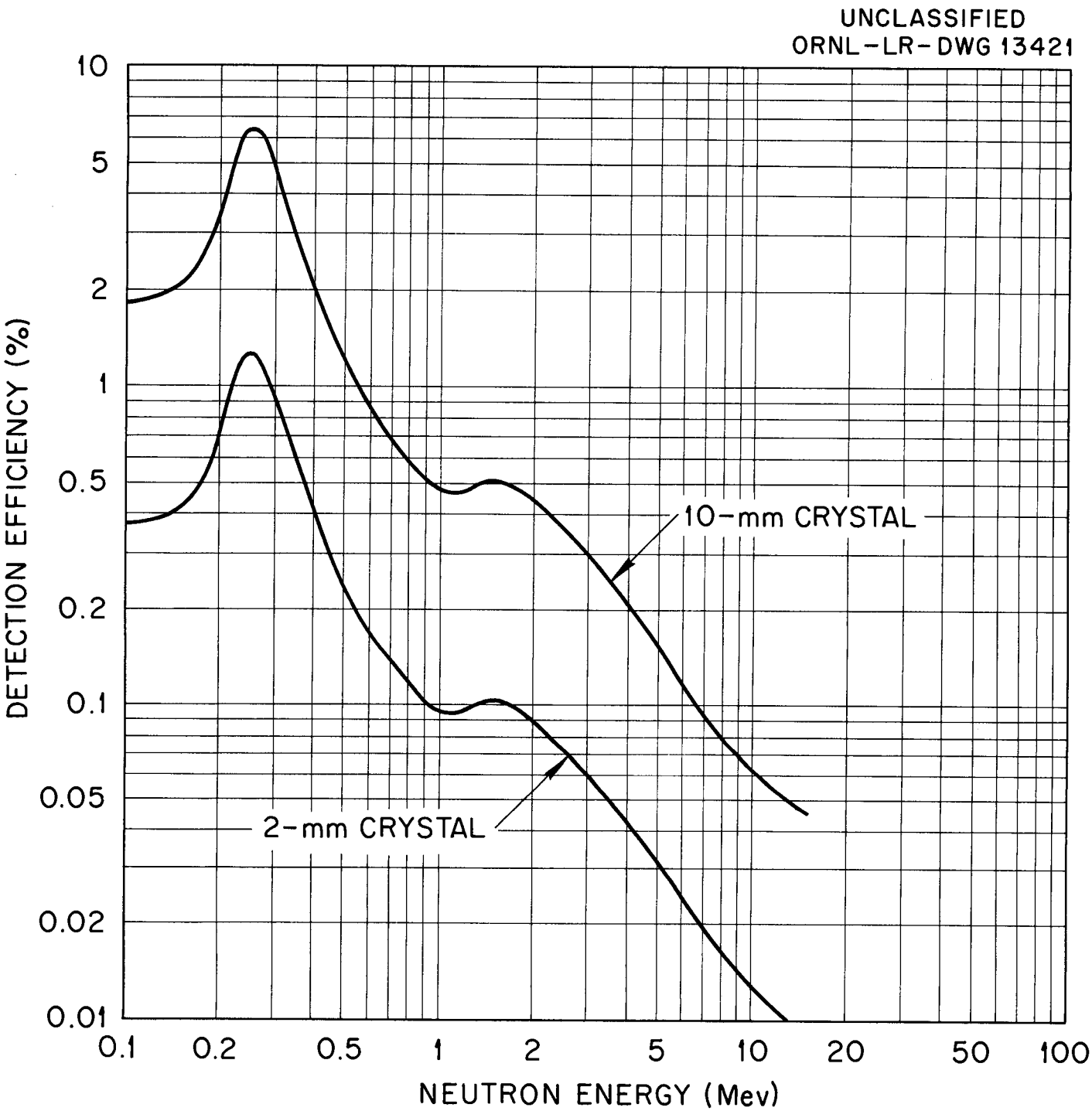

Fig. 1. Detection Efficiency of Li^6I as a Function of Neutron Energy

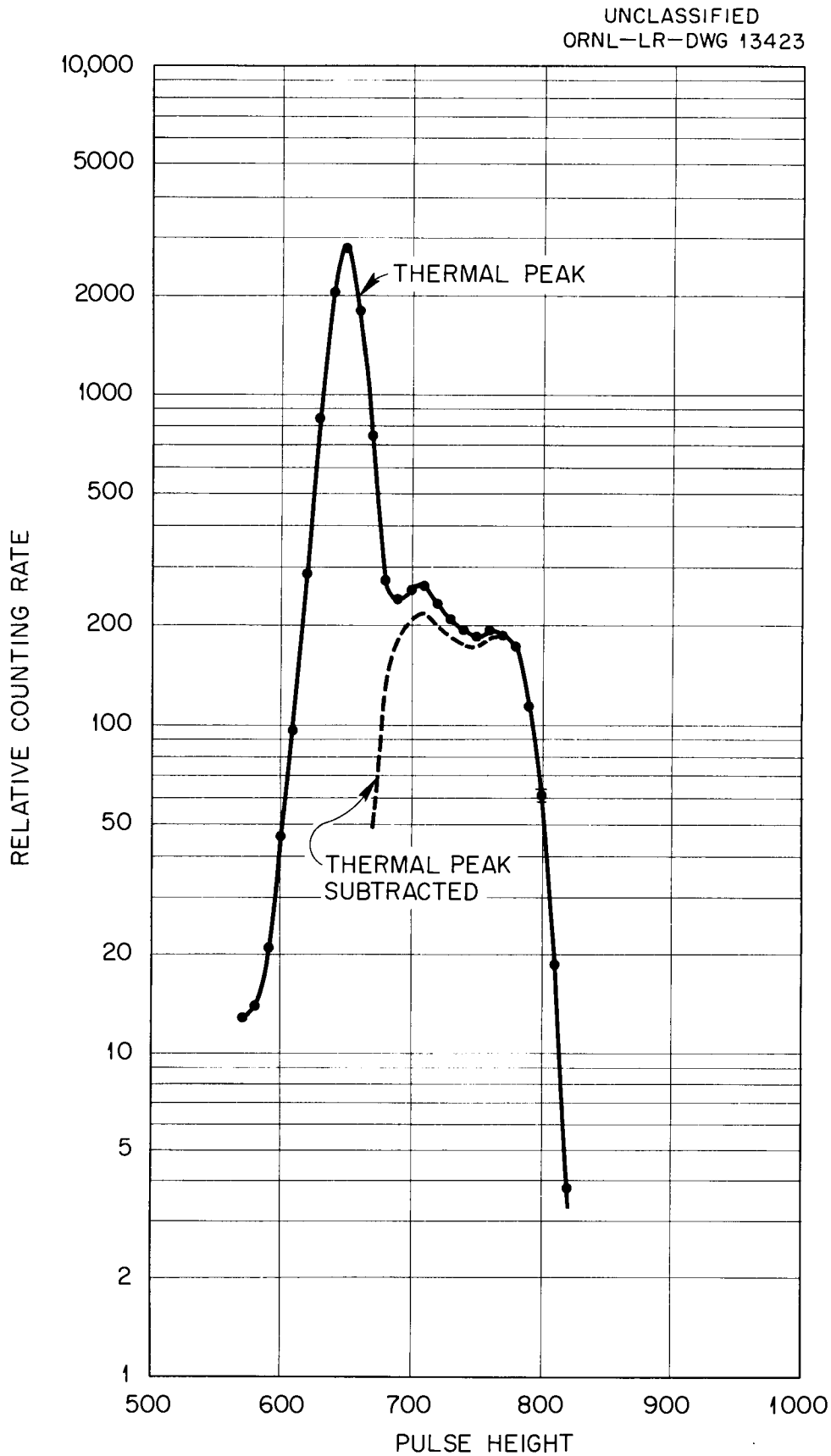

Fig. 2. Scintillation Response of Li^6I (0.025 % Eu) to Fast Neutrons. Crystal: 24-mm-dia x 2 mm thick; $E_n = 0.63$ Mev.

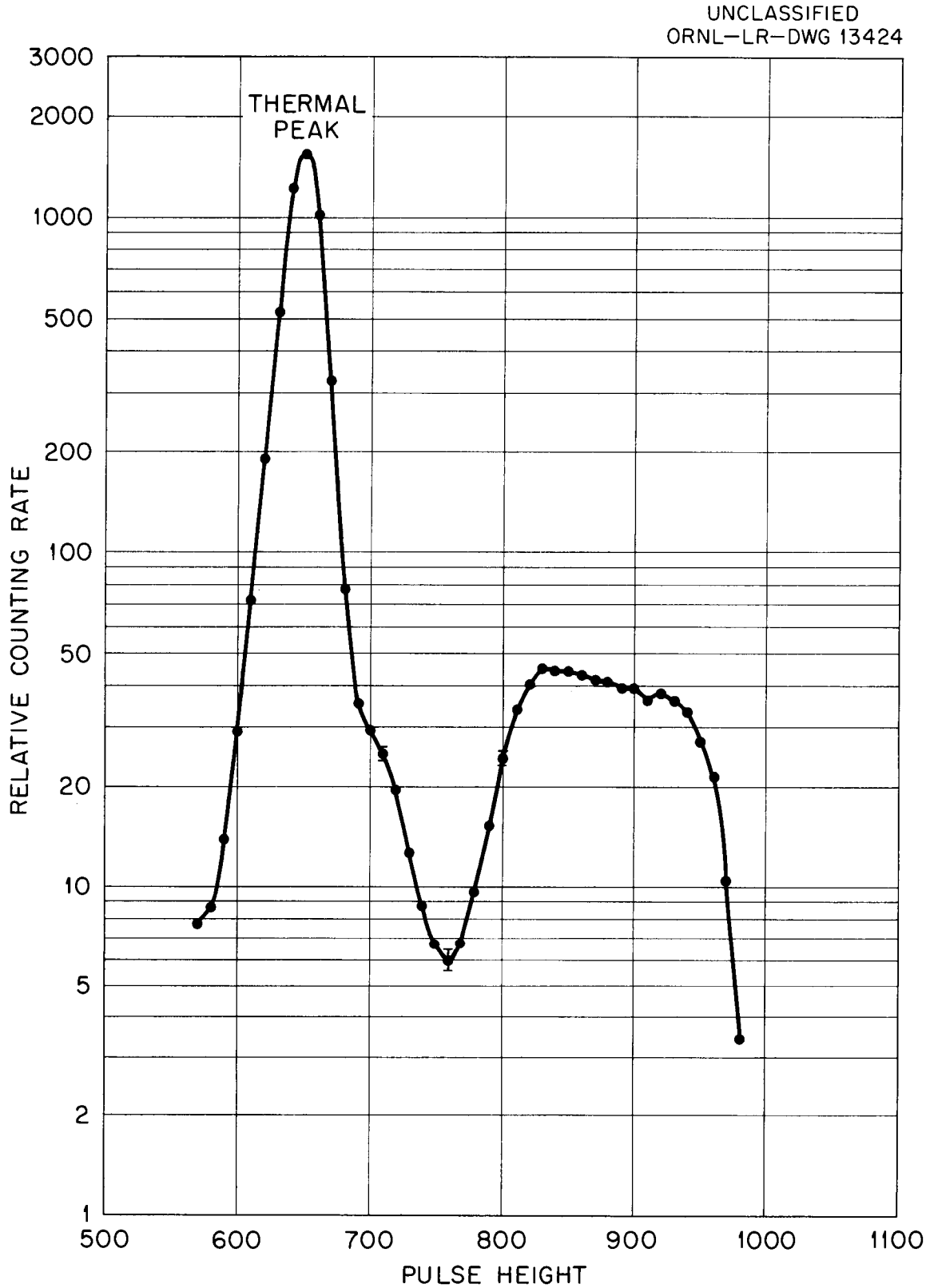

Fig. 3. Scintillation Response of Li^6I(0.025 % Eu) to Fast Neutrons. Crystal: 24-mm-dia. x 2 mm thick; E_n = 1.57 Mev.

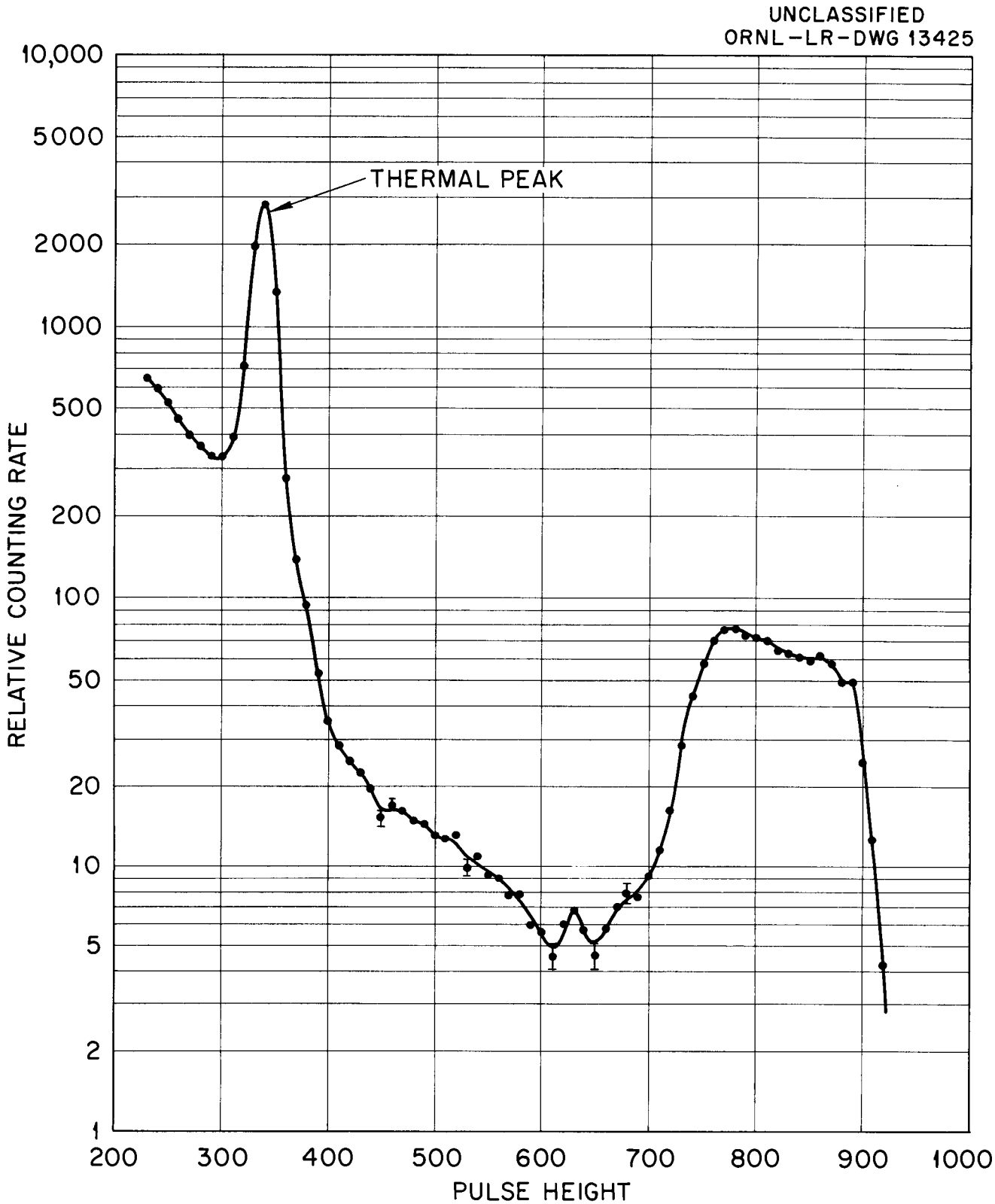

Fig. 4. Scintillation Response of Li^6I (0.025 % Eu) to Fast Neutrons. Crystal: 24-mm-Dia X 2 mm Thick; $E_n = 5.79$ Mev.

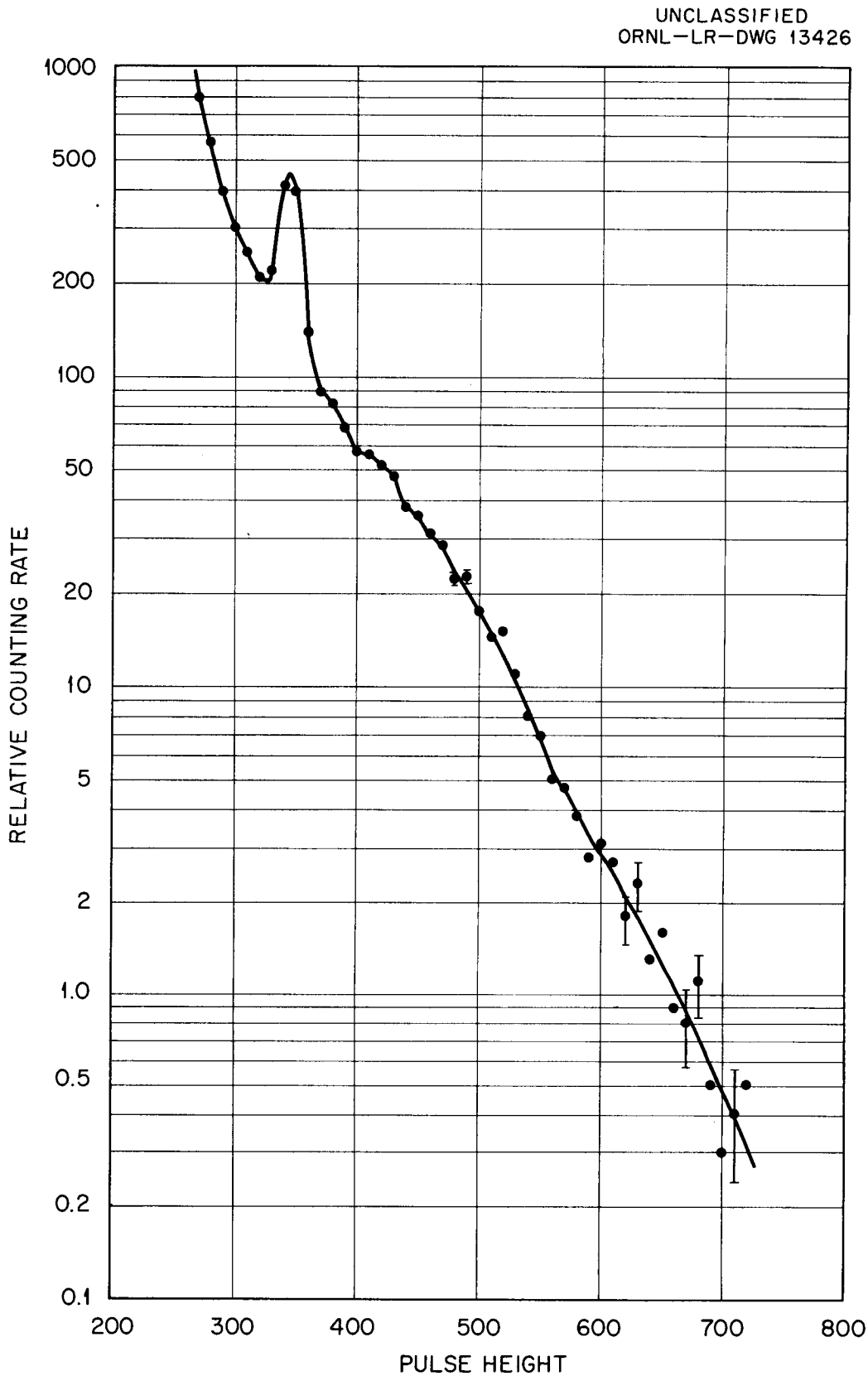

Fig. 5. Scintillation Response of Li^7I (0.046 % Eu) to Fast Neutrons. Crystal: 24-mm-dia x 8 mm thick; $E_n = 5.79$ Mev.

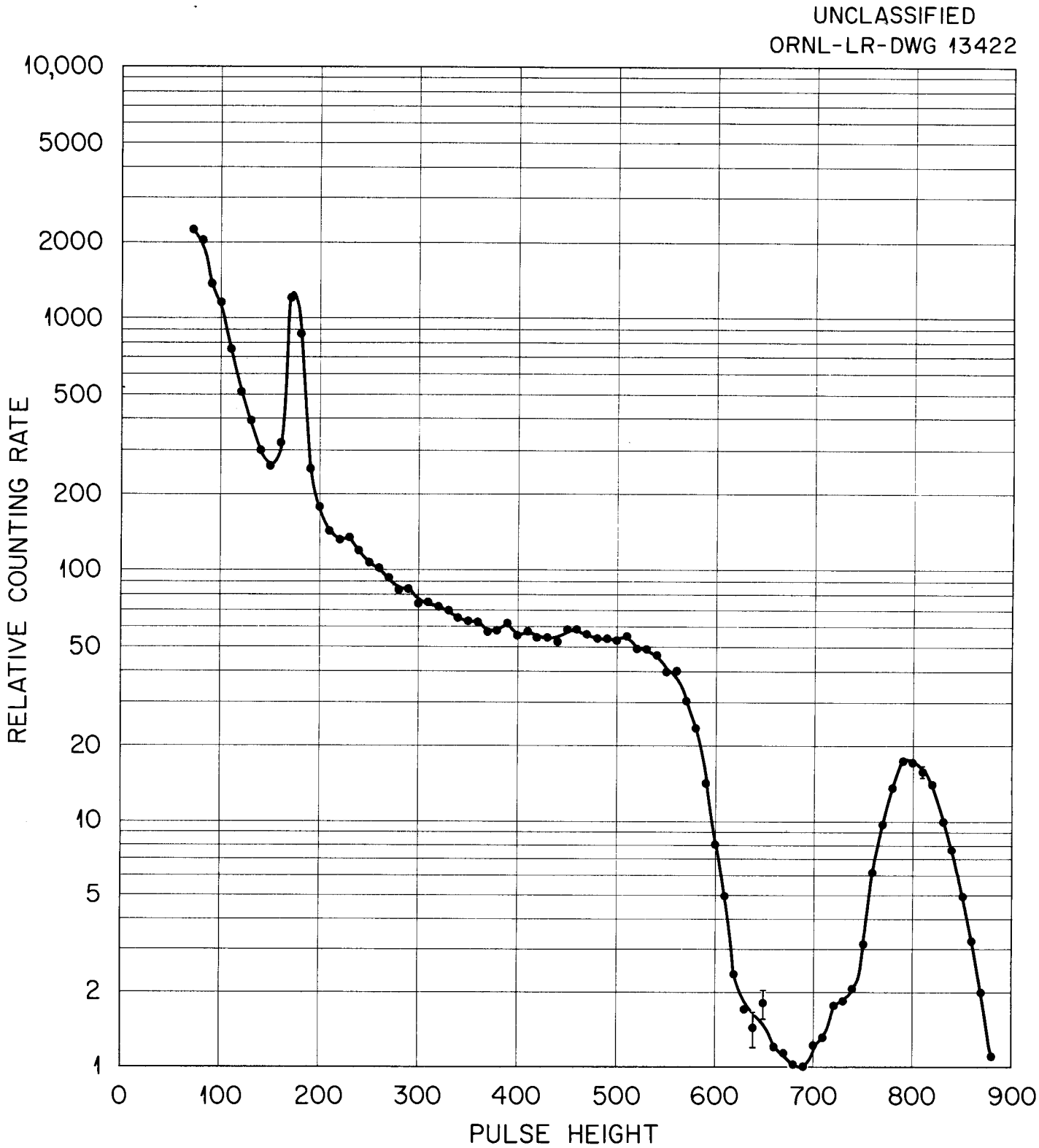

Fig. 6. Scintillation Response of Li^6I(0.025% Eu) to Fast Neutrons. Crystal: 24-mm-dia. x 2 mm thick; E_n = 14.9 Mev.

case of 14.9 Mev neutrons there are other fast-neutron reactions which can contribute to the background; e.g., $Li^6(n,p)He^6$ and $Li^6(n,d)He^5(n)He^4$. This does not necessarily mean, however, that neutrons in the 1-8 Mev region of the fission spectrum will be obscured by the background from the higher energy component; the fission neutron spectrum falls off very rapidly in energy so that the background from high energy neutrons will still be small.

Figure 7 shows a plot of pulse height vs. total energy released for the Li^6I(0.025% Eu) crystal. The data are plotted as full width of the peak at half maximum. It is seen that the midpoints of the peaks can be joined by a straight line, indicating that the relationship between pulse height and neutron energy is linear throughout the range of interest.

Measurements of fast-neutron pulse height spectra have been carried out on other crystals of LiI(Eu) with various concentrations of europium activator and Li^6 isotope. The spectra observed have all been basically similar to those shown in Figs. 2, 3, 4, and 6. Pulse height spectra from fast neutrons on a 10 mm thick crystal of LiI(0.1% Eu), with the natural concentration of Li^6, have been reported in ORNL-1798, p. 32.

Another variable which can affect the scintillation properties of a crystal is its temperature. In order to examine the effect of varying the temperature, pulse height spectra from 5.3 Mev neutrons on Li^6I(Eu) have been recorded at several temperatures. These spectra are shown in Fig. 8 [Li^6I(0.025% Eu)] and Fig. 9 [Li^6I(0.06%Eu)]. Figures 8 and 9 demonstrate two interesting effects. First, the scintillation efficiency increases with decreasing temperature. In Fig. 8 the pulse height of the thermal-neutron peak and the 5.3 Mev neutron peak is increased by a factor of 1.7 on cooling from room temperature to -138°C. Second, the fast-neutron peak assumes a nearly Gaussian shape at the lowest temperatures, and the resolution is substantially improved over that at room temperature. The resolution indicated in these spectra is somewhat deceptive, in that it is the full width at half maximum divided by the pulse height of the maximum, following the usual convention. From the standpoint of neutron energy, however, the zero of energy occurs at the position of the thermal peak, so that the <u>neutron energy</u> resolution is greater than that shown.

The considerable improvement in fast-neutron response observed in these crystals upon cooling has provided the motivation for a continued study of pulse height spectra at low temperatures. It will be of immediate interest to examine the spectra at various neutron energies, and at even lower temperatures. It is hoped that cleaner spectra may be obtained by collimating the fast-neutron beam through a shield of lithiated paraffin, so as to cut down the number of degraded neutrons reaching the crystal.

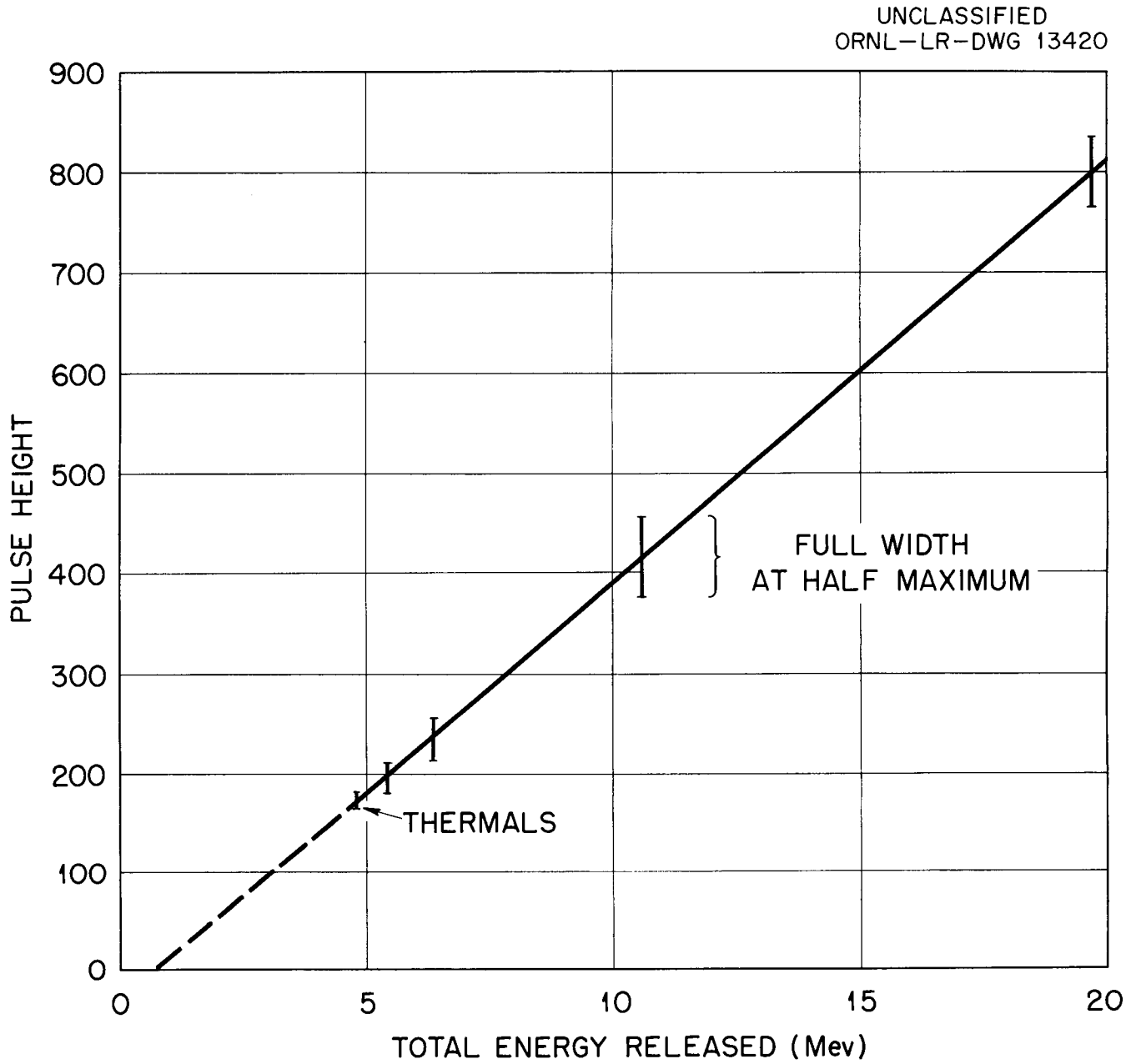

Fig. 7. Pulse Height vs. Total Energy Released for Li^6I (0.025 % Eu), 2 mm thick.

UNCLASSIFIED
ORNL-LR-DWG 13427

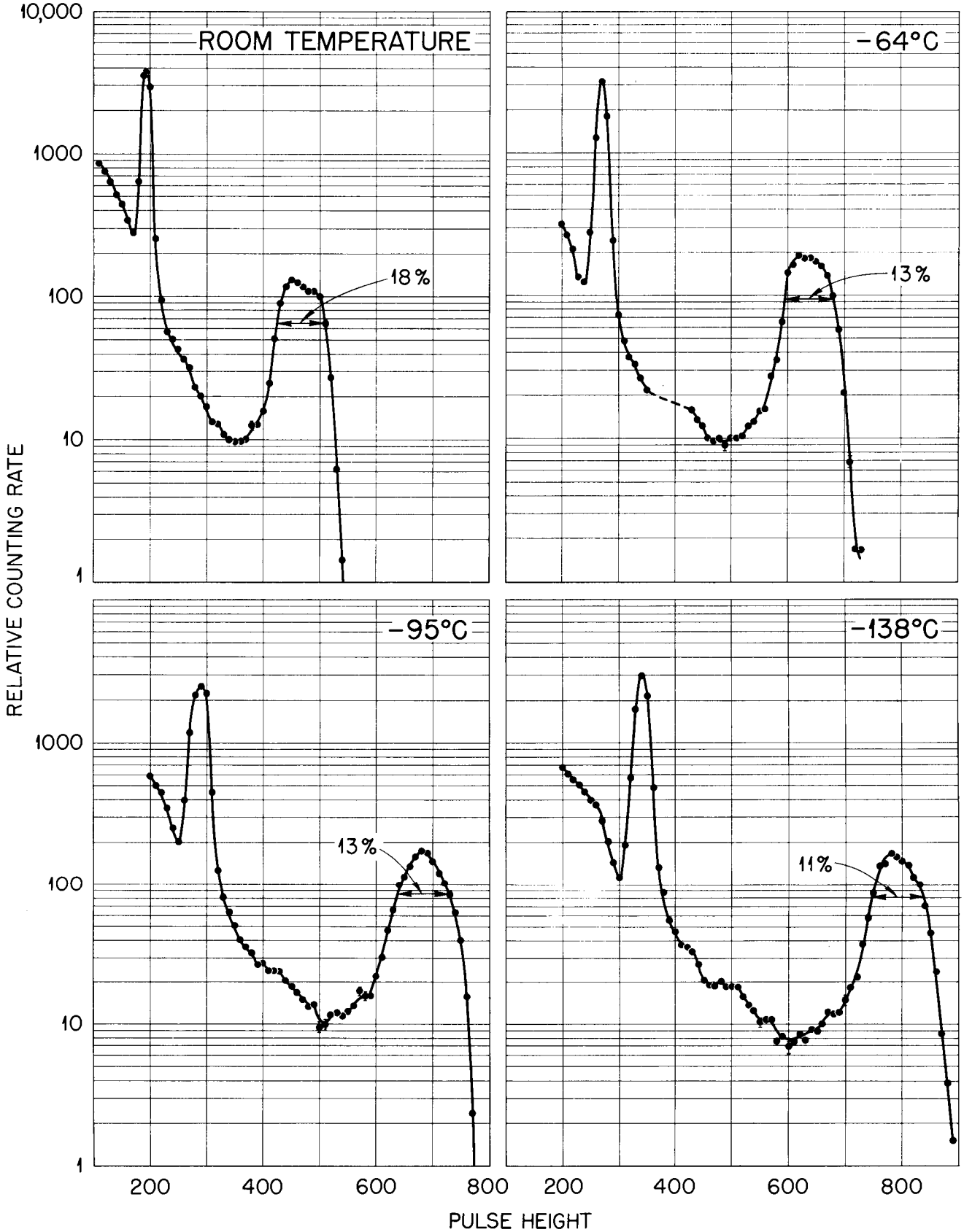

Fig. 8. Scintillation Response of Li^6I(0.025% Eu) to Fast Neutrons. Crystal: 24-mm dia x 2 mm Thick; E_n = 5.3 Mev.

UNCLASSIFIED
ORNL-LR-DWG 13428

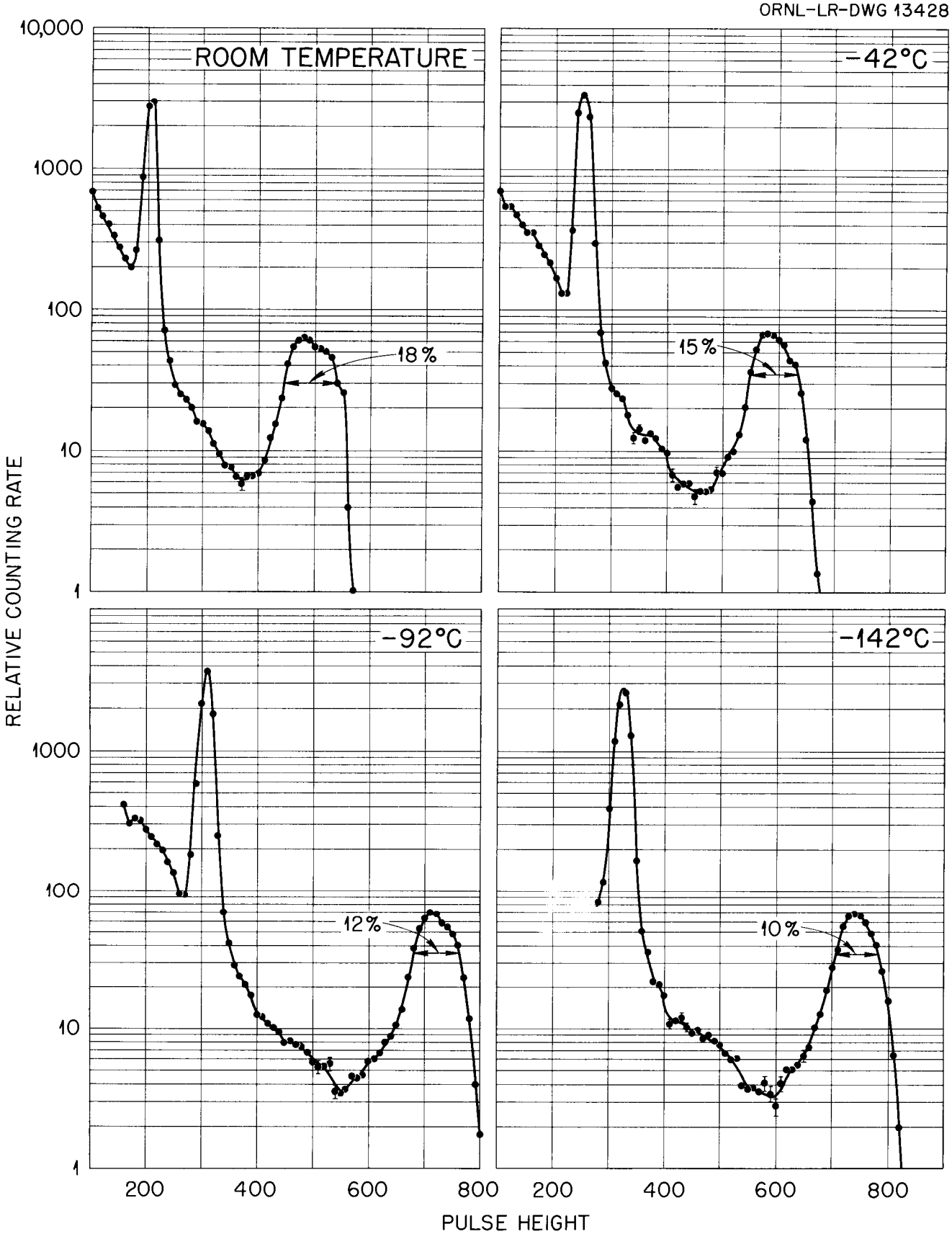

Fig. 9. Scintillation Response of Li^6I(0.06% Eu) to Fast Neutrons. Crystal: 24-mm dia. x 2mm Thick; $E_n = 5.3$ Mev.

Paper II-B

INVESTIGATION OF THE HORNYAK BUTTON AS A FAST-NEUTRON DOSIMETER

F. J. Muckenthaler
Oak Ridge National Laboratory

INVESTIGATION OF THE HORNYAK BUTTON AS A FAST-NEUTRON DOSIMETER

by

F. J. Muckenthaler

Oak Ridge National Laboratory

Four Hornyak buttons, (70-4)[a] 25-μ,[b] .750-in.-thick; (70-4) 25-μ, .150-in.-thick; (70-4) 25-μ 1-in.-thick with 1/8-in. lucite rods vertical in the crystal; (70-4) 3-5-μ 1-in.-thick have been compared to the Hurst-type fast-neutron dosimeter to determine the energy range over which their dose rate was equivalent to the Hurst-type. monoenergetic neutrons were obtained from a 3 Mev Van de Graaff generator here at the Laboratory using protons and deuterons on tritium and deuterons on deuterons. This gave energy variations from approximately 100 kilovolts to about 17 Mev. The comparison showed that above 1.5 Mev the dose rate ratio between the Hornyak button and dosimeter oscillated about one. The ratio at lower energies was greatly improved by increasing the ZnS lucite ratio and decreasing the button thickness. The maximum ratio observed for the optimum thickness and concentration used so far was about three at a neutron energy of approximately several hundred kilovolts. Such an optimization process will be continued.

The Hornyak button is a homogeneous mixture of lucite and ZnS pressed into cylinders of various thicknesses. These are then encased in a light shield and mounted on a phototube. The impinging neutrons produce proton recoils which in turn excite the activated ZnS particles. These then emit photons whose wavelengths lie within the sensitive regions of the phototube. The pulses are fed into a preamplifier, an A-1 amplifier, and then into a scaler or 20-channel analyzer. The button is calibrated in the same manner as the Hurst-type dosimeter, using a Po-Be source of known intensity at a known distance.

The success of the button as a dosimeter and its usefulness in shielding measurements depends on several things. Its range of neutron detection should lie from near 100 kev energy to as high as 15 Mev. It should be capable of weighting each individual proton recoil within the crystal, that is, it should do within the crystal what the integrator does for the Hurst-type dosimeter.

a. 70 parts lucite, 4 parts ZnS by wt.
b. Particle size, dia.

The crystal should be small so that the point of detection is well-known. It should, in general, be an isotropic detector. Along with all this, it should be capable of working in a high gamma-ray background, biasing out any effect the gamma rays may have. Too, the sensitivity of the detector to temperature change should be negligible. The detection efficiency should also be equal to or greater than the presently used dosimeter. Not all of these requests have been satisfied but data to date is encouraging.

Biasing out the effects of gamma rays on the Hornyak button can be done several ways. One is to run the neutron PHS curve for a Po-Be neutron source and for the unknown neutron source to be measured and then set the bias where these two curves become parallel. This must be done where the gamma field is greatest. If the strength of the gamma-ray field is approximately known ahead of time, the button may be set up in the same manner as is done for the dosimeter. This means that a Co^{60} gamma-ray source should be placed so that the field surrounding the button is known. If operation is to be in a 1 r/hr field maximum, the gain of the system and the high voltage are adjusted so that when a bias of 6 volts is used, the scaler will record about 25 to 35 counts/min. If the gamma-ray background is to be 100 r/hr, the over-all gain of the system is merely changed so that the same 25 to 35 counts/min are obtained.

Some time ago measurements were made by the Bulk Shielding Facility group with both the Hurst-type dosimeter and a Hornyak button in the water surrounding the Bulk Shielding Reactor (Fig. 1). A 3-in.-thick lead shield which was held a constant distance from the detector on the reactor side reduced the gamma-ray flux to less than 1 r/hr. For these measurements the detectors were used in conjunction with an A-1 amplifier and a 20-channel analyzer. The four Hornyak button curves in Fig. 1 are all from the same run, but they are plotted as a function of a lower limit on the pulse height selector. One hundred and twenty channels on the analyzer compares to a coverage of 100 volts on the pulse height selector. The data at each point on curve 1 is the sum total of counts obtained between channels 6 and 43 at that particular water thickness. Curve 2 gives the counts between channels 10 and 43, etc. Since the curves remain parallel with this variation in the pulse height selector setting, it is assumed that gamma rays were not contributing to the counting rate even at the lower settings. From this data it can be seen that the sensitivity of this particular button and phototube combination is less than that of the dosimeter but that curves from the two detectors are parallel.

The effect of varying the temperature of the detector and phototube was investigated (Fig. 2) using a Po-Be neutron source. Curve 1 represents the change in counting rate when only the Hornyak button temperature was changed (effected by inserting a 4-in. length of lucite light piper between

Response of Hurst-type Dosimeter and Hornyak Button
at Various Distances from the Bulk Shielding Reactor

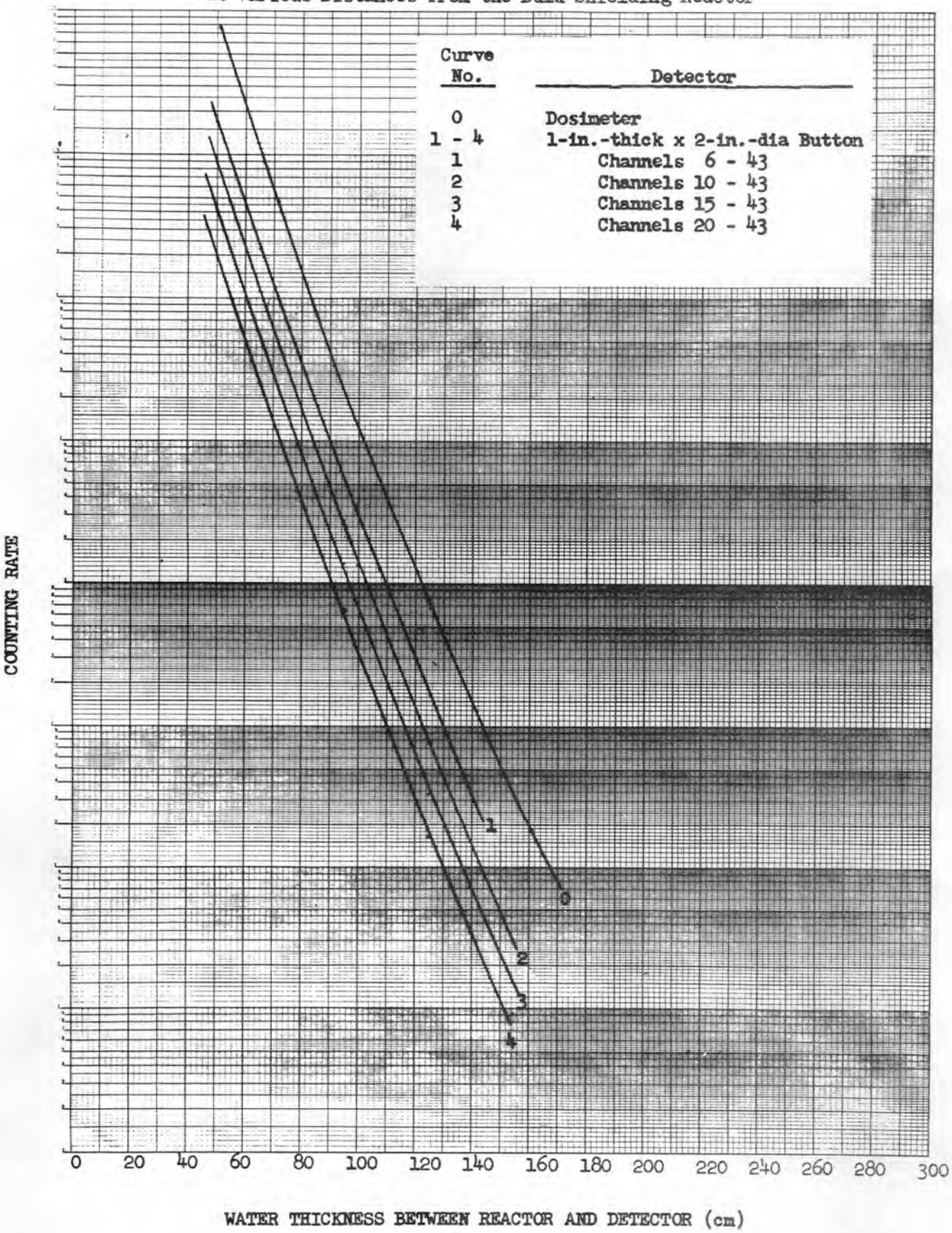

Fig. 1

Response of the Hornyak Button to a Po-Be Neutron Source as a Function of Temperature

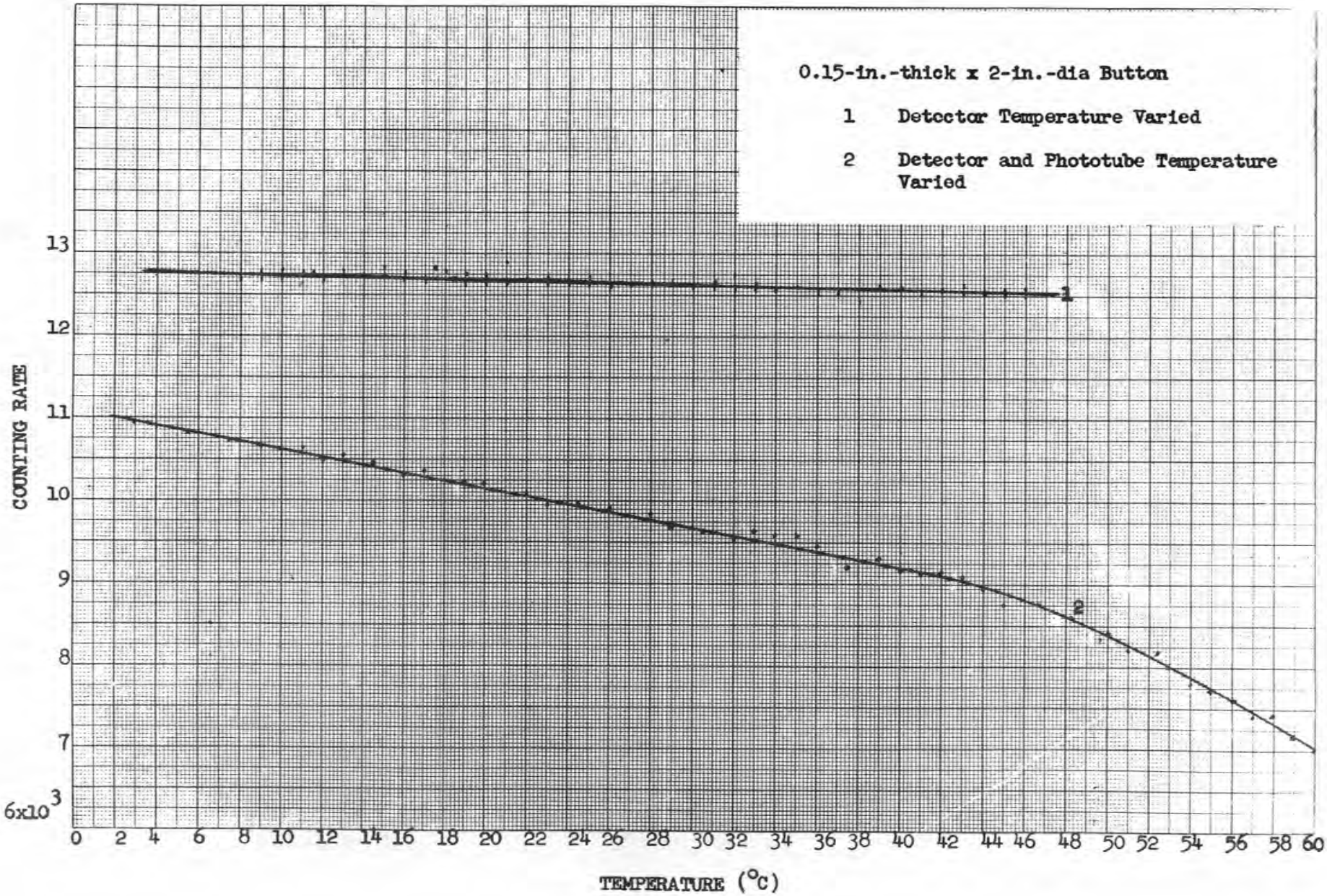

Fig. 2

the detector and phototube). The change in counting rate is less than 4% over 40°C. Curve 2 shows what happened when both the phototube and Hornyak button temperature was varied; the sudden change in slope at the upper end of the temperature range is due to change in the photocathode surface. In this case the counting rate varies about 17% over 40°C.

It is hoped that by decreasing the ZnS particle size the slope of the PHS curve for the Po-Be neutrons would be much less. This would be advantageous because it would allow one to operate at a higher PHS with little loss in counting rate. As can be seen in Fig. 3, the change is not large but in the right direction. Along with this process of trying to improve the neutron detecting efficiency through the use of small size particles, it was hoped that just the opposite effect would take place regarding gamma rays. Figure 3 also shows what happened in that respect. The over-all electronic gain for the system was increased by a factor of about 3 to bring the neutron response for the (70-4)[a], 3 to 5-μ-dia particle button equal to that of the 25-μ-dia particle button at one PHS. In doing this, the gamma-ray response was increased to such an extent that it would be necessary to operate at about twice the previous PHS to obtain a counting rate independent of gamma rays. As can be seen, this counting rate is also somewhat less. The over-all gain was increased again to bring the (70-4), 3 to 5-μ-dia particle button response equal to the other two at a common point. By using a smaller concentration of ZnS the number of small pulses increases and the number of large pulses decreases.

Probably the best procedure for determining the dosimetry capabilities of the Hornyak button is to compare it directly with the Hurst-type dosimeter using monoenergetic neutrons. This has been done for several button composition, particle sizes, and thicknesses. The source of the monoenergetic neutrons was the 3-Mv Van de Graaff generator here at the Laboratory. The neutron energies were obtained using protons on tritium, deuterons on deuterons, and deuterons on tritium. The three ranges of resulting energies thus covered were approximately 100 Kev to 1.5 Mev, 2.5 to 5.5 Mev, and 14 to 17 Mev. With the exception of a few runs both button and the dosimeter were placed at an angle of 15 deg with the generator beam, thus insuring that both counters saw the same intensity and same energy neutrons. For the 2.5- and 14-Mev neutrons, it was necessary to move the counter to an angle of 90 deg with the generator beam. For any individual set of runs the distance between center of detection and source remained the same.

Both the dosimeter and the Hornyak button were set up such that a bias of 6 volts was used with an over-all gain that gave 30 counts/min when placed in a 1 r/hr gamma-ray field. The pulses from the Hornyak button were fed into a 20-channel analyzer and those from the dosimeter were fed into a 20-channel analyzer as well as into an integrator. Only four buttons were used, (70-4),

---

a. 70 parts lucite, 4 parts ZnS by weight.

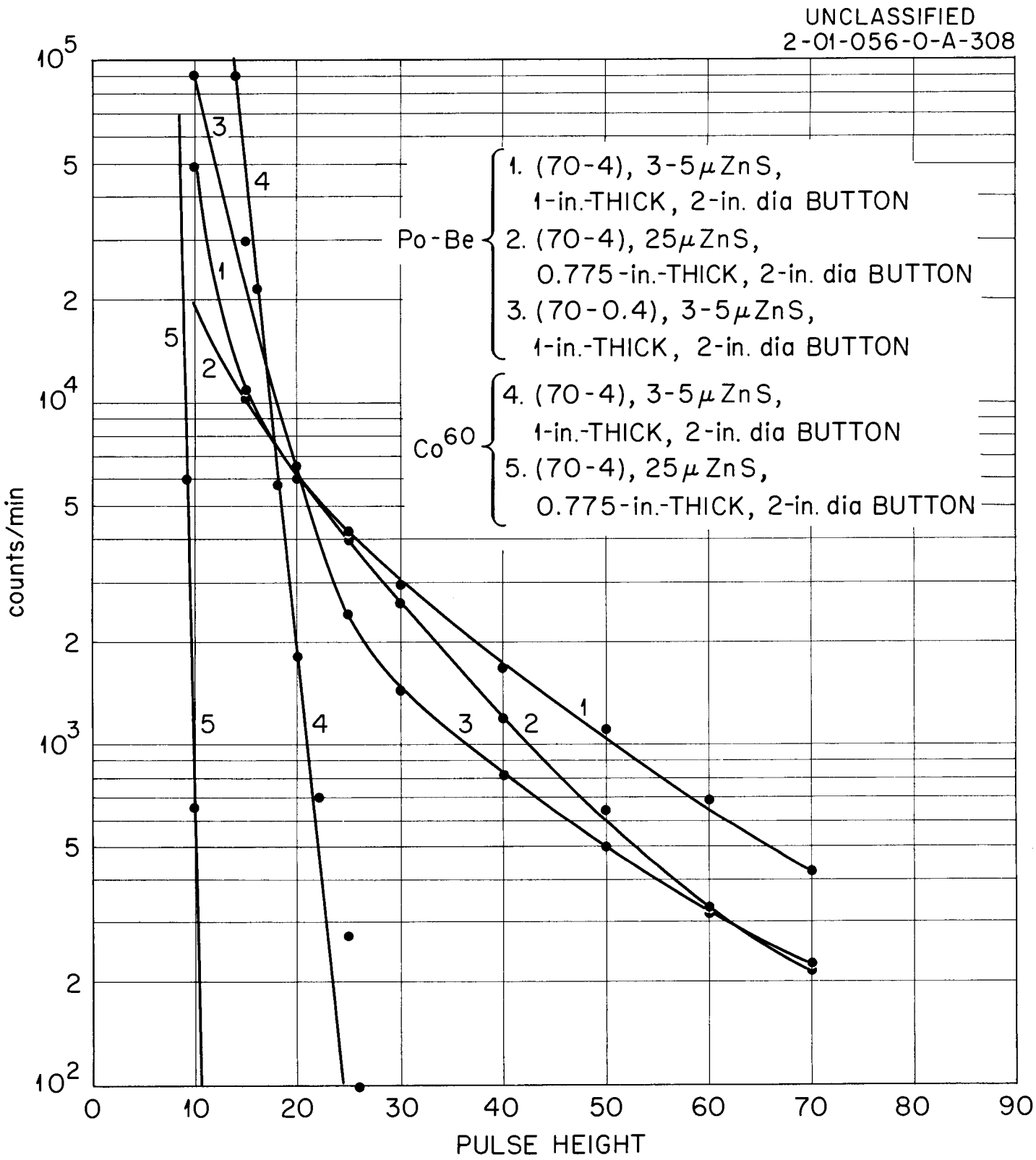

Fig. 3. Response of Hornyak Buttons to Po-Be and Co^{60} Source.

25-μ-dia, 0.750-in.-thick; (70-4), 25-μ-dia, 0.150-in.-thick; (70-4), 25-μ-dia, 1-in.-thick with 1/8-in. lucite light pipers in the crystal; and (70-4), 3 to 5-μ-dia, 1-in.-thick. To eliminate any error due to counting time or beam intensity, both counters were run at the same time for the same amount of beam current.

Some of the results from these runs are shown in Fig. 4. Plotted here is a ratio of the dose rate as measured by the dosimeter to that measured with the Hornyak button as a function of neutron energy. For the button which was (70-4), 25-μ-dia, and 750-mil-thick the ratio is quite high at low energies, approaching 1 near 1.5 Mev. Above this energy the ratio is near 1. For a button which was (70-0.4), 3-5-μ-dia, and 1-in.-thick the ratio is much smaller at the low energies, approaching 1 at less than 1 Mev. For a (70-4), 25-μ-dia, 1-in.-thick button with 1/8-in. lucite rods in it the curve is essentially the same as for the 750 mils thick button. When the thickness for the (70-4), 25-μ-dia button was decreased to 150 mils, the lower energy ratio drops to that shown here for the 3 to 5-μ-dia button, but approaches 1 in the same manner as the 750-mil crystal.

A check was made on the efficiency of the Hornyak button using the (70-4), 25-μ-dia, 750-mil-thick crystal. For a neutron energy of 0.165 Mev it is about 0.001%; at 0.5 Mev it is about 0.02%; and at 1.5 Mev it is about 0.216%. The dosimeter at this latter energy is about 2% efficient. The calculations are based on the number of neutrons passing through the counter determined from the beam current, differential cross section, and number of atoms of gas in the target.

Other runs on the Van de Graaff were made more recently using only the p, T reaction. The compositions of the Hornyak buttons used were (70-4), (70-20) and (70-50) with a 25-μ-dia particle size. One (70-4) button had a 3 to 5-μ-dia particle size. This time the thickness of the buttons was varied in an attempt to find some combination that would reduce the dose ratio at the lower energies. The results plotted in Figs. 5, 6 and 7 are the dose rate ratios against proton energy. Since this is preliminary data, no attempt was made to calculate the neutron energies. It can be noticed that as the thickness of the crystal decreases, the lower energy ratio improves. At about a 20-mil-thickness the point of diminishing returns appears to be reached.

The best curve from each of the Figs. 5, 6 and 7 are plotted in Fig. 8 which shows that as the concentration is increased the tendency is for more of the low energy neutrons to be observed with the Hornyak button. The present information does not give a full optimization of all components involved. The data does seem to indicate a need for larger ZnS concentrations in the crystal and optimum crystal thickness. No check has been made regarding response to gamma rays at these higher concentrations. More work is needed in regard to both the 25-μ-dia and the 3 to 5-μ-dia particle crystals.

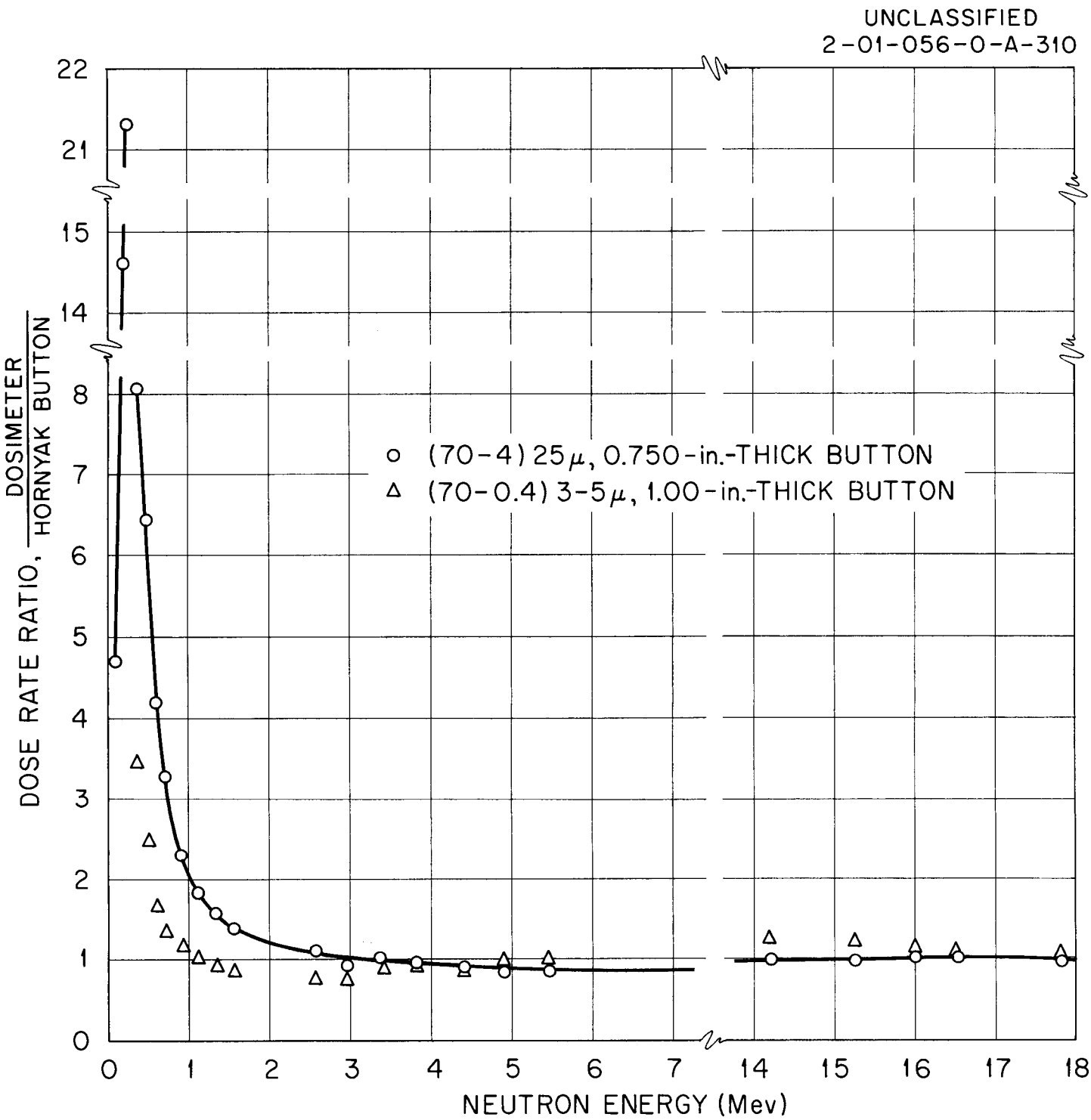

Fig. 4. Dose Rate Ratio for Various Hornyak Buttons

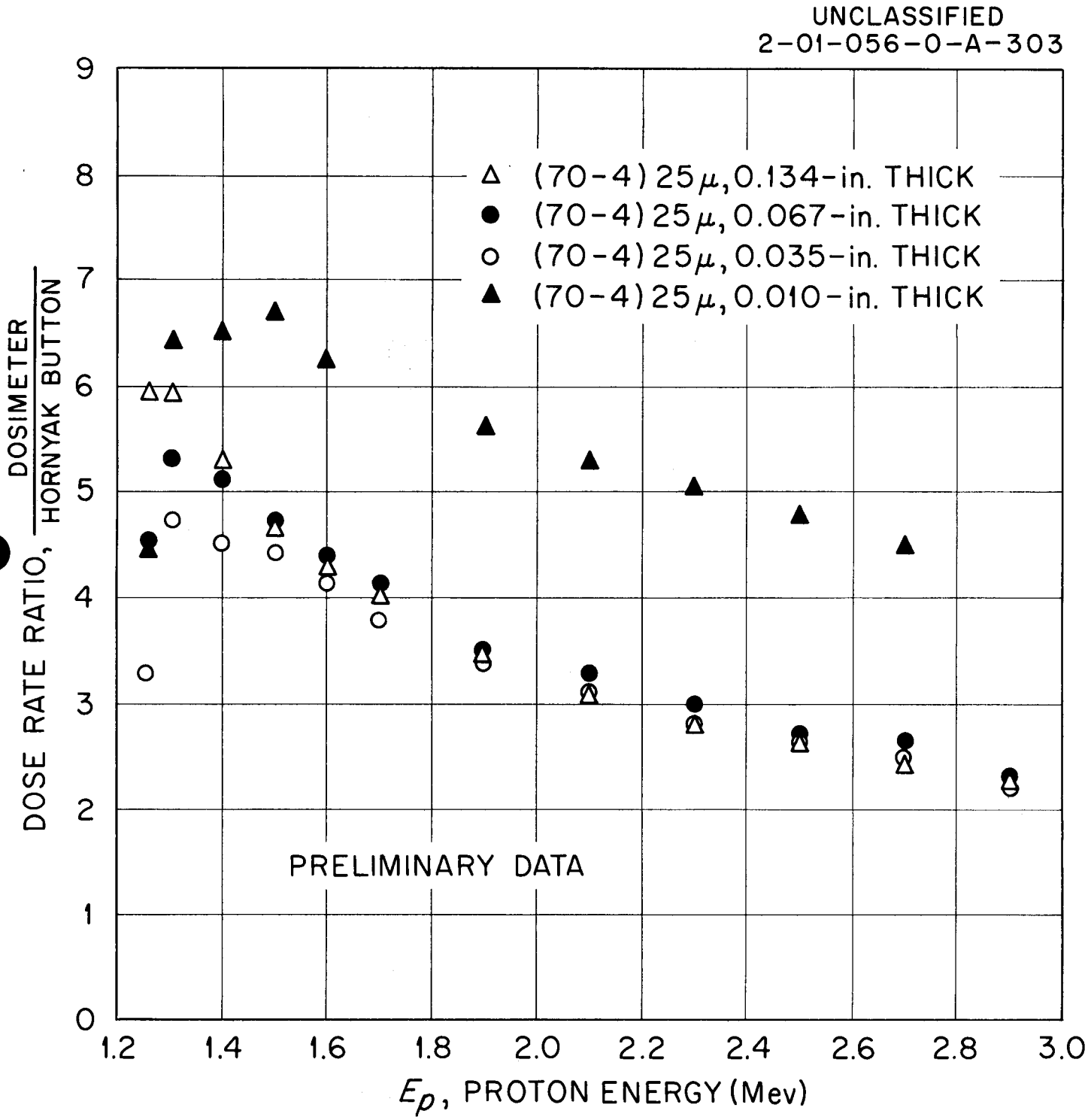

Fig. 5. Dose Rate Ratios for Various Hornyak Buttons

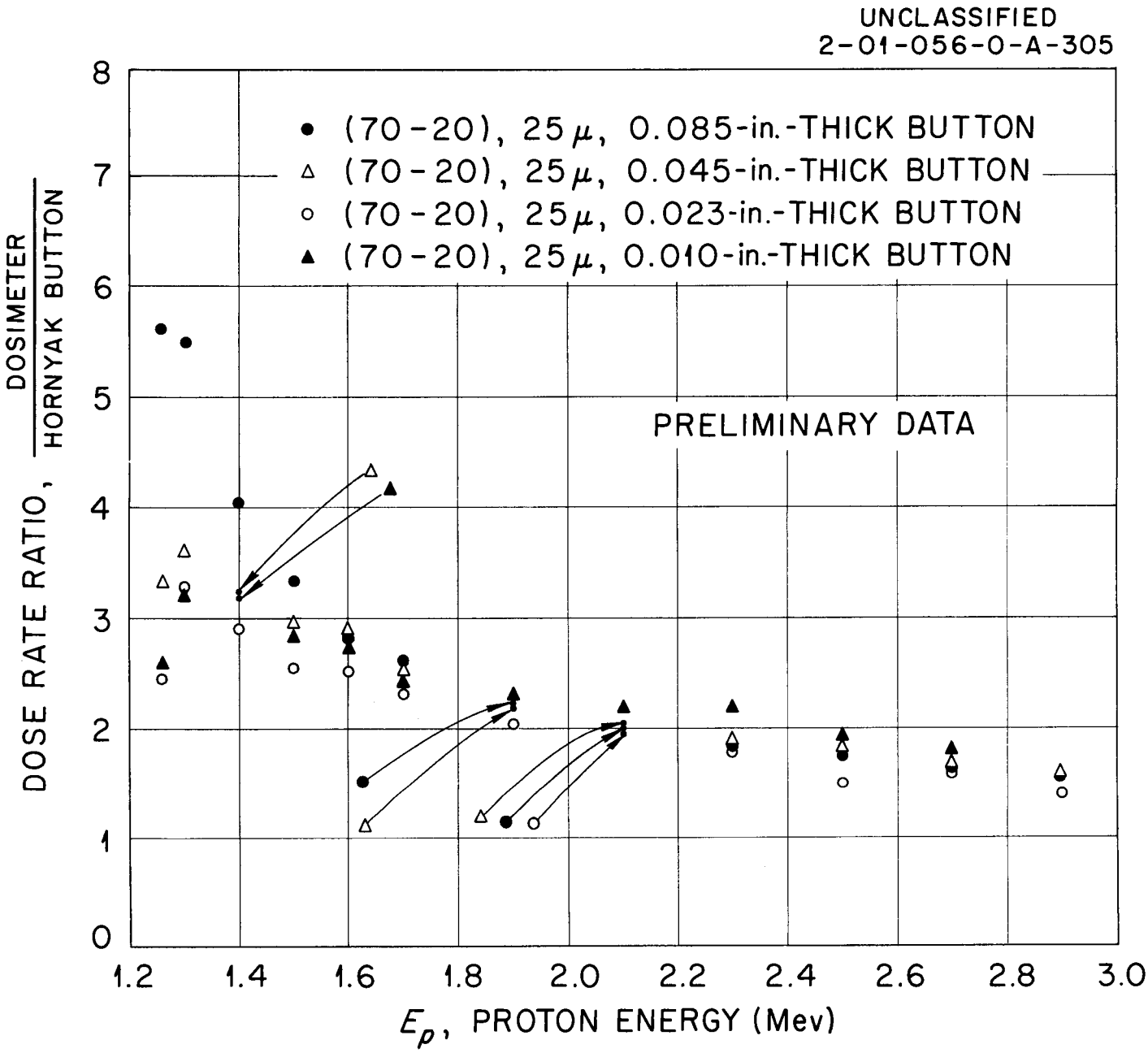

Fig. 6. Dose Rate Ratios for Various Hornyak Buttons.

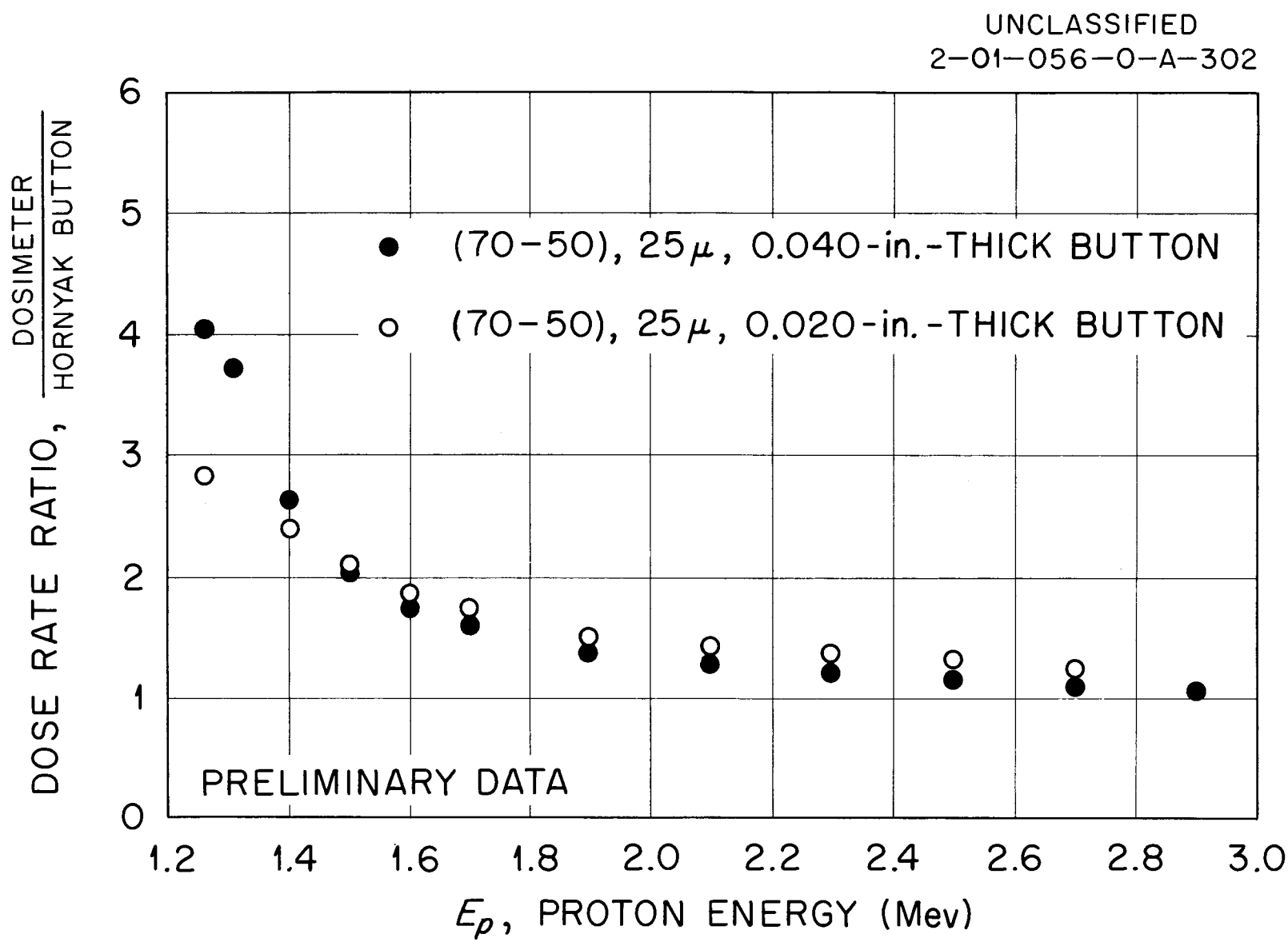

Fig. 7. Dose Rate Ratios for Various Hornyak Buttons.

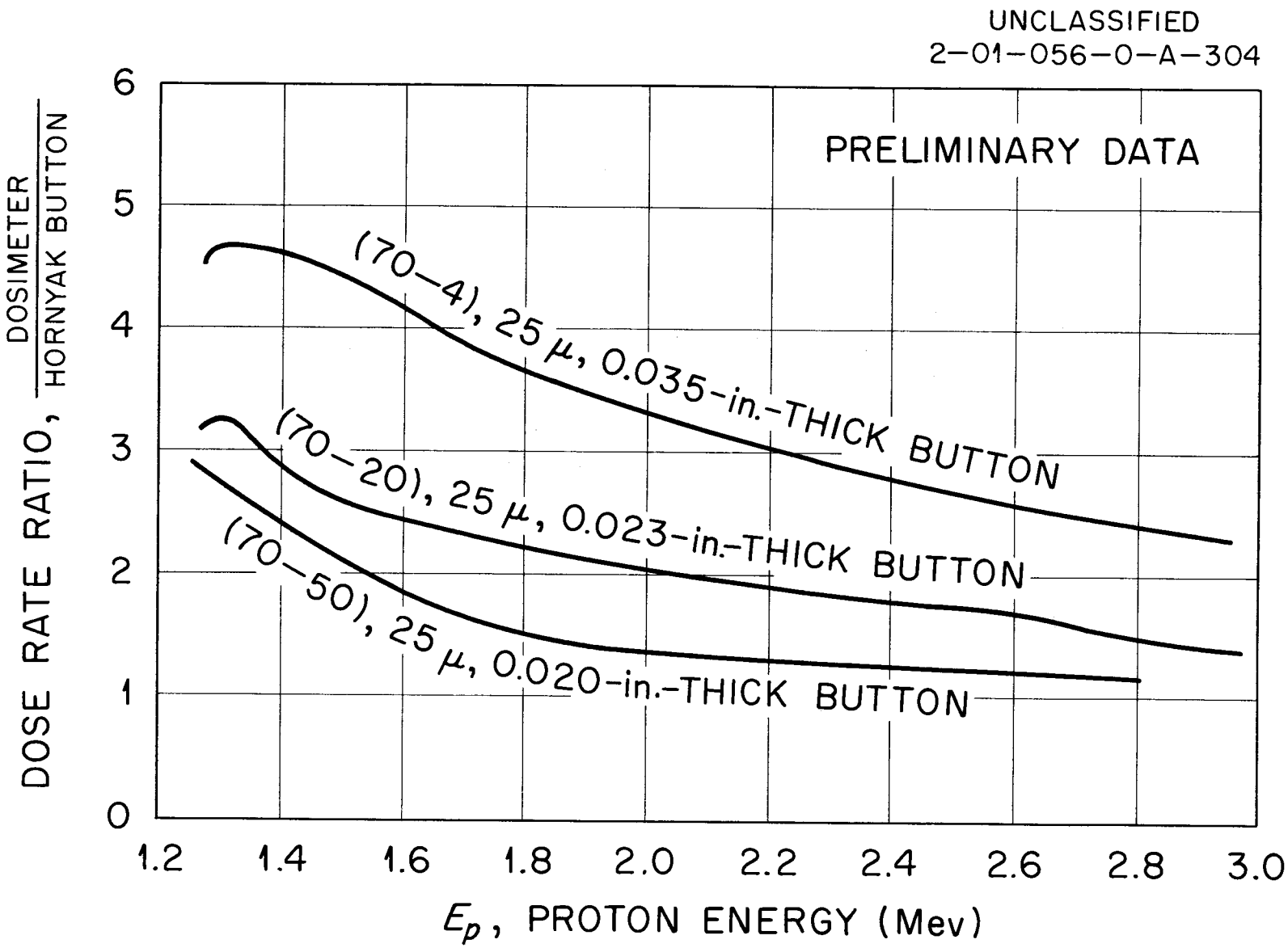

Fig. 8. Dose Rate Ratios for Various Hornyak Buttons.

Paper II-C

NUCLEAR RADIATION HEATING*

B. L. Byrum and J. A. Biggerstaff
Martin, Baltimore

*Published at Martin as Report No. ER-8018.

[redacted]

FOREWORD

This work has been supported in part by the Bureau of Aeronautics and the Office of Naval Research contract No. Nonr-1612(00).

ACKNOWLEDGEMENTS

The authors wish to thank Messrs. H. E. Stern, T. S. Webb, and T. R. Strayhorn (each with Convair, Fort Worth) for a critical reading of the manuscript.

[redacted]

ABSTRACT

The problem of heat generation in a reactor gamma shielding material is defined, and a technique that is adequate for establishing preliminary design requirements is developed. The results are presented in a manner facilitating application by the designer of the best pertinent experimental data which may be made available from time to time.

The salient simplifying assumptions are:

1) geometry may be represented by a plane slab (gamma shielding) of finite thickness and infinite extent bounded by a reactor core region and a neutron shielding region;

2) neutron fluxes in the slab follow simple exponential distributions (thermalization of fast neutrons is not considered);

3) gamma rays which leave the slab do not return;

4) neutrons scattered from the plane slab region into the reactor core region do not return to the slab (albedo of source region is zero for neutrons);

5) albedo of the neutron shielding region is known for neutrons;

6) primary neutron and gamma ray currents incident upon the slab are known;

7) certain nuclear parameters (discussed in the text) are known for the case of interest;

8) annihilation photons are absorbed near their points of origin; and

9) first order corrections for multiple Compton scatterings are sufficient.

Although considered adequate for preliminary design, the simple exponential function (representing the volumetric source strength of gamma rays arising in the shield) may be modified, when warranted, on the basis of appropriate experimental data.

As an example, the heat generation distribution in a slab of iron six inches thick is estimated for a given set of parameters.

I. INTRODUCTION

The treatment of nuclear radiation heating discussed in this paper was developed at the Martin Company, and was presented in rough form at the Convair Shielding Symposium during August, 1955. The underlying theory, parametric curves, and a sample application of the technique are presented herein.

A. DEFINITION OF GENERAL PROBLEM

Radiation heating, which may cause severe thermal stresses and creep in reactor external shells and reactor shields, confronts both the reactor designer and the shield designer. The radiation heating problem is characteristic of power reactors, where it influences the design of reactor shells and requires special provisions for dumping heat generated in reactor shields.

An evaluation of thermal stresses resulting from radiation heating requires the resolution of three interconnected problems:

1) determination of the magnitude and distribution of energy associated with the radiation;

2) ascertainment of the heat transfer rates and temperature distributions based on the physical properties of the material and the manner in which heat is being removed from the material; and

3) calculation of the thermal stresses resulting from the temperature distribution derived from the heat transfer solution.

B. DEFINITION OF SPECIFIC PROBLEM

The purpose of this paper is to discuss the first of the aforementioned problems. Results derived therefrom will facilitate the definition of shield cooling requirements. Although the derivation specifically applies to a slab of finite thickness and infinite extent, designs involving practical geometries can be based upon the results.

Complexity is inherent in any attempt to determine the magnitude and distribution of energy associated with reactor radiation. The analytical treatment must account for the geometries and physical properties of the absorbing media, and for the energy spectra, geometries and spatial distributions of the sources, as well as for the energy and angular distributions of the radiation leakage entering the shield. Resolution of the problem leads to consideration of the following areas:

1) self shielding characteristics of the reactor core, and determination of neutron and gamma leakage therefrom;

2) absorption of energy from core gammas in the reactor shell and shield;

3) absorption of energy from capture gammas due both to thermal neutrons and to fast neutrons that have been thermalized in the reactor shell and shield;

4) absorption of fast neutron energy in the reactor shell and shield due to elastic scattering;

5) absorption of energy manifested in gammas arising from inelastic scattering of fast neutrons in the reactor shell and shield; and

6) absorption of energy arising from (n,α), (n, p), and (n, f) reactions where shielding materials are contemplated which may have significant cross-sections for these reactions, as might be the case, for example, in a power-breeder reactor.

Specifically, the task is to express the contributions to shield heating from thermal neutrons, fast neutrons, core gammas, capture gammas, charged particles, Compton scattered gammas, inelastic scattered gammas, and fission fragments (in exotic shielding materials) as functions of the source strength, energy spectra, and spatial coordinates involved.

II. METHOD OF APPROACH

The approach employed here is intended to provide preliminary design data.

Due to the large number of variables and to the lack of basic knowledge, analytical solutions are based upon several simplifying assumptions. It is usually necessary to consider a number of discrete energies in the core gamma leakage because a single energy is seldom representative of the emitted energies. Each gamma group is characterized by a different absorption probability in a given material. Determination of the inelastic scattering contribution is generally restricted by the lack of data on inelastic cross sections. The leaking neutrons are subdivided into two or more energy groups. The various means of determining neutron and gamma core leakages are not discussed.

It is logical and convenient to define an effective energy absorption coefficient (μ') for gammas in the slab material:

$$\mu' \equiv \mu'_{PE} + \mu_{PP} + \mu_{c,d} + f\mu_{c,s}$$

where

μ_{PE} ≡ fraction of energy deposited in medium per centimeter of travel due to photoelectric process

μ_{PP} ≡ fraction of energy deposited in medium per centimeter of travel due to pair production

μ_c ≡ fraction of gamma rays that undergo Compton scattering per centimeter of travel

$= \mu_{c,d} + \mu_{c,s}$

$\mu_{c,d}$ ≡ fraction of energy that is deposited in medium per centimeter of travel due to Compton scattering

$\mu_{c,s}$ ≡ fraction of energy that is scattered per centimeter of travel due to Compton scattering

f ≡ fraction of energy of secondary gamma ray that is absorbed locally after primary Compton scattering

By judicious choice of the fraction f, a first order approximation of the multiple scattering effect may be accomplished. It should be noted that since

$$f\mu_{c,s} < \mu_c - \mu_{c,d}$$

it generally represents a small contribution to the effective energy absorption coefficient.

III. HEATING DUE TO NEUTRON-INDUCED GAMMAS

An evaluation of the heat generation arising from (n,γ) reactions is probably the most complex problem to be encountered in radiation heating studies and is the one involving the most uncertainties. A realistic evaluation of these sources of heat demands a knowledge of the neutron flux in every portion of the region under consideration, the neutron capture probability and the energy distribution of the resulting gamma radiation, as well as a detailed investigation of the particular geometry under consideration.

An approach to this problem has been made by Enlund (Ref. 1), who defines the heating in a semi-infinite volume bounded by a plane upon which thermal neutrons are incident. An integrated treatment for a slab of finite thickness is presented here, together with suggested analogies between the capture and inelastic scattering processes.

In the following sections it is assumed that the rate of decay of compound nuclei has reached the rate of formation.

With reference to Fig. 1, let the point $\underline{x}'$ denote any arbitrary $x(0 \leq x < b)$ in the neighborhood of which the heat generation rate per unit volume per unit time due to contributions from a given type of event taking place at all points (x, y, φ) in the volume under consideration is to be determined. Let the given event be the emission of capture or inelastic scattering gamma rays by the atoms of the material composing the slab, then

$$H(x') = \int_{x=0}^{b} \int_{y=0}^{\infty} \int_{\varphi=0}^{2\pi} dH(x, x', y, \varphi) \tag{1}$$

and

$$dH(x, x', y, \varphi) = \frac{EP(x)\, y\, dy\, d\varphi\, dx\, \mu'\, e^{-\mu \ell}\, \frac{ds\, d\ell}{4\pi \ell^2}}{ds\, d\ell}$$

where

b ≡ slab thickness

E ≡ energy of gamma

$P(x)$ ≡ volumetric gamma source strength

μ ≡ total interaction cross section of the material for gammas of energy E ≡ $\mu_{PE} + \mu_{PP} + \mu_c$

μ' ≡ effective energy absorption coefficient of the material for gammas of energy E ≡ $\mu_{PE} + \mu_{PP} + \mu_{c,d} + f\mu_{c,s}$

ℓ^2 ≡ $|x - x'|^2 + y^2$

Let $H_1(x')$ and $H_2(x')$ denote the capture gamma heat generation rate per unit volume in the neighborhood of $\underline{x}'$ due to fast neutrons and thermal neutrons, respectively. Then, from Eq. (1),

$$H_1(x') = \frac{\mu' E}{2} \int_{x=0}^{b} P(x)\, E_1(\mu |x - x'|)\, dx \tag{2}$$

Eq. (2) may be integrated after selection of the function $P(x)$.

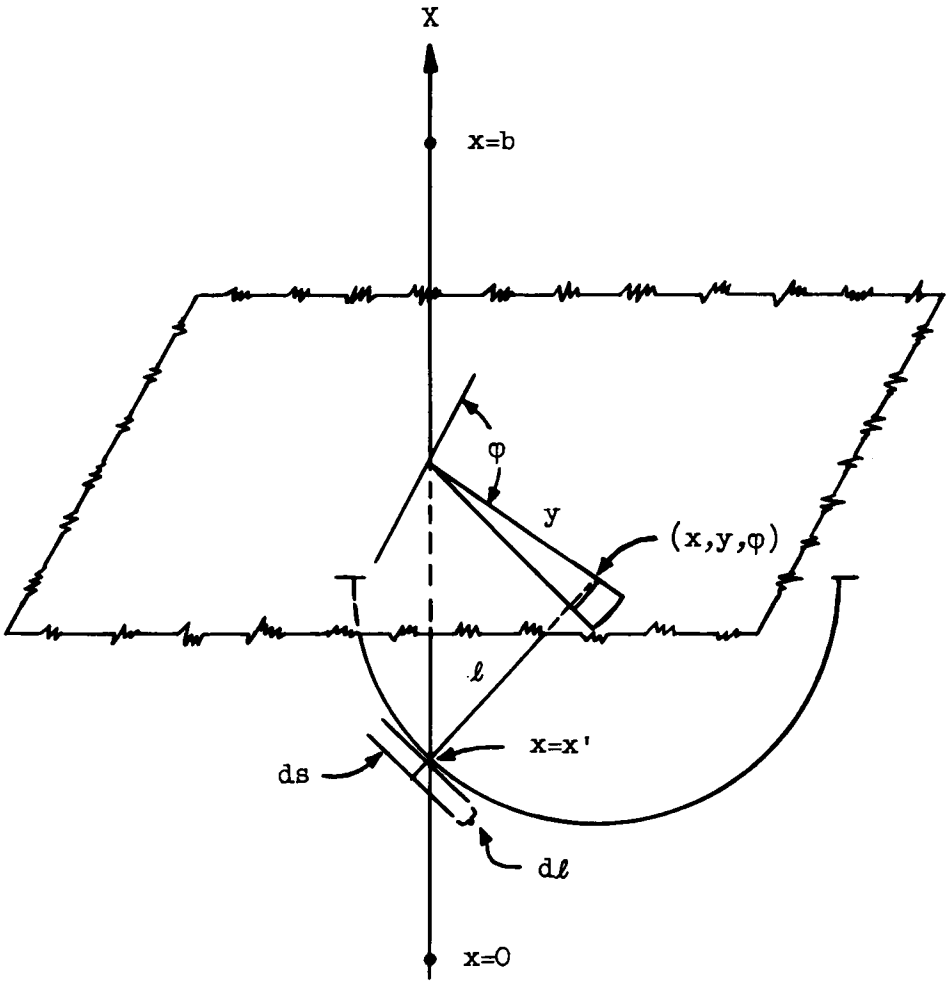

Fig. 1: Slab Geometry: Slab Source Distribution

A. FAST NEUTRON CAPTURE

Assuming that the function P(x) can be derived from a simple diffusion theory prediction of the neutron flux in a plane slab of finite thickness and infinite extent, it follows that

$$P(x) = C_1 e^{-K_1 x} + C_2 e^{K_1 x} \tag{3}$$

where

$$C_1 \equiv \frac{4(\eta_1 - K_1) J_1 \Sigma_1^a}{(1 + 2 K_1 D_1)(\eta_1 - K_1) - (1 - 2 K_1 D_1)(\eta_1 + K_1) e^{-2K_1 b}}$$

$$C_2 \equiv \frac{4 J_1 \Sigma_1^a - (1 + 2 K_1 D_1) C_1}{1 - 2 K_1 D_1}$$

$$\eta_1 \equiv \frac{1}{2 D_1} \quad \frac{\beta_1 - 1}{\beta_1 + 1}$$

$\beta_1 \equiv$ fast neutron albedo of the neutron shielding region bounding the slab at x = b, Fig. 1

$K_1^2 \equiv \Sigma_1^a / D_1$

$J_1 \equiv$ fast neutron current incident upon the slab (note that J_1 denotes the incident rather than the net neutron current at x = 0, Fig. 1)

Σ_1^a ≡ macroscopic absorption cross section of the slab material for fast neutrons

D_1 ≡ "diffusion" coefficient for fast neutrons in the slab material

Substituting the right side of Eq. (3) into Eq. (2), it is shown in the appendix that

$$H_1(x') = \left[C_1 \xi(x') + C_2 \Lambda(x')\right] \frac{\mu' E}{2K_1} \tag{4}$$

where

$$\xi(x') \equiv \int_{x=0}^{b} e^{-K_1 X} K_1 E_1 (\mu |x-x'|)\, dx$$

$$= Q_1^- (\alpha, K_1 X') + e^{-K_1 X'} Q_2^- (\alpha, K_1 Z)$$

$$\Lambda(x') \equiv \int_{x=0}^{b} e^{K_1 X} K_1 E_1 (\mu |x-x'|)\, dx$$

$$= Q_1^+ (\alpha, K_1 X') + e^{K_1 X'} Q_2^+ (\alpha, K_1 Z)$$

$$Q_1^- \equiv E_1 \left[\alpha (K_1 X')\right] + e^{-K_1 X'} \left\{ \ln \left| \frac{\alpha}{\alpha - 1} \right| - E_1 \left[(\alpha - 1) K_1 X'\right] \right\}$$

$$Q_2^- \equiv \ell n \frac{\alpha+1}{\alpha} + E_1 \left[(\alpha+1)K_1 Z \right] - e^{-K_1 Z} E_1 \left[\alpha(K_1 Z) \right]$$

$$Q_1^+ \equiv - E_1 \left[\alpha(K_1 X') \right] + e^{K_1 X'} \left\{ \ell n \frac{\alpha+1}{\alpha} + E_1 \left[(\alpha+1)K_1 X' \right] \right\}$$

$$Q_2^+ \equiv \ell n \left| \frac{\alpha}{\alpha-1} \right| - E_1 \left[(\alpha-1)K_1 Z \right] + e^{K_1 Z} E_1 \left[\alpha(K_1 Z) \right]$$

$$\alpha \equiv \frac{\mu}{K_1}$$

$$Z \equiv b - x'$$

$$\gamma \equiv \lim_{t \to \infty} \left(- \ell n\, t + \sum_{n=1}^{t} n^{-1} \right) = 0.5772157 \cdots$$

$$E_1(\chi) \equiv \int_{s=\chi}^{\infty} e^{-s} \frac{ds}{s} \equiv - \Upsilon(-\chi)^*$$

* $\Upsilon(-\chi)$ is generally tabulated as $E_i(-\chi)$.

$$\Upsilon(\chi) \equiv \int_{s=0}^{e^{\chi}} \frac{ds}{\ell n s} = - \int_{t=-\chi}^{\infty} e^{-t} \frac{dt}{t} = - E_1 (-\chi)$$

The dimensionless symbols Q_1^- and Q_1^+ are to be associated with the heat generation rate due to gamma sources in the region $0 \leq x \leq x'$, and are derived from the exp $(-K_1 x)$ and exp $(K_1 x)$ portions, respectively, of the function P(x). The quantities Q_2^- exp $(-K_1 x')$ and Q_2^+ exp $(K_1 x')$ have the corresponding physical significance in the region $x' \leq x \leq b$.

Curves are presented in Section VIII showing the various Q's as functions of Kx' or Kz in the range $0 < \alpha \leq 10$. These curves are useful for evaluation of neutron-induced gamma heating.

B. THERMAL NEUTRON CAPTURE

The expression for the capture gamma heat generation rate in a small region about $\underline{x}'$ due to thermal neutrons can be obtained from Eq. (4) by replacing the quantities η_1, K_1, J_1, Σ_1^a, D_1, and β_1 by their respective correspondents for thermal neutrons (η_1 by η_2, etc.). The reciprocal of the quantity K_1, for example, would be replaced by the diffusion length of thermal neutrons in the material.

It is noted that the model does not lend itself to accounting for the thermal neutron source due to slowing down of fast neutrons in the slab material. A correction for this source could be included in the function P(x). In many cases, however, the refinement that would be obtained does not warrant the increased complexity of the integration.

C. INELASTIC SCATTERING GAMMAS

The contribution to the heat generation rate due to inelastic scattering gammas may be estimated from Eq. (4) by replacing η_1, K_1, J_1, Σ_1^a, D_1, and β_1 by their respective correspondents for neutrons in the inelastic scattering energy range. For example, Σ_1^a would be replaced by Σ_{in}^s — a suitably weighted macroscopic inelastic scattering cross section of the material for neutrons.* The reciprocal of the relaxation length for neutrons engaged in inelastic scattering would differ from K_1, in general, since the neutrons undergoing inelastic scattering are usually in a different energy range from neutrons engaged in fast capture. Usually inelastic scattering occurs at higher neutron energies than those predominating in fast capture. It is noted that $\underline{E}$ would be replaced by E_{in}, the energy of the inelastic scattering gamma, and that $\underline{\mu}$ and $\underline{\mu}'$ are functions of gamma energy.

D. CONSIDERATION OF SECONDARY GAMMA ENERGY DISTRIBUTION

In those cases where a neutron interaction may give rise to gammas of various discrete energies (Ref. 2), Eq. (4) may be applied by dividing the gammas into $\underline{m}$ groups. The quantities associated with neutrons (J, η, etc.) will be the same for all groups, while $\underline{\mu}$, $\underline{\mu}'$, and $\underline{E}$ will vary. Denoting the values for the $\underline{i}$th group by the subscript $\underline{i}$, Eq. (4) becomes

$$H_1(x') = \sum_{i=1}^{m} \Gamma_i n_i \tag{5}$$

where

$$\Gamma_i \equiv \frac{1}{2K_1}\left[C_1\left(Q_{1i}^- + e^{-K_1 x'} Q_{2i}^-\right) + C_2\left(Q_{1i}^+ + e^{K_1 x'} Q_{2i}^+\right)\right]$$

$$n_i \equiv \mu_i' E_i q_i$$

q_i ≡ number of gammas in $\underline{i}$th group per neutron interaction ($\Sigma q_i \neq 1$, in general)

* This substitution is to be made in Eq. (3), but $\underline{\text{not}}$ in the equation connecting $\underline{D}$ and $\underline{K}$.

It is convenient to normalize each term of the sum in Eq. (5) to the value of n_j; letting

$$A_i \equiv \frac{n_i}{n_j}$$

it is seen that Eq. (5) may be written

$$H_1(x') = n_j \sum_{i=1}^{m} \Gamma_i A_i = n_j \sum_{i=1}^{m} A_i \frac{H_1(x')}{n_i} \qquad (6)$$

where the subscript j represents any of the gamma groups, $1 \leq j \leq m$.

IV. HEATING DUE TO CORE GAMMAS

With reference to Fig. 2, the contribution to the heat generation rate in the neighborhood of a point $\underline{x}$ within the slab due to a core gamma group of energy $\underline{E}$ may be estimated as follows:

$$G(x,n) = \int_{y=0}^{\infty} \int_{\phi=0}^{2\pi} \frac{y d\phi \, dy}{ds \, d\ell} \frac{J \cos^n \theta}{\pi \ell^2} e^{-\mu \ell} \mu' E \, ds \, d\ell \qquad (7)$$

where $J \cos^n \theta \exp(-\mu\ell)/\pi\ell^2$ is assumed to adequately represent the number of photons of the pertinent gamma group in the neighborhood of $\underline{x}$ due to gammas entering the slab through the elementary area ($y d\phi \, dy$). It should be noted that $\underline{J}$ must be taken so that

$$I = \int_{\theta=0}^{\pi/2} \frac{J \cos^n \theta}{\pi} 2\pi \sin\theta d\theta = \frac{2J}{n+1}$$

where $\underline{I}$ represents the number of photons per unit area of the given gamma group incident on the slab. It is assumed that $\underline{I}$ (and hence $\underline{J}$) is independent of $\underline{y}$ and $\underline{\phi}$. For simplicity the build-up of gamma energy has been neglected, but it will be a significant factor for thicknesses of more than one or two mean free paths in heavy elements. In these cases a correction for this effect should be made by estimating an average buildup factor.

Let $v = \mu\ell$, then since $\ell^2 = x^2 + y^2$, $y dy = \ell d\ell$ and $\cos\theta = x/\ell$, Eq. (7) may be written:

$$G(x,n) = 2 \mu' (\mu x)^n EJ \int_{v=\mu x}^{\infty} \frac{e^{-v} dv}{v^{n+1}} \qquad (8)$$

or

$$\frac{G(x,n)}{2\mu' EJ} = (\mu x)^n E_{n+1}(\mu x) \, , \; n=0, 1, 2 \ldots \qquad (9)$$

where $E_{n+1}(\mu x)$ may be found by use of the recursion formula

$$E_{n+1}(\mu x) = \frac{e^{-\mu x}}{n(\mu x)^n} - \frac{E_n(\mu x)}{n} \tag{10}$$

and the previous definition of $E_1(x)$ following Eq. (4). These functions, are tabulated for n = 1, 2 and 3 in the argument range $1 \leq x \leq 20$ (Refs 3 and 4).* The function $G(x,1)/2\ \mu' EJ$ was computed for various values of $\mu x \leq 20$ and is presented in the appendix.

*The exponential integral function of first order, $E_1(x)$, is tabulated in Refs. 8 and 9 for both positive and negative arguments over a wide range.

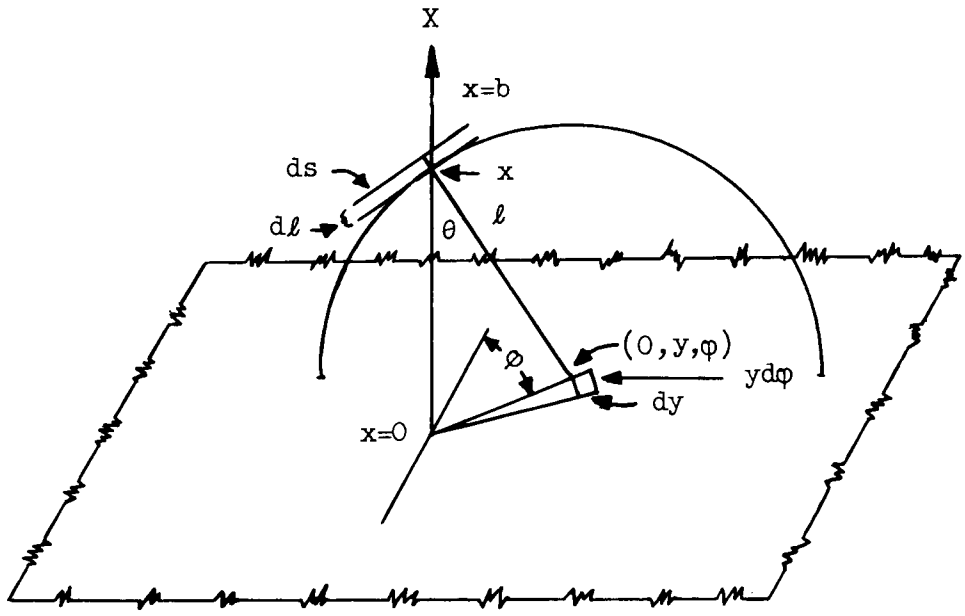

Fig. 2: Slab Geometry: Plane Source Distribution

V. HEATING DUE TO NEUTRON ELASTIC SCATTERING

Although generally negligible, the direct neutron contribution to the heat generation rate may be estimated from Eq. (11) in cases of interest.

Let H_e denote the heat generation rate per unit volume due to elastic scattering of fast neutrons in the materal, then

$$H_e = \alpha_1 (C_1 e^{-K_1 x} + C_2 e^{K_1 x}) \, \Sigma_e^s / \Sigma_1^a \qquad (11)$$

where the new symbols are defined as follows:

α_1 ≡ average loss of energy per elastic scattering collision =

$$1/2 \left[1 - \left(\frac{A-1}{A+1} \right)^2 \right] (1 - \overline{\cos \Theta'}) \, E_n$$

A ≡ atomic weight of the material

E_n ≡ energy of neutron prior to primary collision in the material

Σ_s ≡ macroscopic scattering cross section for fast neutrons in the material

$\overline{\cos\Theta'}$ ≡ average cosine of the scattering angle (note that $\overline{\cos\Theta'} = 0$ or $2/3A$) for isotropic scattering in the laboratory or center-of-mass system, respectively.

VI. HEATING DUE TO OTHER SELECTED REACTIONS

The contribution to the heat generation rate from (n,p), (n,α) and (n,f) reactions may be divided into two parts:

1) that from gamma radiation associated with these reactions and

2) that from dissipation of kinetic energy associated with charged particles emitted in these reactions.

The gamma ray contribution may be calculated from Eq. (4) by replacing $\underline{\mu}$, $\underline{\mu}'$, $\underline{E}$, Σ_1^a, J_1, K_1, etc. by their correspondents for the reaction under consideration. Note that the macroscopic cross section for the reaction under consideration would replace Σ_1^a in Eq. (3), but that the equation connecting D and K would remain in terms of the Σ^a associated with the appropriate neutron group.

The charged particle contribution is deposited locally and may be determined from Eq. (11) by replacing Σ_s, J_1, K_1, etc. by their correspondents and replacing α_1 by α_2, the energy released in the reaction minus the energy of gamma radiation accompanying the reaction.

VII. AVAILABILITY OF DATA

The foregoing treatment assumes that values of the various parameters are readily available. Unfortunately, this is not the case at the present time.

Values of μ_{PE}, μ_{PP}, $\mu_{c,s}$ and $\mu_{c,d}$ are fairly well known; for example, where the electron binding energy is negligible the Compton coefficients may be determined directly from the Klein-Nishina equation (Refs 4, 5, and 6). The lack of neutron data, however, suggests that this is an area in which a great deal of basic research may profitably be done. Particularly needed are branching ratios for the different neutron - induced reactions as a function of neutron energy.

VIII. PARAMETRIC CURVES

This section contains parametric curves which may be used to facilitate the calculation of heating due to gamma rays.

Figures 3 through 5 present Q_1^+ and Q_1^- versus KX with α as a parameter. These terms are defined in Eq. (4).

Figures 6 through 9 present curves for Q_2^+ and Q_2^- versus KZ (where $Z \equiv b - x'$), with α as a parameter, and in addition nomographs for obtaining values of $Q_2^+ \exp(KX')$ and $Q_2^- \exp(-KX')$. Again the terms are defined in Eq. (4). In the appropriate nomograph, the value of $Q_2^{\pm} \exp(\pm KX')$ is read at the intersection of the $Q_2^{\pm} \exp(\pm KX')$ axis and the straight line joining the intersection of the KZ and $Q_2^{\pm}$ axes with KX' on the left hand axis.

The functions $Q_1^{\pm}$ and $Q_2^{\pm}$ are to be associated with heating due to induced gamma rays. In Figs. 10 through 12 curves are presented which are to be associated with heating due to reactor core gammas, and the function $\frac{G(X, 1)}{2\mu' EJ}$ is plotted as a function of μX. These terms are defined in Section IV.

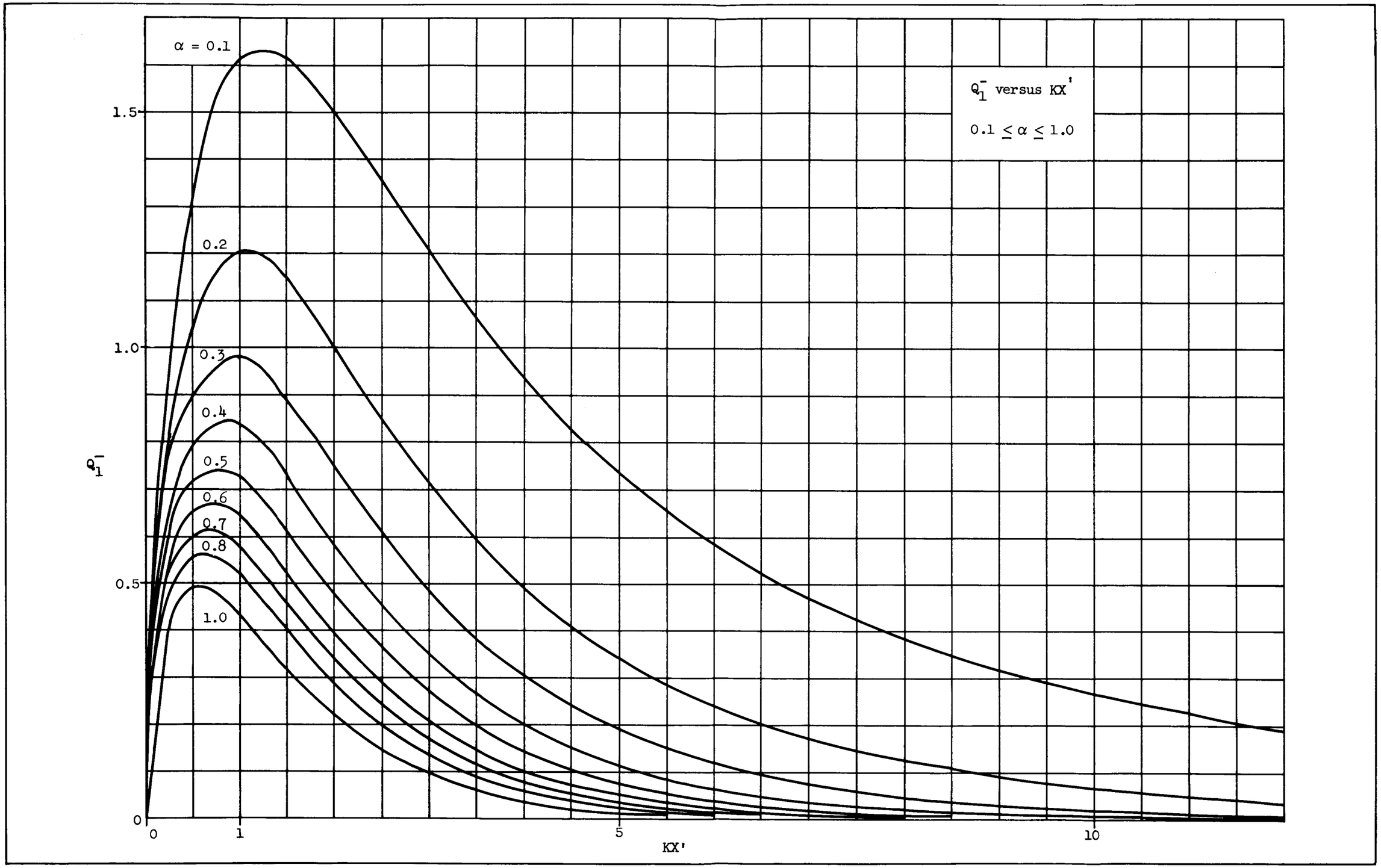

Fig. 3. Q_1^- Versus KX' $(0.1 \leq \alpha \leq 1.0)$

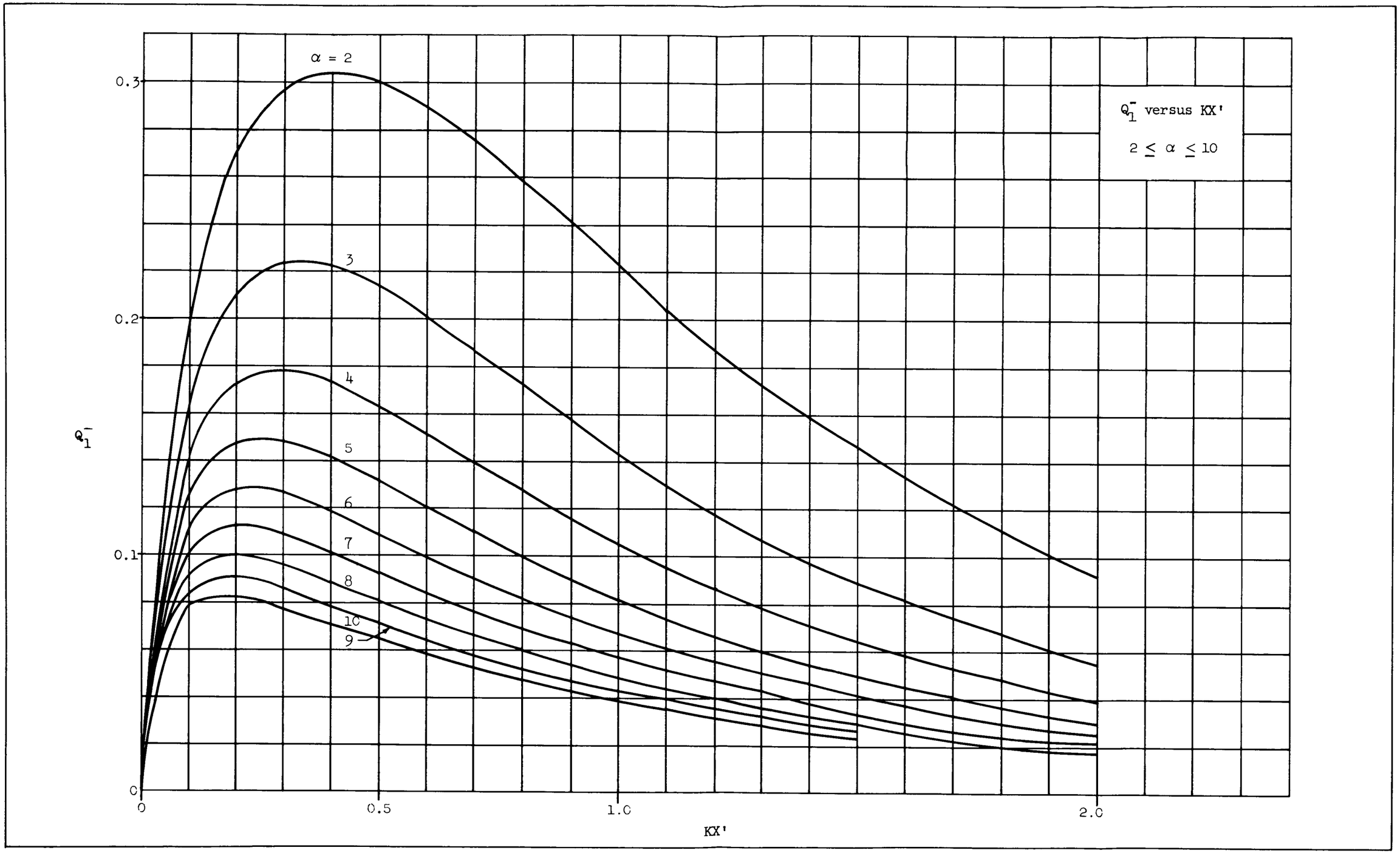

Fig. 4. Q_1^- Versus KX' $(2 \leq \alpha \leq 10)$

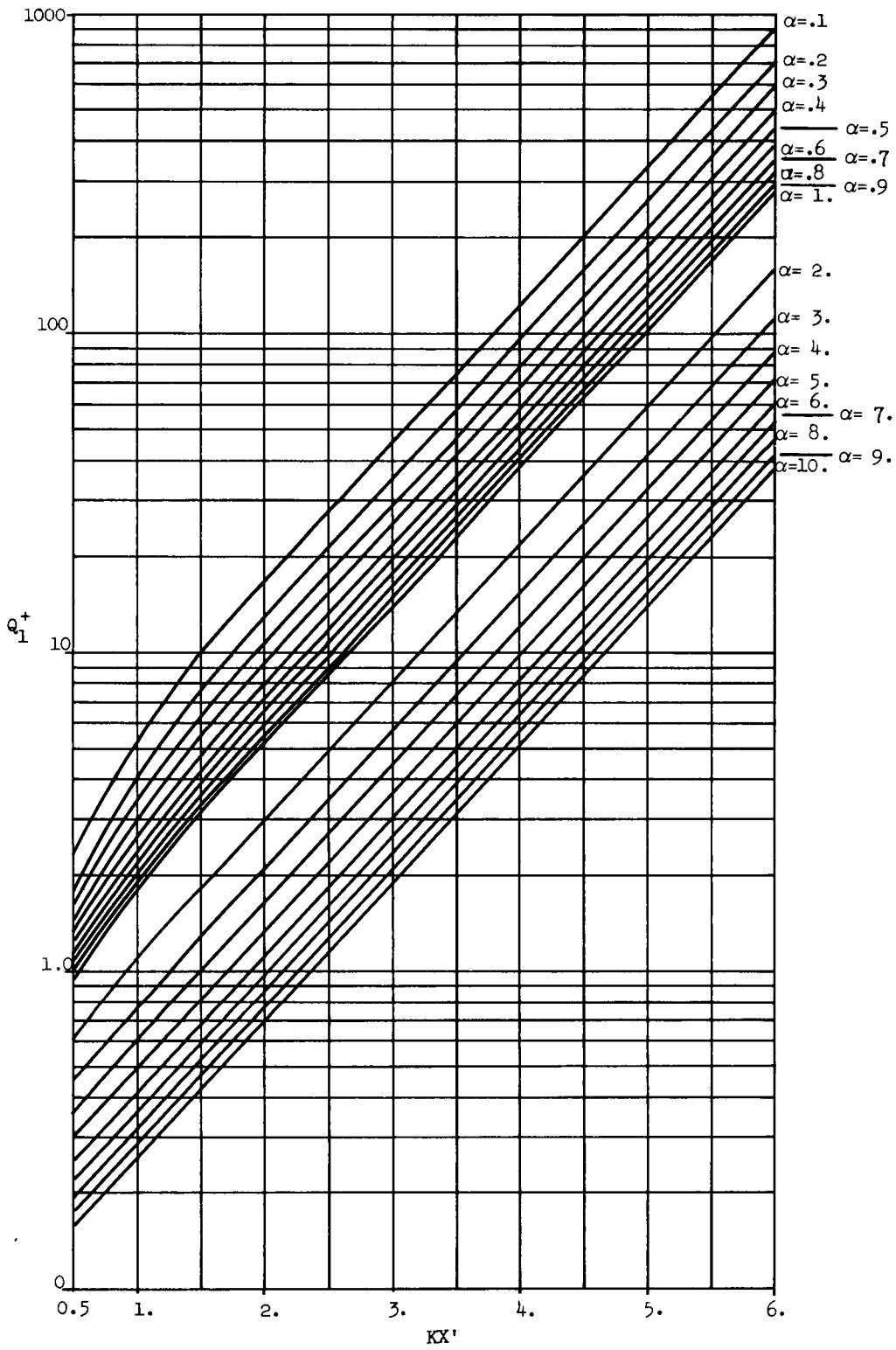

Fig. 5. Q_1^+ Versus KX' $(0.1 \leq \alpha \leq 10)$

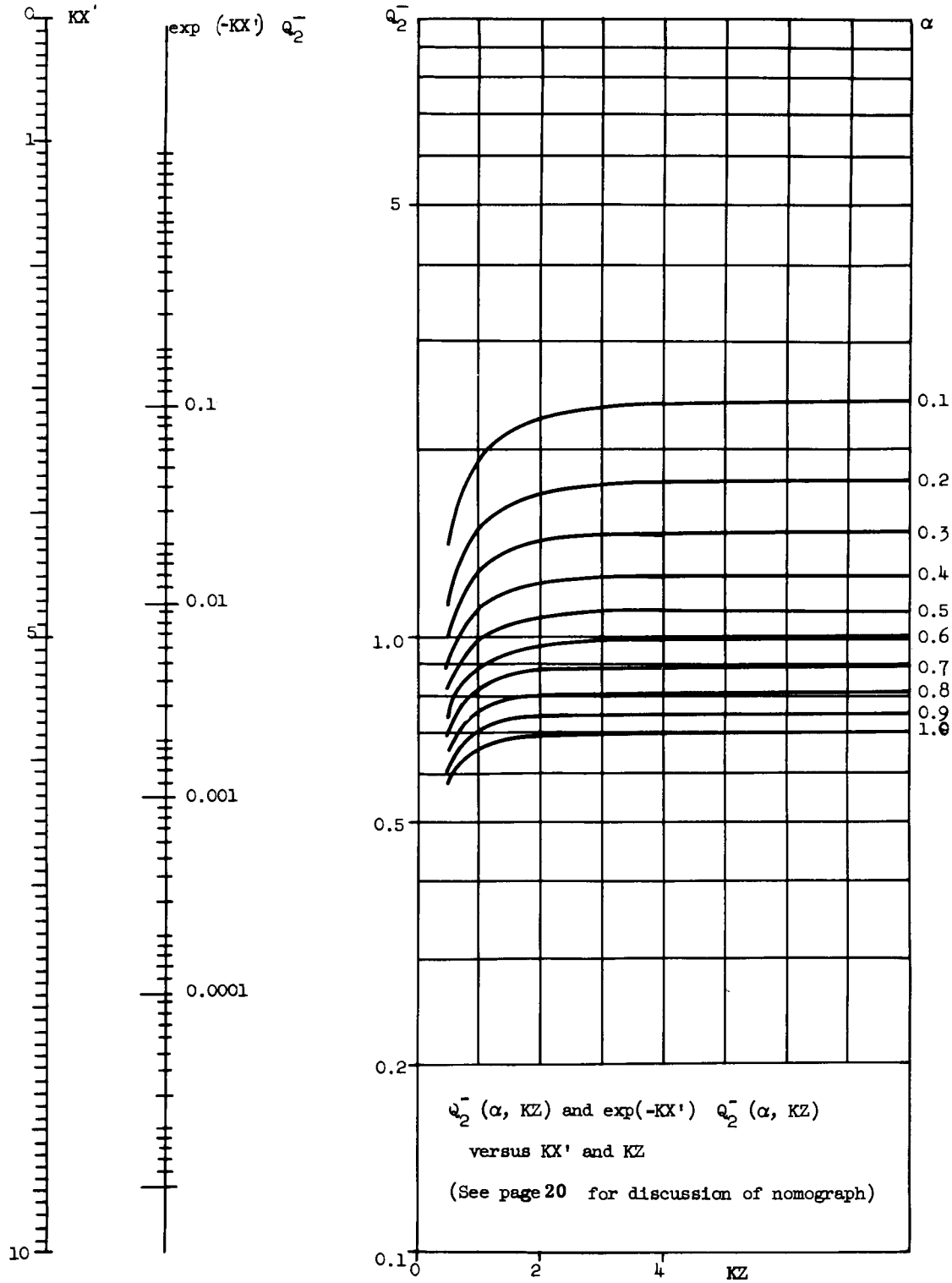

Fig. 6. Q_2^- Nomograph $(0.1 \leq \alpha \leq 1)$

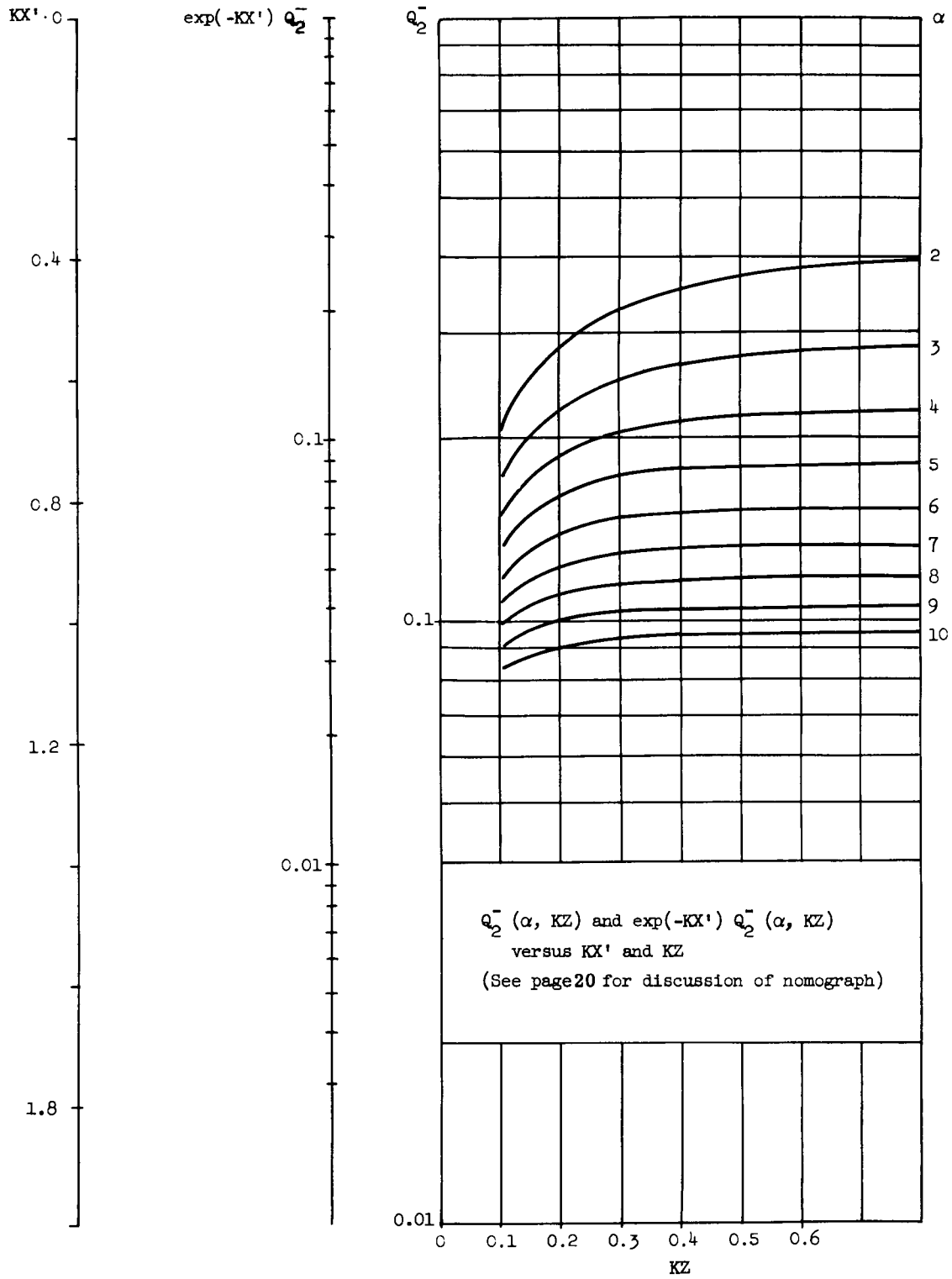

Fig. 7. Q_2^- Nomograph $(2 \leq \alpha \leq 10)$

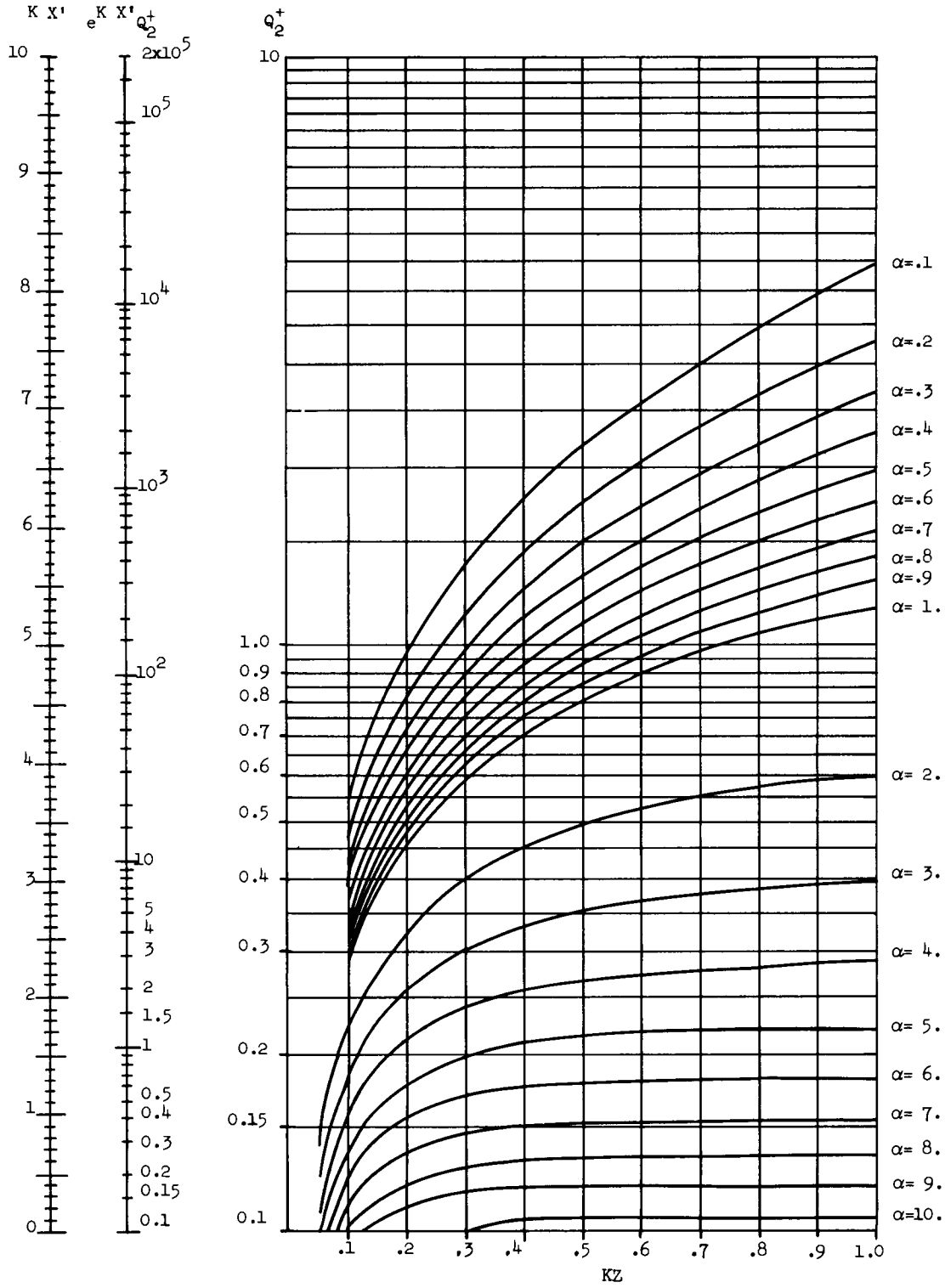

Fig. 8. Q_2^+ Nomograph ($0.1 \leq \alpha \leq 10$, $KZ \leq 1$)

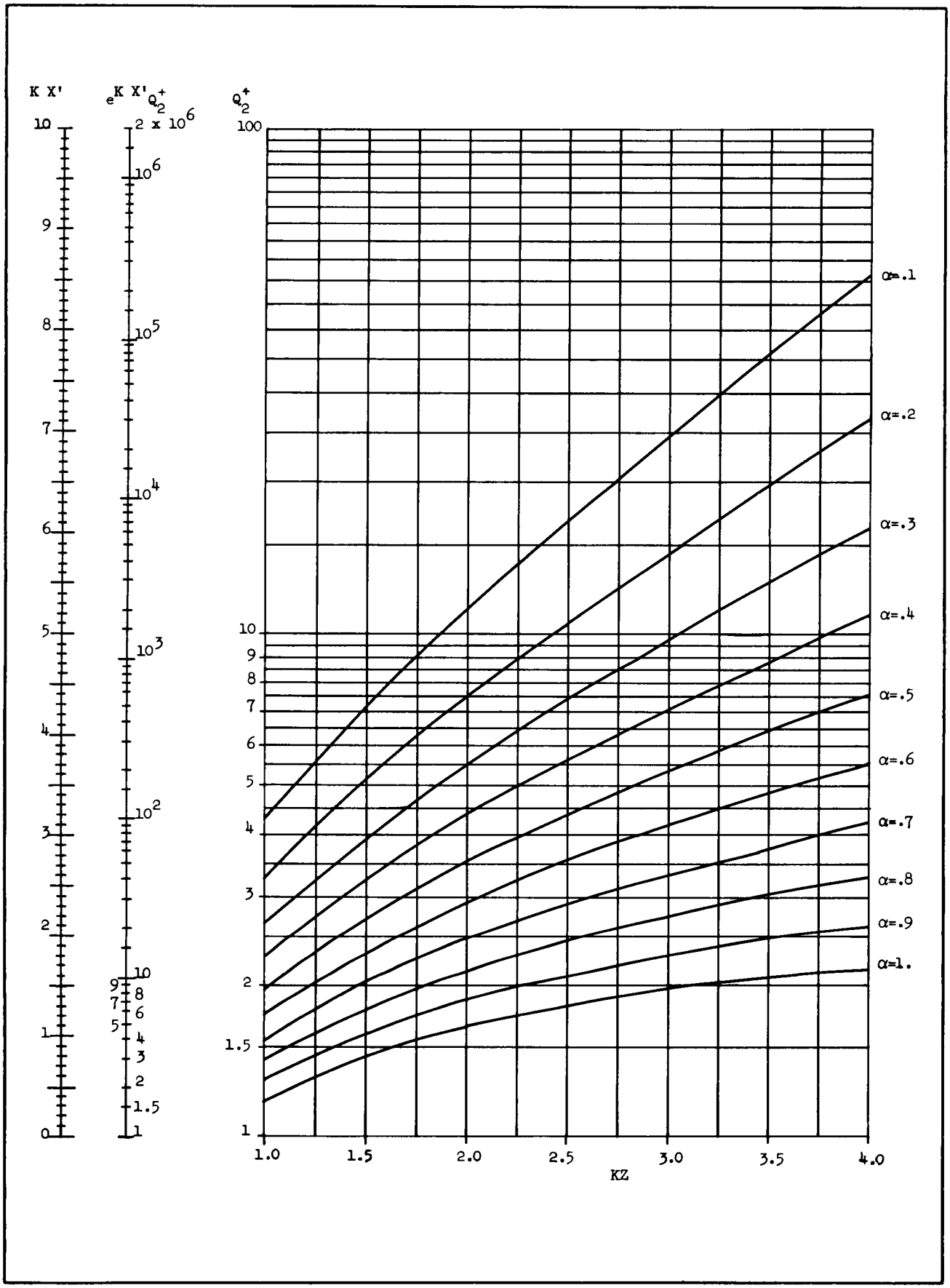

Fig. 9. Q_2^+ Nomograph ($0.1 \leq \alpha \leq 1$, $1 \leq KZ \leq 4$)

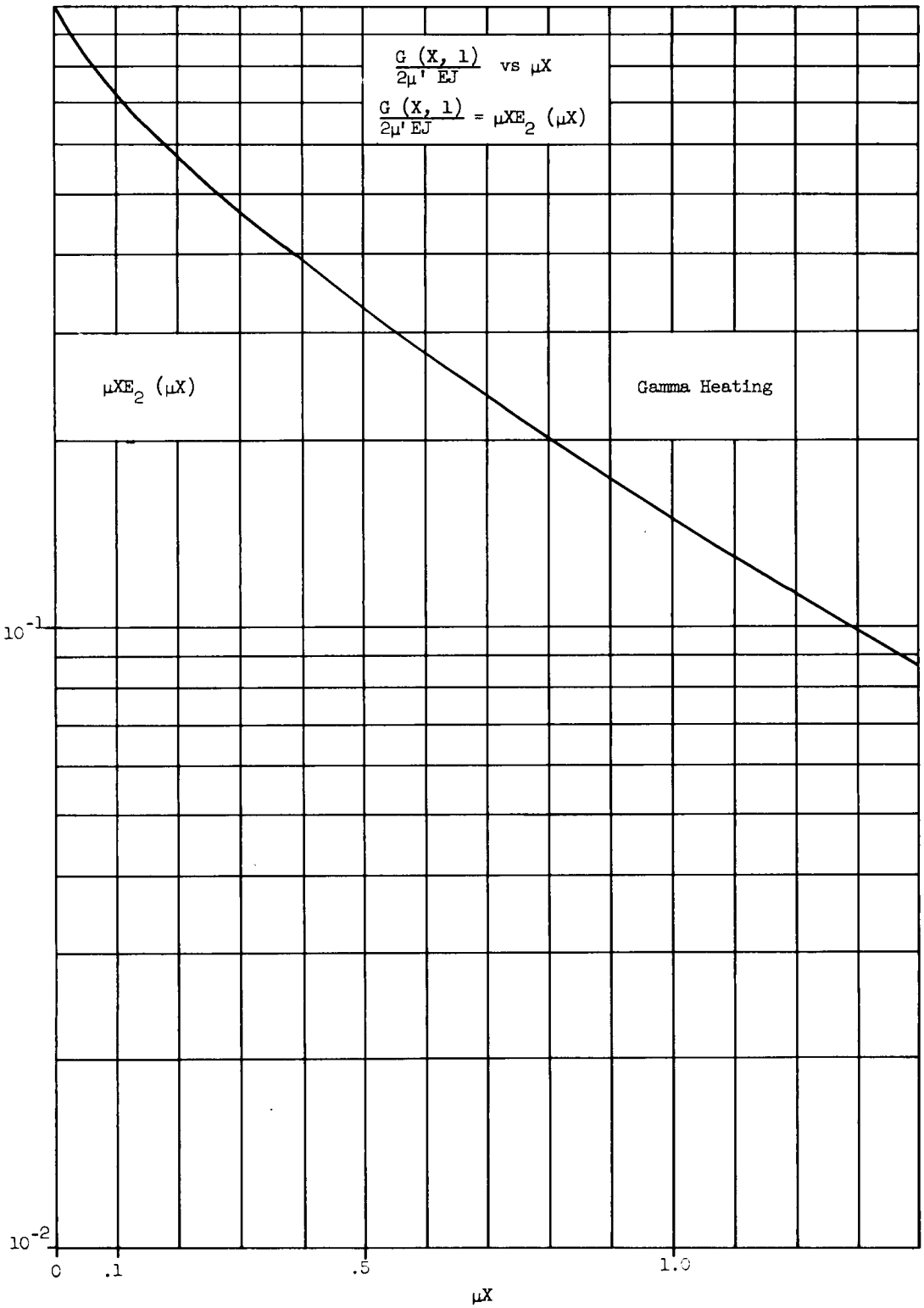

Fig. 10. $\mu X\ E_2(\mu X)$ Versus μX ($\mu X \leq 1.4$)

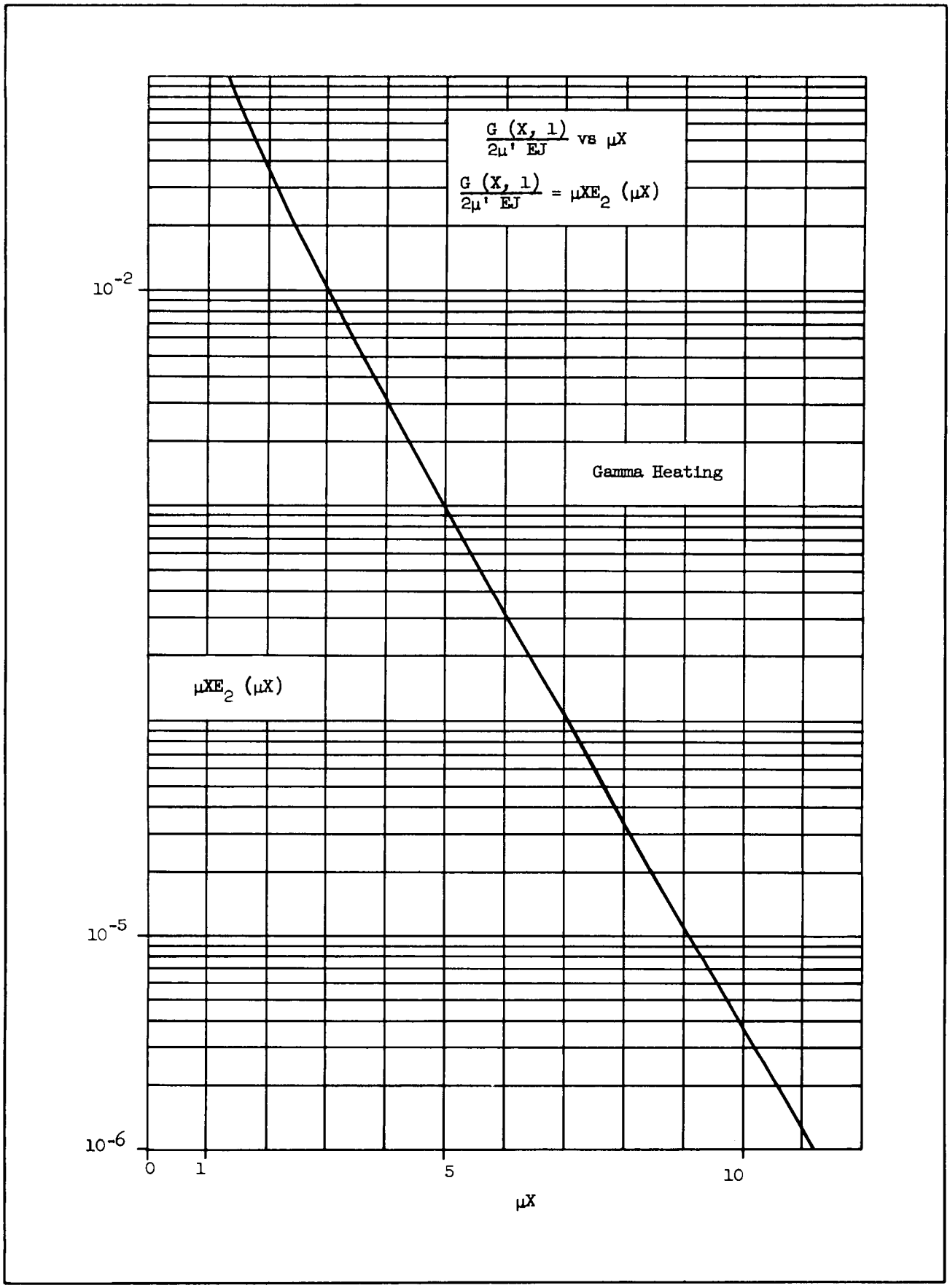

Fig. 11. $\mu X\ E_2(\mu X)$ Versus μX $(1.4 \leq \mu X \leq 11)$

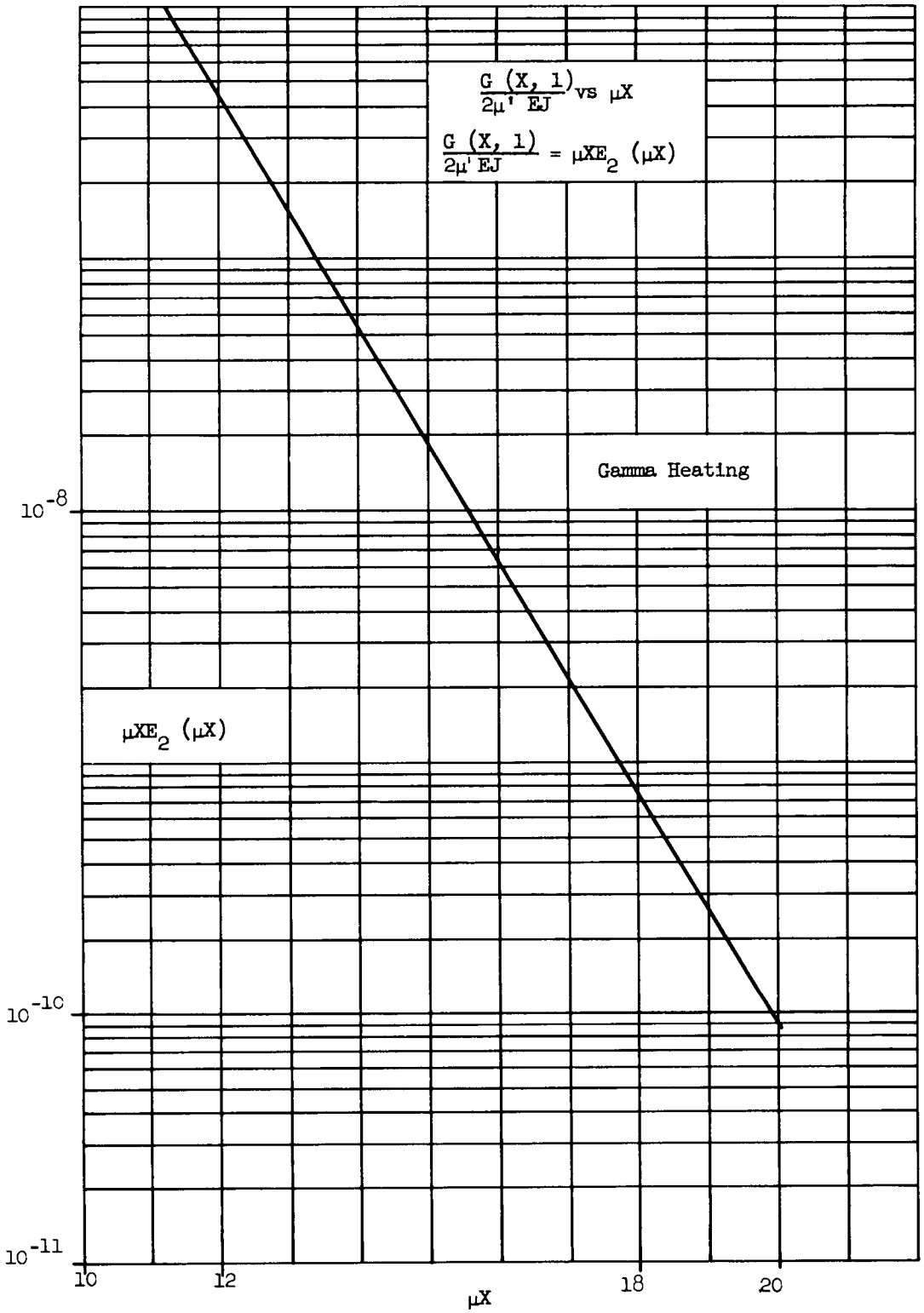

Fig. 12. $\mu X E_2(\mu X)$ Versus μX ($11 \leq \mu X \leq 20$)

IX. EXAMPLE

As an example of the application of the formulas derived for the heat generation in a plane slab, values have been calculated for the various heat contributions in a slab of iron. Iron has been chosen for this example because more complete information is available for iron than for most materials.

A. TABULATION OF SELECTED PARAMETERS

The following values of the parameters have been selected:

Slab thickness = 6 in. = 15.3 cm

Incident fast neutron current = 1×10^{12} neutrons/cm^2-sec

Incident thermal neutron current = 1×10^{12} neutrons/cm^2-sec

6-Mev gamma current = 1×10^{13} gammas/cm^2-sec

3-Mev gamma current = 2×10^{13} gammas/cm^2-sec

1-Mev gamma current = 5×10^{13} gammas/cm^2-sec

Core gamma distribution = $I \cos \theta$

$f = 0.85$

$K_1 = 0.0428 \text{ cm}^{-1}$

$K_2 = 0.788 \text{ cm}^{-1}$

$\Sigma_1^a = 0.0025 \text{ cm}^{-1}$

$\Sigma_{in.}^s = 0.0508 \text{ cm}^{-1}$

$\beta_1 = 0.5$ (This is an assumed value. It is selected because it gives an interesting result.)

$\beta_2 = 0.821$ (A water medium is assumed.)

The values of the incident neutron and gamma currents were selected for convenience in the calculations. The values of K, Σ_1^a and Σ_{in}^s were taken from Dr. L.G. Alexander's lectures (Oak Ridge School of Reactor Technology) on reactor engineering.

B. HEAT GENERATED BY CORE GAMMAS

For each of the selected core gamma energies a G(X) is computed from the curves in Section VIII. These functions are presented in Fig. 13.

C. HEAT GENERATED BY THERMAL NEUTRON CAPTURE

The gamma energy groups for thermal neutron capture are (Ref. 3):

i	E_i	$\bar{E}_i$	μ_i	q_i	A_i
1	0-1 Mev	0.5 Mev	0.607 cm^{-1}	0.54*	0.1912
2	1-3	2.0	0.331	0.10*	0.0772
3	3-5	4.0	0.252	0.24	0.2825
4	5-7	6.0	0.244	0.22	0.3763
5	7	7.5	0.228	0.50	1.0000

* Estimated value

Using the normalization procedure outlined in Eqs. (5) and (6), a composite Q_1^- and Q_2^- are defined for the thermal capture process in iron. These are presented in Fig. 14. The corresponding Q^+'s are not shown because exp (-2 Kb) is approximately zero for this particular example. The heat generation rate is given in Fig. 15.

D. HEAT GENERATED BY FAST NEUTRON CAPTURE

Since this is not a major contribution (K_1 is small), one 7.5 Mev gamma per capture is assumed. The resulting heat generation is also plotted in Fig. 15.

E. HEAT GENERATED BY INELASTIC SCATTERING

A number of measured scattering cross-sections have been tabulated by Feld (Ref. 7). Although cross sections and energies for several of the possible reactions are well known, the data are not complete. For this example an average energy of 2.0 Mev for the emitted gamma ray is chosen. The results are given in Fig. 15.

F. DISTRIBUTION OF HEAT GENERATION

The sum of the contributions shown in Figs. 13 and 15 are shown in Fig. 16. Integration under the curve yields an areal heat generation rate of 15.2 watts/cm^2. For a spherical shell of 65 cm radius (mean area = 5.30×10^4 cm^2) and the above thickness, the total heat generation rate, neglecting geometrical distortion, is 8.8×10^5 watts.

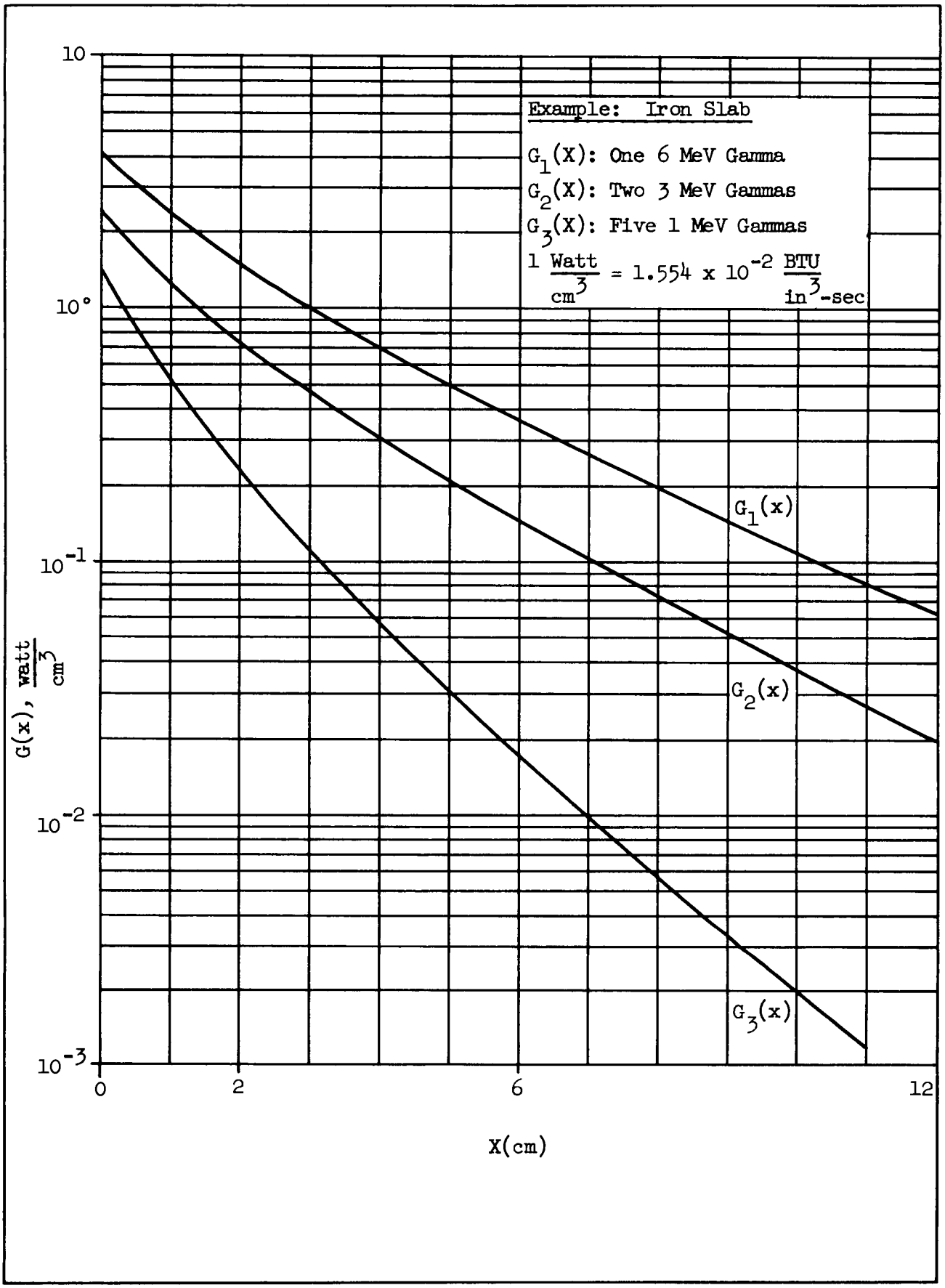

Fig. 13. G(X) Versus X (iron slab)

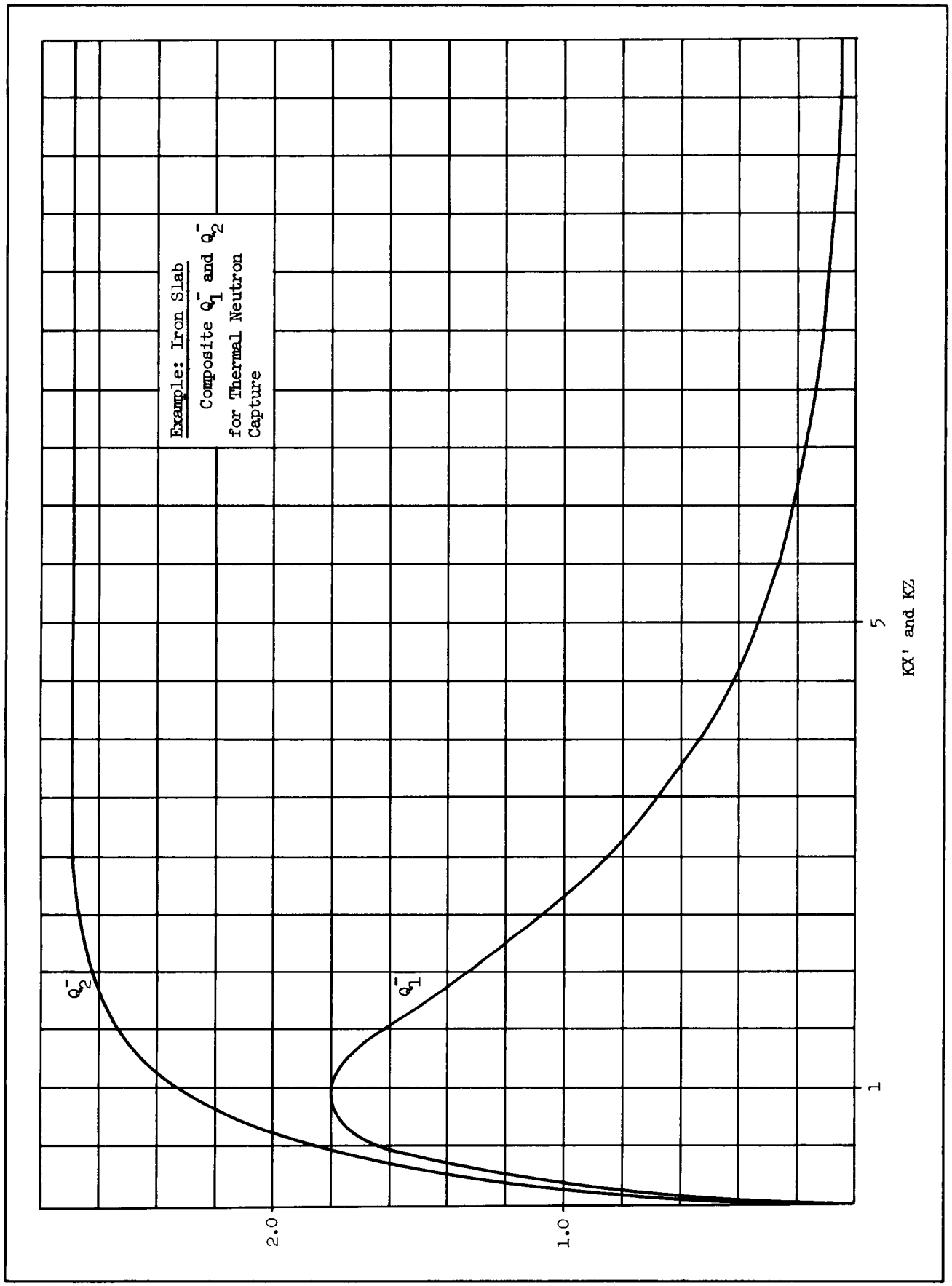

Fig. 14. Composite Q_1^- and Q_2^- for Thermal Neutron Capture (iron slab)

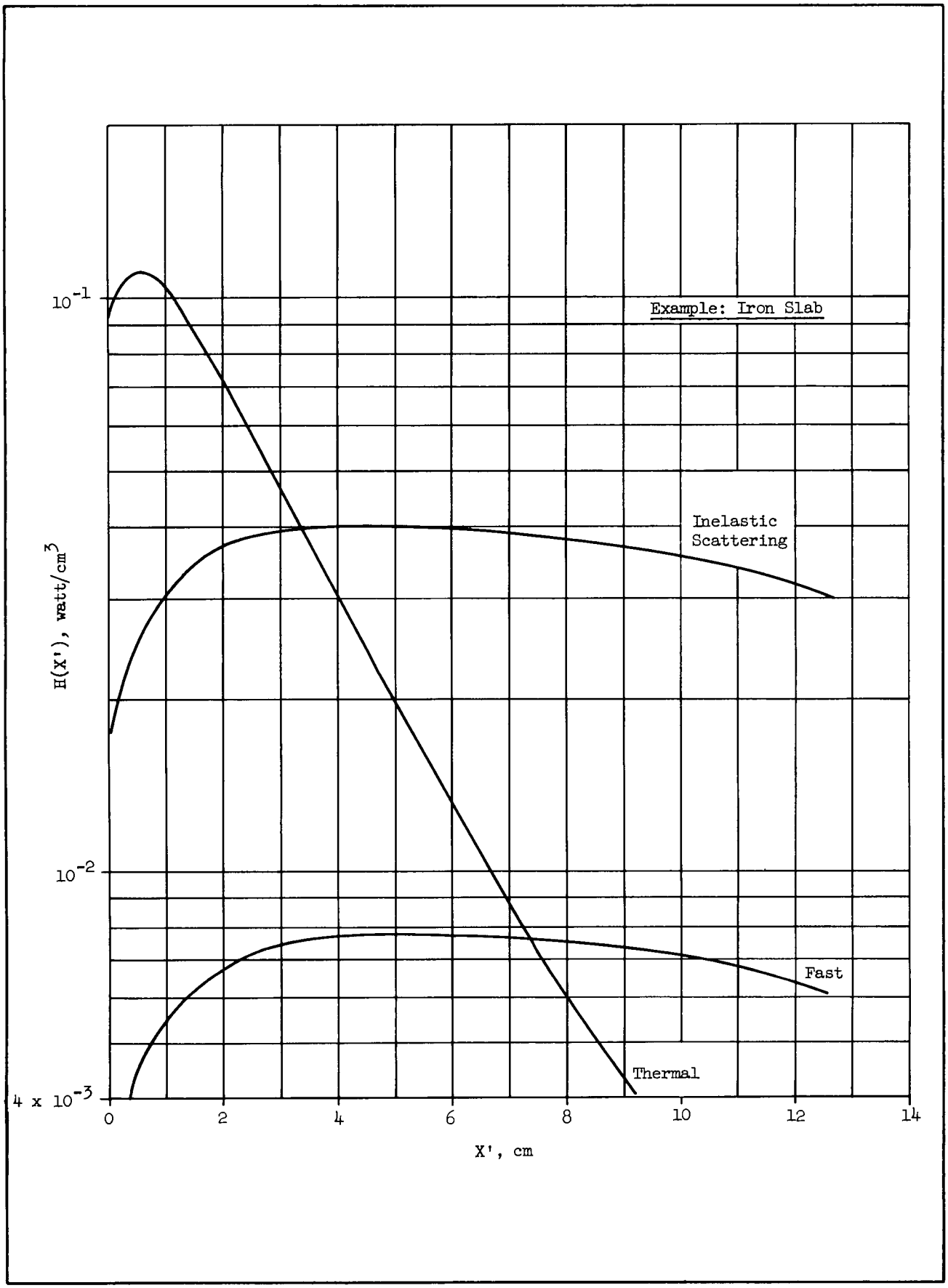

Fig. 15. Heat Generation Rate Versus X' for Inelastic Scattering, Fast Neutrons, and Thermal Neutrons (iron slab)

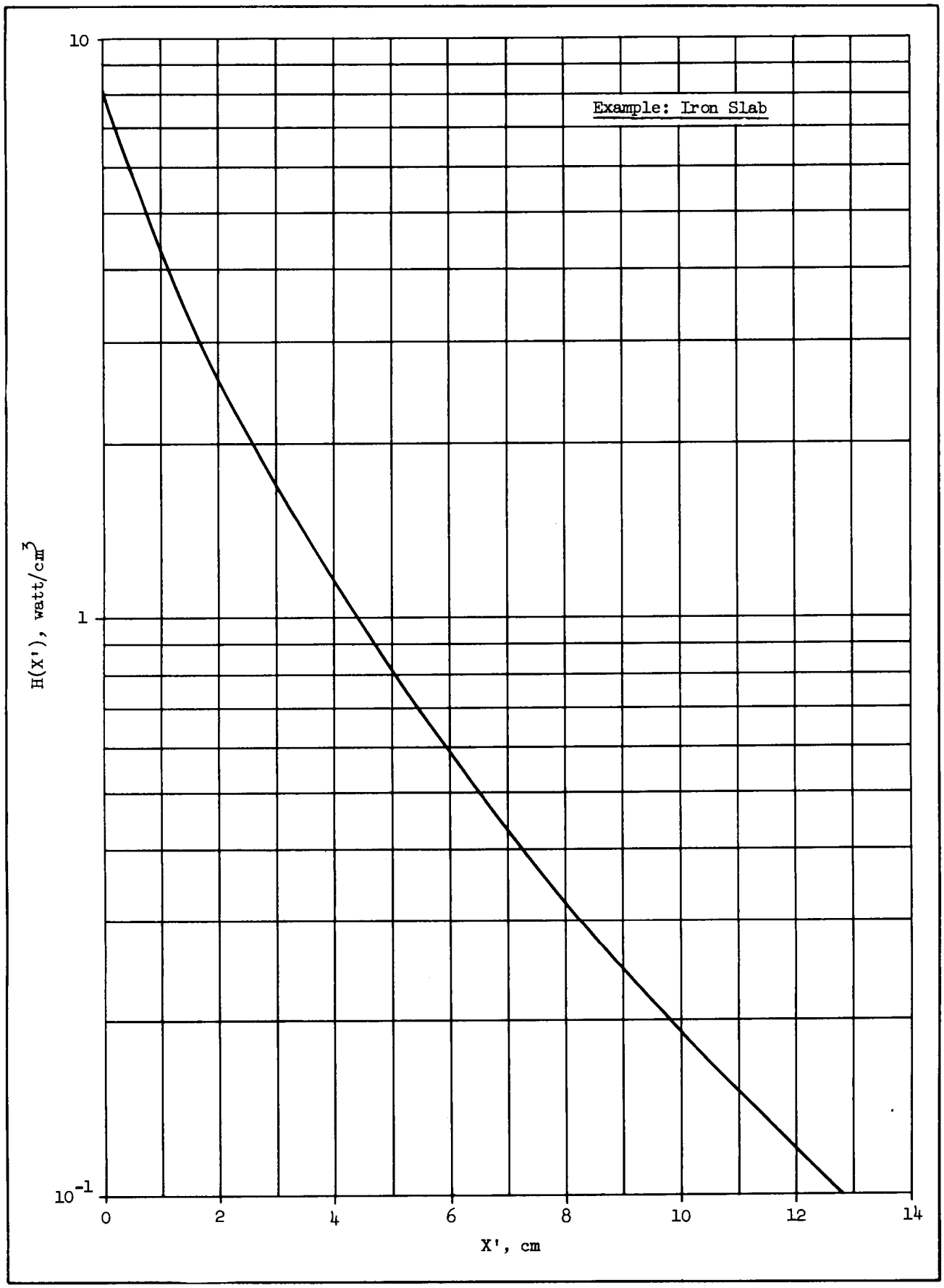

Fig. 16. Heat Generation Rate Versus X' for all Processes Considered (iron slab)

X. APPENDIX

This appendix contains details of the theory which were omitted in the text in the interest of brevity and clarity and are presented here for the sake of completeness.

A. DERIVATION OF EQ. (2)

With reference to the text,

$$H(x') = \int_{x=0}^{b} \int_{y=0}^{\infty} \int_{\varphi=0}^{2\pi} d\,H(x, x', y, \varphi) \qquad (1\text{-A})$$

$$= \int_{x=0}^{b} \int_{y=0}^{\infty} \int_{\varphi=0}^{2\pi} \frac{E\,P(x)\,y\,dy\,d\varphi\,dx\,\mu'\,e^{-\mu\ell}}{4\pi\,\ell^2}$$

With reference to Fig. 1, it is seen that $\ell^2 = |x - x'|^2 + y^2$, and that when $y = 0$ or ∞, $\ell = x - x$ or ∞, respectively. Furthermore, $ydy = \ell d\ell$, since $\underline{x}$ is constant for any integration over $\underline{y}$. Therefore, Eq. (1-A) may be written:

$$H(x') = \frac{\mu' E}{4\pi} \int_{x=0}^{b} P(x)\,dx \int_{\ell = |x - x'|}^{\infty} e^{-\mu\ell}\,\frac{d\ell}{\ell} \int_{\varphi=0}^{2\pi} d\varphi$$

$$= \frac{\mu' E}{2} \int_{x=0}^{b} P(x)\,dx \int_{\ell = |x - x'|}^{\infty} e^{-\mu\ell}\,\frac{d\ell}{\ell}$$

$$= \frac{\mu' E}{2} \int_{x=0}^{b} P(x)\,E_1\,(\mu|x - x'|)\,dx \qquad (2\text{-A})$$

B. DERIVATION OF EQ. (3)

It is assumed that the neutron flux in the plane slab under consideration can be derived from simple diffusion theory.

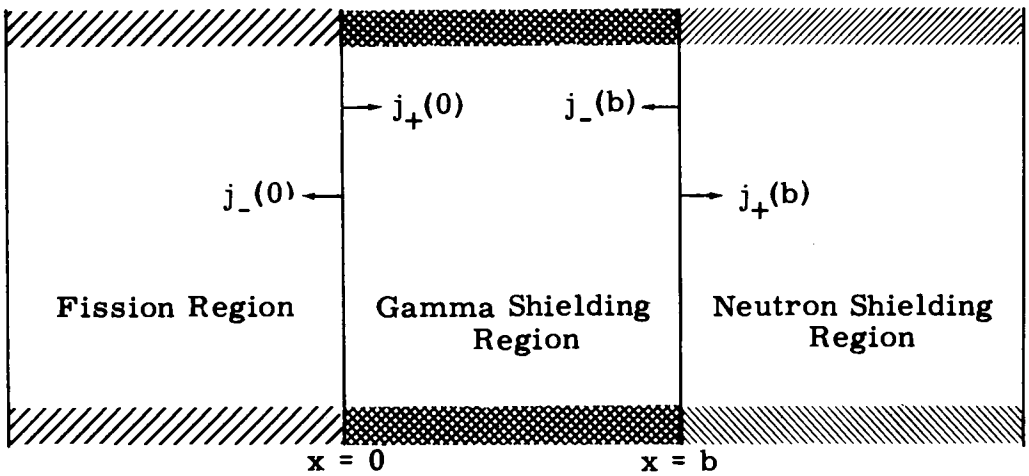

With reference to the text and to the above diagram, it is seen that the diffusion equation

$$\nabla^2 \varphi(x) - K^2 \varphi(x) = 0 \qquad (3 - A)$$

is to be solved subject to the following boundary conditions:

1) $\alpha \; j_+(0) = j_-(0)$

2) $\beta \; j_+(b) = j_-(b)$

where

$\varphi \equiv$ neutron flux in gamma shielding region

$K^2 \equiv \Sigma_a/D$

$\alpha \equiv$ albedo of gamma shielding region

$\beta \equiv$ albedo of neutron shielding region

Integration of Eq. (3-A) gives

$$\varphi(x) = A\, e^{-Kx} + B\, e^{Kx} \tag{4-A}$$

Then, since

$$\alpha = \frac{1 + 2D \dfrac{\nabla\varphi(o)}{\varphi(o)}}{1 - 2D \dfrac{\nabla\varphi(o)}{\varphi(o)}} = \frac{1 - 2KD \dfrac{A - B}{A + B}}{1 + 2KD \dfrac{A - B}{A + B}} \tag{5-A}$$

application of boundary conditions 1) and 2) above yields Eqs. (6-A) and (7-A), respectively:

$$B = \frac{4\ j_+(0) - A\,(1 + 2KD)}{1 - 2KD} \tag{6-A}$$

$$A = \frac{4\ j_+(0)\ (\eta - K)}{(1 + 2KD)\,(\eta - k) - (1 - 2KD)\,(\eta + K)\exp(-2Kb)} \tag{7-A}$$

where

$$\eta \equiv \frac{1}{2D}\ \frac{\beta - 1}{\beta + 1}$$

Hence, it is seen that

$$P(x) = \Sigma\ \varphi(x) = C_1\, e^{-Kx} + C_2\, e^{Kx} \tag{8-A}$$

where C_1 and C_2 are defined in Eq. (3).

C. DERIVATION OF EQ. (4)

Upon substituting the P(x) obtained in Eq. (8-A), Eq. (2) or (2-A) becomes

$$H(x') = \frac{\mu' E}{2K} \quad (C_1 \, \xi + C_2 \, \Lambda) \tag{9-A}$$

where

$$\xi(x') \equiv \int_{x=0}^{b} e^{-Kx} \, K \, E_1 \, (\mu |x - x'|) \, dx \tag{10-A}$$

$$\Lambda(x') \equiv \int_{x=0}^{b} e^{Kx} \, K \, E_1 \, (\tilde{\mu} |x - x'|) \, dx \tag{11-A}$$

Consider

$$\xi(x') = \int_{x=0}^{b} e^{-Kx} \, K \, dx \int_{\omega = \mu|x - x'|}^{\infty} e^{-\omega} \, \frac{d\omega}{\omega}$$

$$= \int_{x=0}^{x'} e^{-Kx} \, K \, dx \int_{s = \mu(x'-x)}^{\infty} e^{-s} \, \frac{ds}{s}$$

$$+ \int_{x=x'}^{b} e^{-Kx} \, K \, dx \int_{t=\mu(x-x')}^{\infty} e^{-t} \, \frac{dt}{t}$$

$$= \xi_1 + \xi_2 \tag{12-A}$$

where

$$\xi_1 \equiv \int_{x=0}^{x'} e^{-Kx} \, K \, dx \int_{v=1}^{\infty} e^{-\mu(x'-x)v} \, \frac{dv}{v} \tag{13-A}$$

$$\xi_2 \equiv \int_{x=x'}^{b} e^{-KX} K dx \int_{w=1}^{\infty} e^{-\mu(x-x')w} \frac{dw}{w} \tag{14-A}$$

Consider

$$\xi_1 = \int_{v=1}^{\infty} K e^{-\mu x' v} \frac{dv}{(K-\mu v)v} \int_{x=0}^{x'} e^{-(K-\mu v)x} (K-\mu v) dx$$

$$= \int_{v=1}^{\infty} K(e^{-KX'} - e^{-\mu x' v}) \frac{dv}{(\mu v - K)v}$$

$$= \int_{v=1}^{\infty} \left(e^{-Kx'} - e^{-\mu x' v}\right) \frac{\mu dv}{\mu v - K} - \int_{v=1}^{\infty} (e^{-Kx'} - e^{-\mu x' v}) \frac{dv}{v}$$

$$= e^{-Kx'} \ln \left|\frac{\mu}{\mu - K}\right| + E_1(\mu x') - e^{-Kx'} E_1(\mu x' - Kx') \tag{15-A}$$

where

$$E_1(\chi) \equiv -\Upsilon(-\chi) \equiv \int_{u=\chi}^{\infty} e^{-u} \frac{du}{u} = -\gamma - \ln\chi - \sum_{n=1}^{\infty} \frac{(-\chi)^n}{n.n!}$$

$$\Upsilon(\chi) = -E_1(\chi) + 2\int_{t=0}^{\chi} \sinh t \frac{dt}{t} = \gamma + \ln|\chi| + \sum_{n=1}^{\infty} \frac{\chi^n}{n.n!}$$

$$E_1(\chi) + \Upsilon(\chi) \equiv -\int_{v=-\chi}^{\chi} e^{-v} \frac{dv}{v} = 2 \sum_{n=0}^{\infty} \frac{\chi^{2n+1}}{(2n+1)(2n+1)!}$$

and the symbol γ is defined in Eq. (4).

Values and expansions for the exponential integral functions (E_1 and $\mathcal{T}$) are accessible (e.g., Refs. 8 and 9). It is to be noted that $\mathcal{T}$, generally tabulated as E_i, is simply the Cauchy principal value of E_1 for $\chi < 0$.

Similarly,

$$\xi_2 = Ke^{-KX'} \int_{w=1}^{\infty} \frac{dw}{(\mu w+K)w} - Ke^{-Kb} \int_{w=1}^{\infty} e^{-\mu(b-X')w} \frac{dw}{(\mu w+K)w}$$

$$= - e^{-KX'} \int_{w=1}^{\infty} \frac{\mu dw}{\mu w+K} + e^{-KX'} \int_{w=1}^{\infty} \frac{dw}{w}$$

$$+ \mu e^{-Kb} \int_{w=1}^{\infty} e^{-\mu(b-X')w} \frac{dw}{\mu w+K} - e^{-Kb} \int_{w=1}^{\infty} e^{-\mu(b-X')w} \frac{dw}{w}$$

$$= e^{-KX'} \ln \frac{\mu+K}{\mu} - e^{-Kb} E_1(\mu b-\mu X') + e^{-KX'} E_1 \left[(b-X')(\mu+K)\right] \qquad (16\text{-A})$$

Now, summing Eqs. (15-A) and (16-A), it is seen that Eq. (10-A) may be written

$$\xi(X') = E_1(\mu X') + e^{-KX'} \left\{ \ln \left| \frac{\mu+K}{\mu-K} \right| - e^{-K(b-X')} E_1(\mu b-\mu X') \right.$$

$$\left. - E_1(\mu X'-KX') + E_1 \left[(b-X')(\mu+K)\right] \right\}$$

$$= Q_1^- (\alpha, KX') + e^{-KX'} Q_2^- (\alpha, KZ) \qquad (17\text{-A})$$

where the new symbols are defined in Eq. (4).

In a manner similar to that used above, it can be shown that Eq. (11-A) may be written

$$\Lambda(X') = e^{Kb} E_1(\mu b-\mu X') - E_1(\mu X') + e^{KX'} \left\{ \ell n \left| \frac{\mu+K}{\mu-K} \right| \right.$$

$$\left. + E_1(\mu X' + KX') - E_1 \left[(\mu-K)(b-X') \right] \right\}$$

$$= Q_1^+ (\alpha,KX') + e^{KX'} Q_2^+ (\alpha,KZ) \qquad (18\text{-A})$$

where the new symbols are defined in Eq. (4).

N.B.

Throughout the report, upper and lower case Z's have the same significance. The same is true for upper and lower case X's.

XI. REFERENCES

1 H.L.F. Enlund, "Energy Absorption of Capture Gammas," ORNL CF-52-6-99 Supplement dated 16 October, 1952, 4 pp.

2 P.S. Mittelman and R.A. Liedtke, "Gamma-Rays from Thermal Neutron Capture," Nucleonics 13, 5 (May, 1955)

3 The Reactor Handbook, Vol. I (Physics), pp 804-808.

4 J.Moteff, Compiler, "Miscellaneous Data for Shielding Calculations," APEX 176 (December, 1954)

5 O. Klein and Y. Nishina; Z. Physik 52, 853 (1929)

6 C.M. Davisson; Revs. Mod. Phys 24, 2, (1952)

7 E. Segre (editor) "Experimental Nuclear Physics, Vol II."

8 E. Jahnke and F. Emde, "Tables of Functions," Fourth Edition, Dover Publications, New York.

9 National Bureau of Standards, "Tables of Sine, Cosine, and Exponential Integrals," New York, 1940.

SECRET

Paper II-D

GAMMA-RAY HEATING IN A 300-Mw CFR SHIELD

C. A. Goetz*
R. M. Davis**
Oak Ridge National Laboratory

*Loan employee from The Martin Company
**Loan employee from Pratt and Whitney Aircraft Company

SECRET

RESTRICTED DATA

"This document contains restricted data as defined in the Atomic Energy Act of 1954. Its transmittal or the disclosure of its contents in any manner to an unauthorized person is prohibited."

[redacted]

GAMMA-RAY HEATING IN A 300-Mw CFR SHIELD

C. A. Goetz*
R. M. Davis**

The heat in the lead and alkylbenzene shield of a 300-Mw circulating-fuel reflector-moderated reactor has been calculated for the following components: (1) primary gamma-rays originating in or near the reactor core, (2) fission product gamma-rays from the heat exchanger, and (3) thermal-neutron capture in the lead and borated (2% boron) alkylbenzene. The third component was subdivided to account for secondary gamma-rays from the lead, hydrogen and boron capture. Alpha particles resulting from thermal-neutron capture boron were also considered.

A study of the gamma-ray heating in the lead and alkylbenzene shield of a 300-Mw circulating-fuel reflector-moderated reactor (Table I) has recently been completed. Throughout the calculation the latest CFRMR-shield mockup experimental data from the LTSF was incorporated as much as possible. The heating in the shield was resolved into three principal components: (1) heating due to primary gamma rays originating in or near the reactor core, (2) heating due to fission-product decay gamma rays from the heat exchanger region, and (3) heating resulting from thermal-neutron captures in the lead and borated (2% boron) alkylbenzene. The third component was subdivided to account for secondary gamma rays from lead, hydrogen, and boron capture. Alpha particles resulting from the thermal-neutron captures by boron were also considered. (This is the only source of heating not due to gamma rays included in the calculations.)

The results of the calculation are plotted in Figs. 1 through 6. The methods of calculation are described below.

---

*Loan employee from The Martin Company.
**Loan employee from Pratt and Whitney Aircraft Company.

[redacted]

[redacted]

PRIMARY GAMMA-RAY HEATING

The primary gamma-ray source includes both prompt and fission-product gamma rays from the core, capture gamma rays from the Inconel core shell cladding, and capture gamma rays from the beryllium. The heating in the alkylbenzene and lead shield resulting from these gamma rays was determined by the procedure outlined below.

The heating in the alkylbenzene was obtained by use of a recent analysis[1] of LTSF measurements in which the important source contributions to the gamma-ray dose rate in water beyond a CFRMR mockup were determined for various lead and water thicknesses. The usual material and geometry transformations were applied to the resulting curves to obtain the dose rate in alkylbenzene behind various lead thicknesses. The dose rate was then converted to heat with the following expression:

$$H_{alkyl,P}(t_{alkyl}, t_{Pb}) = K_1 \frac{r_c}{r} D_{P,LT}(a,z,t_{Pb}) H(a,z) \frac{\sigma_R}{\sigma_{LT}} c_1 c_2 c_3$$

where

$H_{alkyl,P}$ = heating due to primary gamma-ray sources (watts/g),

t_{alkyl} = thickness of alkylbenzene (cm),

t_{Pb} = thickness of lead (cm),

K_1 = factor to convert from dose rate to heat

= 2.58×10^{-9} (watts/g)/(r/hr),

r_c = outside radius of reactor core (33.0 cm),

r = radius to a point in the reactor at which heating is computed (cm),

$D_{P,LT}(a,z,t_{Pb})$ = primary dose rate (r/hr) in the LTSF at a distance z from the LTSF source plate with a radius a (a = 35.5 cm),

$H(a,z)$ = transformation from the dose rate of a finite disc (radius a) source to that from an infinite plane source

[redacted]

[redacted]

$$= \frac{E_1(\mu z)}{E_1(\mu z) - E_1\left(\mu z \left[1 + \left(\frac{a}{z}\right)\right]^2\right)^{1/2}},$$

σ_R/σ_{LT} = ratio of reactor to LTSF source plate equivalent surface source strength for neutrons,

$$\sigma_R = \frac{P_R}{4\pi r_c^2},$$

P_R = reactor power (3×10^8 watts),

$$\sigma_{LT} = \frac{P_{LT}}{\pi a^2},$$

P_{LT} = LTSF source plate power (3.5 watts)*,

c_1 = change in attenuation due to replacing the 4-in.-thick test heat exchanger mockup with a particular reactor heat exchanger composition and thickness (based on exponential attenuation at 6.8 Mev),

c_2 = change in attenuation due to addition of small claddings, correct pressure shell thickness and composition, etc.,

$c_1 \times c_2$ = 0.460,

c_3 = change in attenuation due to substitution of alkylbenzene-350 at 330°F, assuming that $\mu_{alkyl} = 0.8\ \mu_{H_2O}$, based on electron density.

The determination of the primary gamma-ray heating in the lead was made in a slightly different manner. Since there were no LTSF curves of primary gamma-ray dose rate as a function of lead thickness, it was necessary to use the transformed LTSF curves mentioned above, i. e., plots of the primary gamma-ray heating in the reactor as a function of alkylbenzene thickness for various lead thicknesses. The lead thicknesses were 0, 1.5, 3, 4.5 and 6 in. By integrating over r from the lead surface to r = infinity, the total heating in the alkylbenzene behind 1.5 in. of lead was evaluated and subtracted from that behind no lead, giving the total amount of energy deposited in the first 1.5-in. thick lead layer in the reactor as follows:

---

*The latest calibration of the new LTSF source plate has yielded a value of 3.5 watts for the old source plate (see papers by W. J. McCool and D. R. Otis this report).

[redacted]

[redacted]

$$\overline{H_{Pb,P}(0 \leq t_{Pb} \leq 1.5 \text{ in.})}$$

$$= \frac{4\pi\rho_{alkyl}\int_{r_o}^{\infty} H_{alkyl,P}(t_{alkyl}, t_{Pb}=0)\, r^2 dr - 4\pi\rho_{alkyl}}{\frac{4\pi\rho_{Pb}}{3}} - - - \frac{\int_{r_o+1.5 \text{ in.}}^{\infty} H_{alkyl,P}(t_{alkyl}, t_{Pb}=1.5 \text{ in.})\, r^2 dr}{\left[(r_o + 1.5 \text{ in.})^3 - r_o^3\right]}$$

where

$\overline{H_{Pb,P}(0 \leq t_{Pb} \leq 1.5 \text{ in.})}$ = average heating due to primary gamma-ray sources in the first 1.5-in. thick lead layers (watts/g),

r_o = inside radius of lead (cm),

ρ_{Pb} = lead density (g/cm^3),

ρ_{alkyl} = alkylbenzene density (g/cm^3),

$H_{alkyl,P}(t_{alkyl}, t_{Pb})$ = heating in the alkylbenzene at a distance t_{alkyl} behind a thickness t_{Pb} of lead (watts/g).

Repeating this procedure for the other lead layers resulted in a histogram of primary gamma-ray heating in the lead. A smooth exponential curve was then fitted to the histogram.

[redacted]

[redacted]

FISSION-PRODUCT GAMMA-RAY HEATING

In the absence of any experimental data for the contribution of fission-product gamma rays from the heat exchanger region, it was necessary to calculate the heating from the fission-product gamma rays. The results of recent spectrometer measurements of fission product photons in the rotating belt experiment at the LTSF were used in the calculation.[1]

The general procedure followed was to evaluate the heating contribution from each of several energies and then to perform a numerical integration over the energy range. The energies chosen were 0.10, 0.25, 0.50, 1.0, 2.0, 3.0, 4.0, 6.0 Mev. The surface source strength (at the outer surface of the heat exchanger region) of photons of energy E was determined first. The energy deposited at a distance from an infinite plane with this source strength was then computed, after which a geometrical transformation was applied to convert to spherical geometry.

The choice of a buildup factor in determining the dose rate from an infinite plane was critical. The preponderance of Inconel between the heat exchanger and the lead suggested the use of the energy absorption buildup factor for nickel when the energy deposition at the inner surface of the lead was computed. (In the actual calculation, the buildup factor for iron was employed, since that for nickel was not available.) When the heating at a point a few mean free paths inside the lead was computed, however, the buildup factor for lead was used. The buildup factor for lead was also applied for the heating in the alkylbenzene at the last lead-alkylbenzene interface. Water buildup factors were employed for results at greater distances into the alkylbenzene.

The following expression was used in the calculation of the heating from the fission-product gamma rays in the heat exchanger:

$$H_{HX}(r) = \int_E H_{HX}(r,E)\, dE$$

where

$$H_{HX}(r,E) = \frac{\mu_a(E)}{\rho} \frac{r_{HX_o}}{r} \frac{S(E)}{2} B_a \left[\sum_i \mu_i(E)\, t_i\right] E_1\left[\sum_i u_i(E) t_i\right],$$

$\frac{\mu_a(E)}{\rho}$ = mass energy absorption coefficient for photons of energy E,

[redacted]

[redacted]

r_{HX_o} = outside radius of reactor heat exchanger (32.872 in.),

$$S(E) = K(E) \frac{P_o}{\mu(E)} L(E),$$

$$K(E) = EN_{fp}(E)\ 3.1 \times 10^{10} \text{ (fissions/sec)/watt},$$

$N_{fp}(E)$ = number of fission product photons emitted per fission per unit energy interval centered about the energy E,

$$P_o = \frac{P_R}{V_f} v_f,$$

P_R = reactor power (3×10^8 watts),

V_f = total fuel volume (20.11 cu ft),

v_f = volume fraction of fuel in heat exchanger (0.274),

$\mu(E)$ = total gamma-ray absorption coefficient for photons of energy E,

$$L(E) = 1 - \frac{r_{HX_i}}{r_{HX_o}} e^{-\mu(E)t_{HX}} + \frac{e^{-\mu(E)t_{HX}} - 1}{\mu_S(E)\ r_{HX_o}},$$

r_{HX_i} = inside radius of reactor heat exchanger (25.842 in.),

t_{HX} = heat exchanger thickness (7.03 in.),

$B_a\left[\sum_i \mu_i(E)t_i\right]$ = energy absorption buildup factor for energy E and $\sum_i \mu_i(E)t_i$ mean free paths,

$$E_1\left[\sum_i \mu_i(E)t_i\right] = \int_{\sum_i \mu_i(E)t_i}^{\infty} \frac{e^{-x}}{x}\, dx.$$

[redacted]

[redacted]

HEATING DUE TO THERMAL NEUTRON CAPTURES IN THE SHIELD

Heating in Lead by Capture Gamma Rays Produced in Lead. The heating in lead by secondary gamma rays resulting from thermal-neutron capture in the lead was calculated, using curves of the thermal-neutron flux in lead which were derived from Lid Tank curves of thermal flux in water behind various thicknesses of lead. The general method of calculation was to construct a series of spherical shells, concentric about the point at which the heating was being determined, and to sum up the contribution from each, calculated by means of the following expression:

$$H_{PB,S_1}(r) = K_2 E \, \Sigma_c \left(\frac{\mu_a}{\rho}\right)_{Pb} \int_{x_1}^{x_2} \int_{\theta_1}^{\theta_2} \phi(r') \, B(\mu x) \, \frac{e^{-\mu x}}{4\pi x^2} \, 2\pi x^2 \sin\theta \, d\theta \, dx$$

where

$H_{Pb,S_1}(r)$ = heating in the lead due to secondary gamma rays produced in the lead (watts/g),

$K_2 = 1.6 \times 10^{-13}$ watts/Mev/sec,

E = energy of lead capture gamma ray (7.4 Mev),

Σ_c = lead capture cross section,

μ_a/ρ = mass energy absorption coefficient,

$\phi(r')$ = thermal-neutron flux at point r' where capture occurs,

x = distance from point r' to point r where the capture gamma ray is absorbed.

Heating in Lead by Capture Gamma Rays Produced in Alkylbenzene. A rough determination was made for the heating in the lead resulting from absorption of hydrogen and boron capture gamma rays produced in the borated alkylbenzene. Heating contributions from several angles θ about the point of absorption were computed, enabling a curve of heating per unit angle vs angle to be drawn. An integration over θ then yielded the desired result. The equation employed was

[redacted]

[redacted]

$$H_{Pb,S_2}(r) = K_2 \Sigma_c \left(\frac{\mu_a}{\rho}\right)_{Pb} \int_0^{\pi/2} \int_{x_o}^{x_1} \phi(r') \, B(\mu x) \, \frac{e^{-\mu x}}{4\pi x^2} \, 2\pi x^2 \sin\theta \, d\theta \, dx$$

where

H_{Pb,S_2} = heating in lead due to secondary gamma rays produced in alkylbenzene (watts/g),

E = energy of boron or hydrogen capture gamma ray (0.5 or 2.2 Mev, respectively),

Σ_c = capture cross section for hydrogen or boron in alkylbenzene.

<u>Heating in Alkylbenzene by Capture Gamma Rays Produced in Lead and Alkylbenzene</u>. The analysis[1] of the LTSF measurements which gave the secondary gamma-ray dose rate in water beyond a CFRMR mockup was employed in calculating the secondary gamma-ray heating in the alkylbenzene. The secondaries consisted of capture gamma rays from lead and from the boron and hydrogen in the alkylbenzene. The heating was determined by means of the following expression:

$$H_{alkyl,\, S_3} = K_1 f_5 f_6 f_7 C_m \frac{r_c}{r} e^{-t_\ell/\lambda_\ell} H(a, z_{Pb})$$

where

H_{alkyl,S_3} = heating in alkylbenzene due to secondary gamma rays produced in lead and alkylbenzene (watts/g),

f_5 = dose rate (r/hr) in alkylbenzene from an infinite plane source of secondary gamma radiation having the same surface source strength as the LTSF CFRMR configuration containing 12 in. of beryllium and 4.5 in. of lead

$= D_{S,LT}(12 \text{ in. Be}, 4.5 \text{ in. Pb}, t_{alkyl}) \, H(a', t_{alkyl})$,

$$f_6 = \frac{D_{S,LT}(t_{Be}, t_{Pb}, t_{alkyl})}{D_{S,LT}(12 \text{ in. Be}, 4.5 \text{ in. Pb}, t_{alkyl})} \text{ (tabulated previously),}^2$$

f_7 = correction for the differences in composition and thickness between reactor and LTSF heat exchangers

[redacted]

[redacted]

$$= e^{-(\Sigma_{HX,R} - \Sigma_{HX,LT})10.16} - e^{-\Sigma_{HX,R}(t_{HX}-10.16)} ,$$

C_m = correction factor to account for small material differences between the LTSF and reactor,

t_ℓ = thickness of alkylbenzene cooling layers in the basic lead shield (cm),

λ_ℓ = neutron relaxation length in alkylbenzene cooling layers (determined to be approximately 6.0 cm),

$H(a,z_{Pb})$ = transformation from the neutron dose rate (at the lead surface) from a disc source (LTSF source plate) to the neutron dose rate from an infinite plane source, taken to be $1/(1 - e^{-84/z_{Pb}})$.

<u>Heating in Alkylbenzene by Alpha Particles Produced in Alkylbenzene.</u> In the calculation of the heating in the alkylbenzene resulting from 2.3-Mev alpha particle production by thermal-neutron capture by the boron, it was assumed that the alpha particle gave up all its energy at the point at which it was produced. The alpha heating in the alkylbenzene was determined by means of the following equation:

$$H_{alkyl,\alpha}(r,t_{Pb}) = \frac{\Sigma_c \phi_R(r,t_{Pb})}{\rho_{alkyl}} (2.3 \text{ Mev}) \left[1.60 \times 10^{-13} \text{ watts/(Mev/sec)} \right]$$

where

$H_{alkyl,\alpha}(r,t_{Pb})$ = heating in alkylbenzene due to alpha particles produced in the alkylbenzene (watts/g),

Σ_c = thermal-neutron capture cross section for boron in alkylbenzene,

$$\phi_R(r,t_{Pb}) = \phi_{LT}(z,t_{Pb})\, H(a,z)\, \frac{\sigma_R}{\sigma_{LT}} \frac{r_c}{r} e^{-t_\ell/\lambda_\ell} C_m f_7,$$

$\phi_{LT}(z,t_{Pb})$ = thermal-neutron flux in Lid Tank behind a thickness t_{Pb} of lead.

[redacted]

[redacted]

Table I.

Parameters of a 300-Mw Circulating-Fuel Reactor
Used in Gamma-Ray Heating Calculation

Reactor or Shield Region	Thickness (in.)	Radius (in.)
Beryllium island		6.700
Sodium passage	0.187	6.887
Inconel-X cladding	0.125	7.012
Core fuel region	5.988	13.000
Inconel-X cladding	0.156	13.156
Sodium passage	0.187	13.343
Beryllium reflector	11.887	25.230
Inconel-X cladding	0.010	25.240
Sodium passage	0.066	25.306
Inconel-X cladding	0.010	25.316
Boron 10	0.200	25.516
Inconel-X cladding	0.010	25.526
Sodium passage	0.066	25.592
Inconel-X cladding	0.250	25.842
Heat exchanger	7.030	32.872
Inconel-X cladding	0.125	32.997
Thermal shield	1.035	34.032
Pressure shell	1.000	35.032
Insulation	1.000	36.032
Insulation Inconel-X shell	0.032	36.064 (91.60 cm)
Alkylbenzene passage	0.375	36.439 (92.56 cm)
Lead	1.000	37.439 (95.10 cm)
Alkylbenzene passage	0.375	37.814 (96.05 cm)
Lead	1.76 (rear)	39.574 (100.52 cm)
	4.56 (front)	42.374 (107.63 cm)
Alkylbenzene	7.25 (rear)	46.824 (118.93 cm)
	14.10 (front)	56.474 (143.44 cm)

[redacted]

[redacted]

2-01-059-56

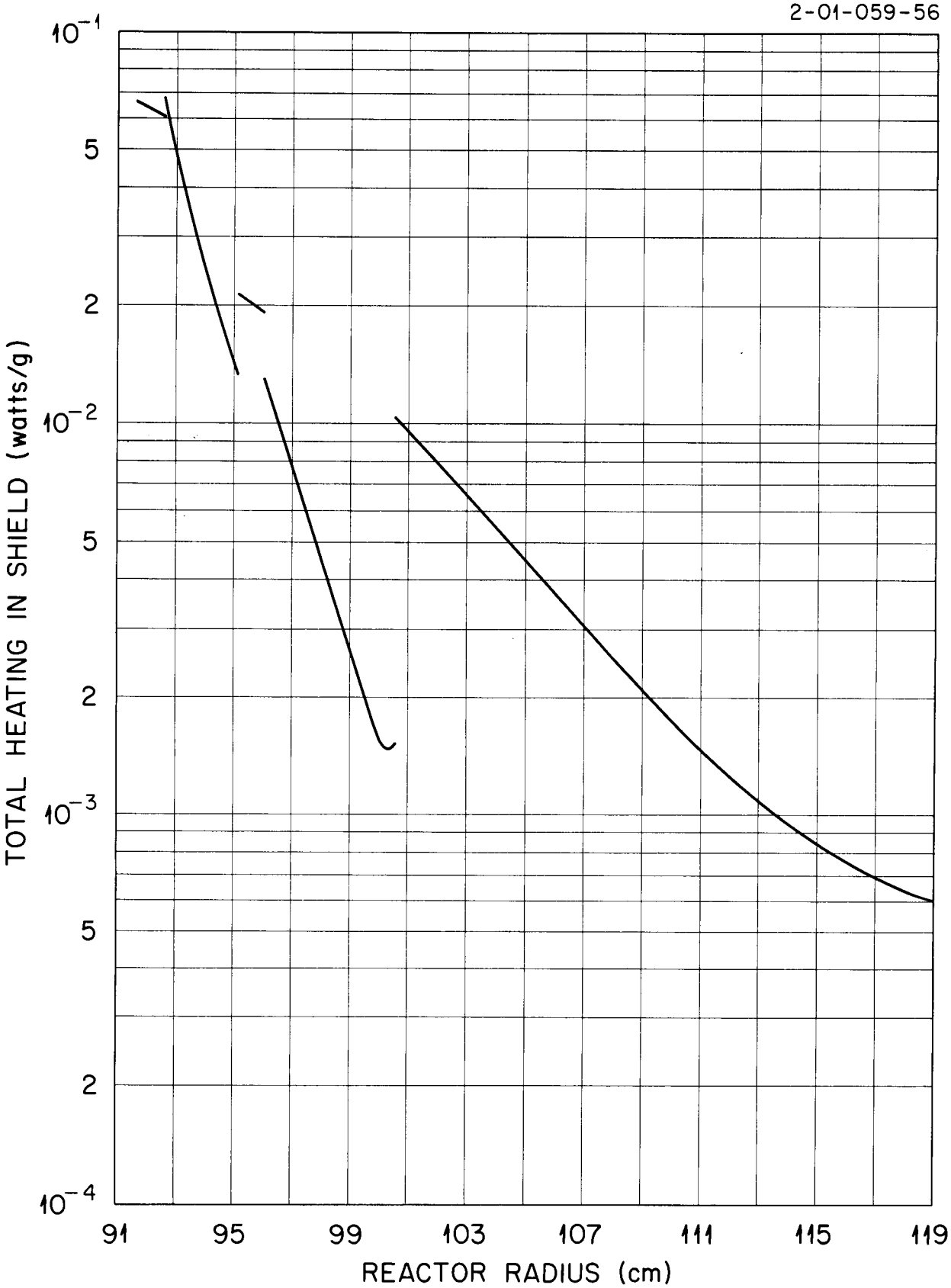

Fig. 1. Total Heating in Rear Portion of 300-Mw CFR Shield.

[redacted]

2-01-059-57

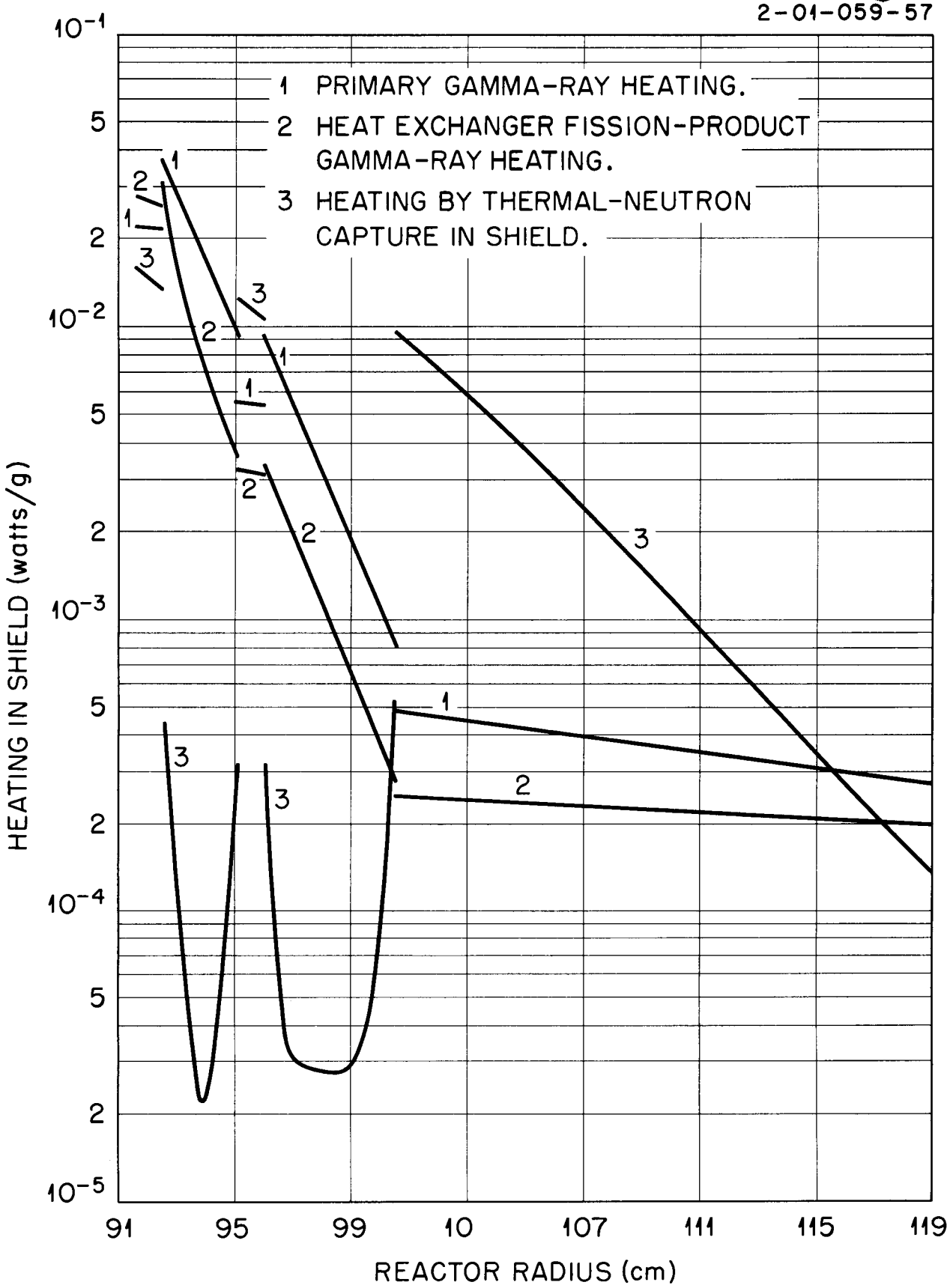

Fig. 2. Components of Total Heating in Rear Portion of 300-Mw CFR Shield.

[redacted]

2-01-059-58

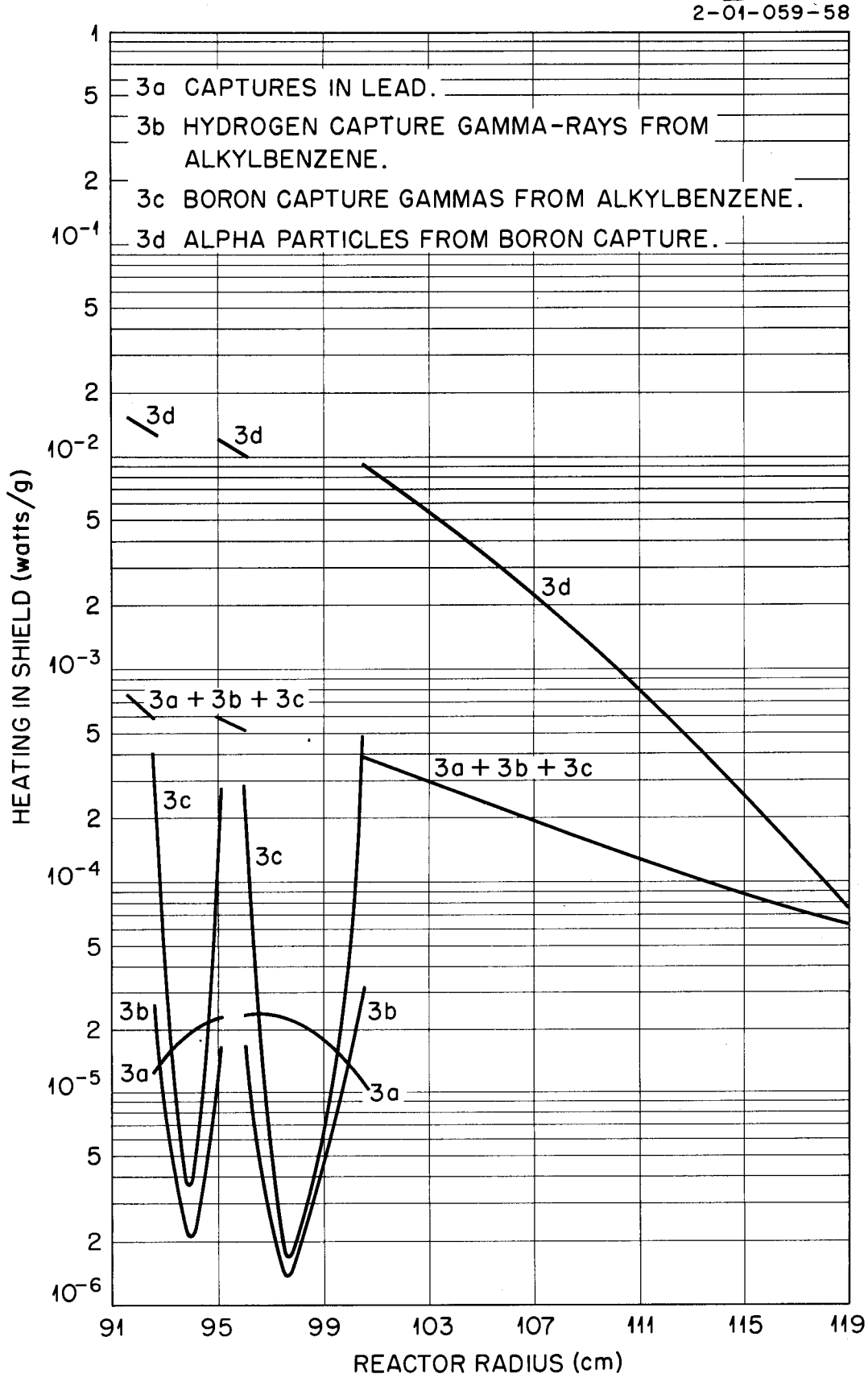

Fig. 3. Components of Heating Due to Thermal-Neutron Capture in Rear Portion of 300-Mw CFR Shield.

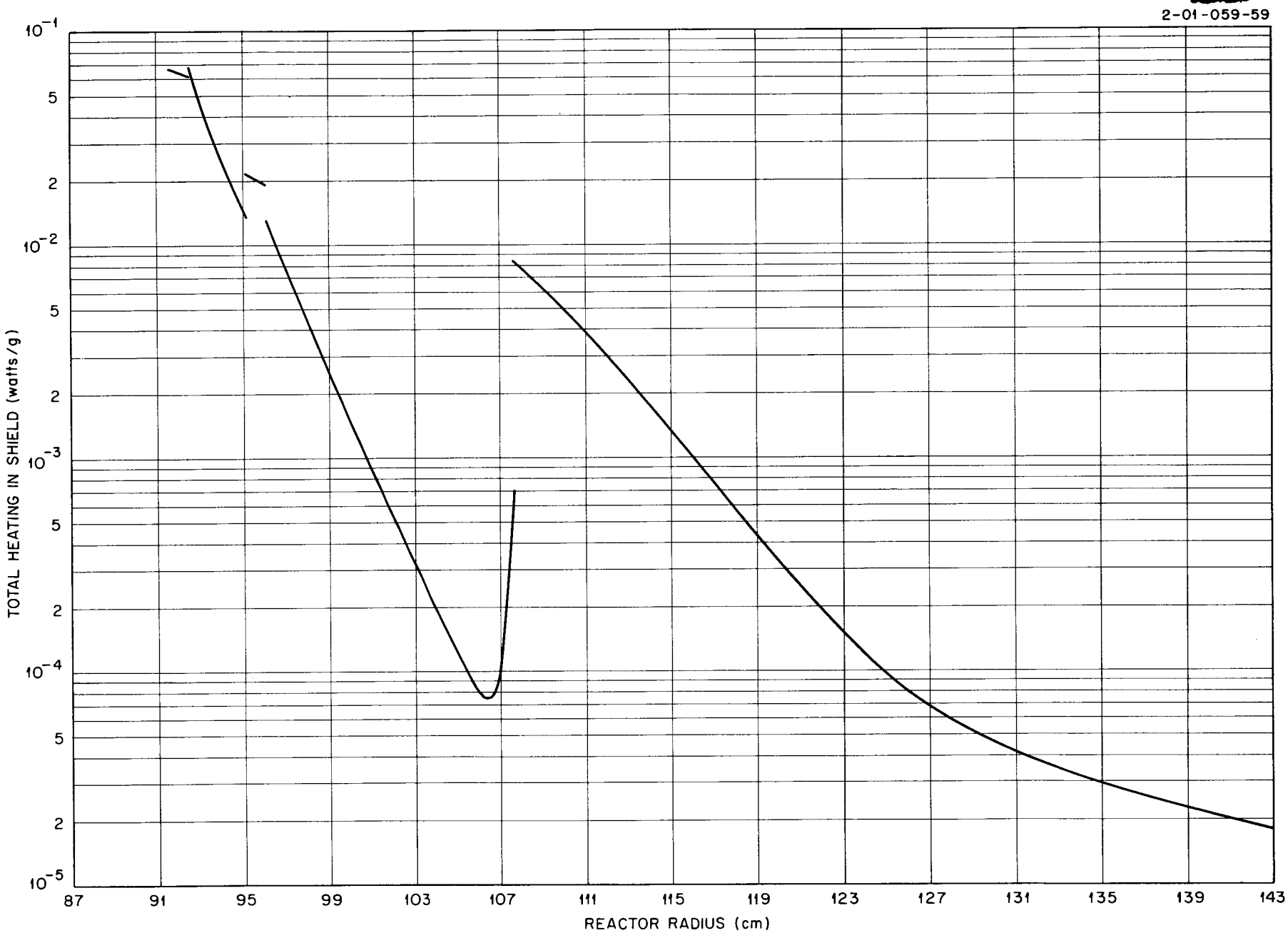

Fig. 4. Total Heating in Forward Portion of 300-Mw CFR Shield.

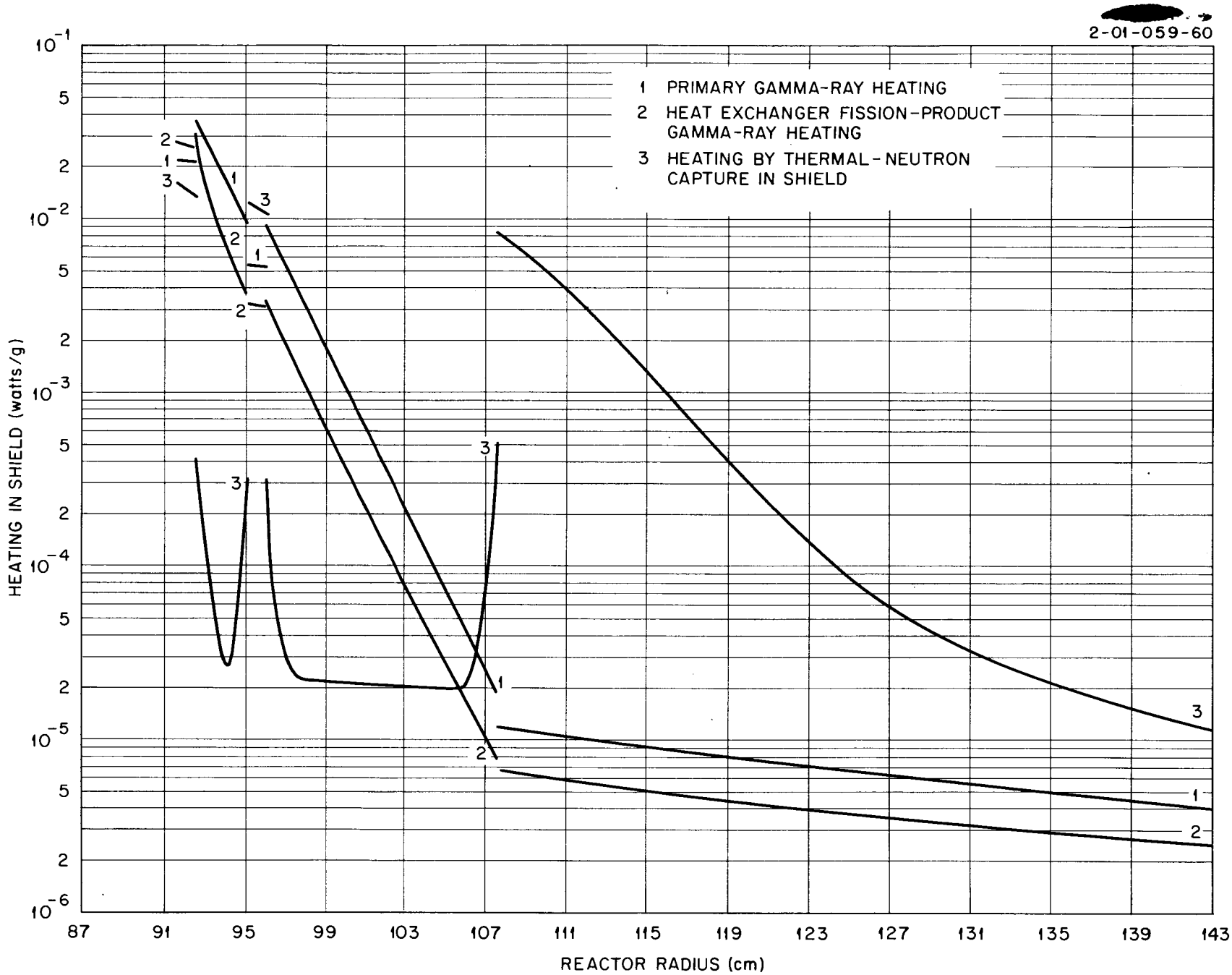

Fig. 5. Components of Total Heating in Forward Portion of 300-Mw CFR Shield.

[redacted]

2-01-059-61

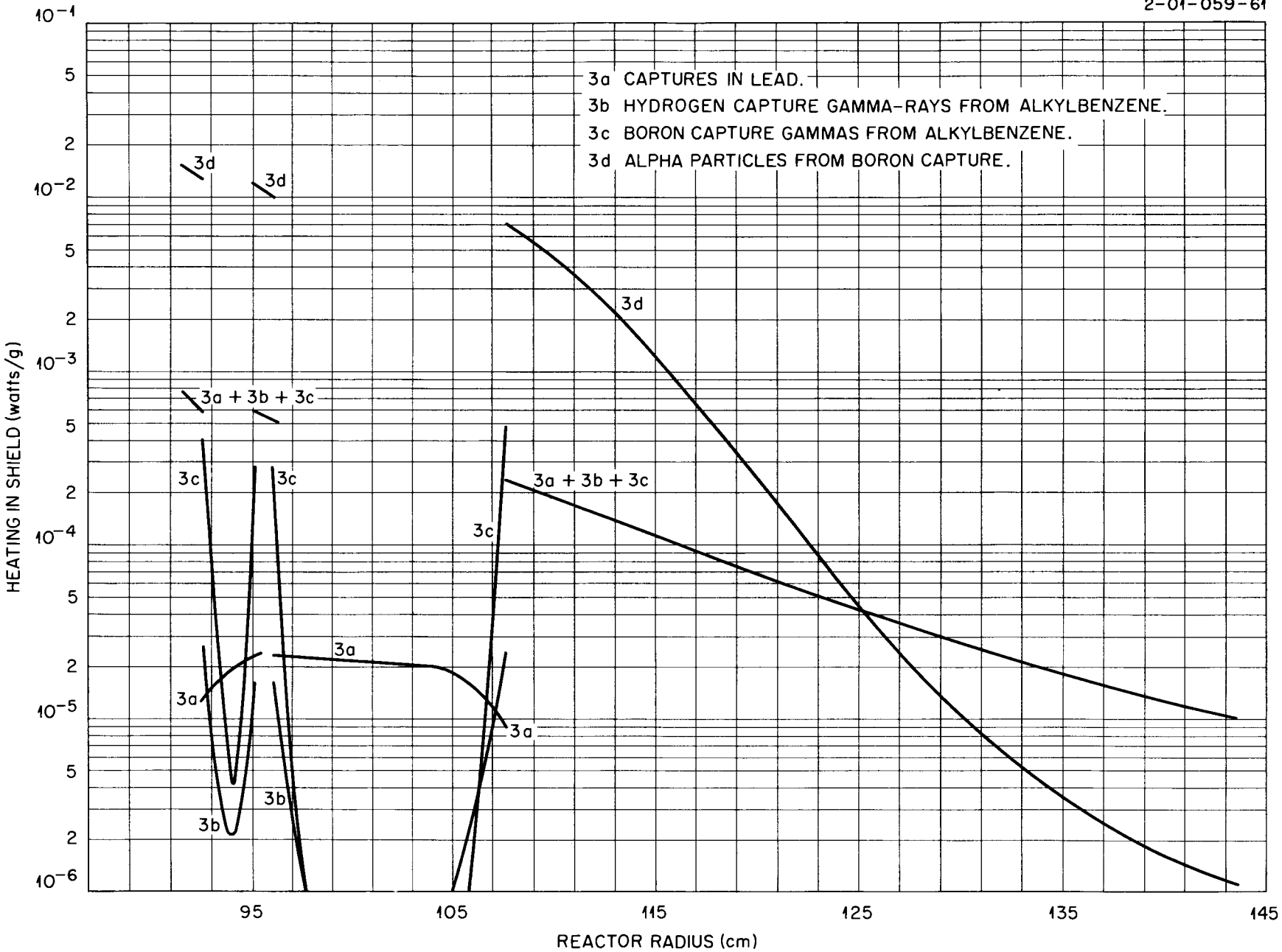

Fig. 6. Components of Heating Due to Thermal Neutron Capture in Forward Portion of 300-Mw CFR Shield.

[redacted]

REFERENCES

1. Peelle, R. W., *et al.*, *ANP Quarterly Progress Report*, December 10, 1955, ORNL-2012, p. 210.

2. Dee, J. B., *et al.*, *ANP Quarterly Progress Report*, December 10, 1955, ORNL-2012, Part IV, p. 28.

[redacted]

SECRET

Paper II-E

NEUTRON INDUCED GAMMA RADIATION*

T. S. Webb
Convair, Ft. Worth

*Published at Convair, Ft. Worth, as Report No. FZM-440.

SECRET

[redacted]

NEUTRON INDUCED GAMMA RADIATION
(Title Unclassified)

by

T. S. Webb

Convair, A Division of General Dynamics Corporation, Fort Worth, Texas

Approximate expressions for the calculation of neutron induced gamma ray dose rates are presented. Thermal and fast reactions in air are considered as well as effects of ground and crew shield captures. Calculated values of total theoretical dose rates are compared to experimental results and reasonable agreement is found in most cases.

INTRODUCTION

A number of recent experiments in the ANP program have indicated an inability in many cases to understand measured gamma ray dose rates in terms of single scattering theories. It is the purpose of the present paper to present several elementary considerations regarding the role of neutron-induced gamma rays in this connection.

To render the problems amenable to hand calculations, several oversimplifying assumptions have been made. While it is true that these seriously affect the quantitative results, it is still believed that the numbers are sufficiently meaningful to allow qualitative conclusions to be drawn regarding the importance of the various contributing effects. This will, of course, allow one to select for further study the more important phenomena in any given case.

The considerations are divided into five main parts: (1) radiative capture of virgin "thermal" neutrons in air, (2) inelastic scattering and reactions of "fast" neutrons in air, (3) "thermal" capture of degraded "fast" and "epithermal" neutrons in air, (4) ground effects, and (5) crew compartment effects.

AEC-3314-CVAC

[redacted]

ATOMIC ENERGY ACT - 1954

[redacted]

PROCEDURE

We consider a point source S and unshielded detector D, each at a height h above the ground, separated by a distance a. The source is assumed to emit S_F, S_E, and S_T "fast", "epi-thermal", and "thermal" neutrons per second, respectively. The definition of these components is somewhat arbitrary, but may be given roughly in terms of the actual source spectrum S(E) as:

$$S_T = E_t^{\frac{1}{2}} \int_0^{\infty} \frac{S(E)dE}{E^{\frac{1}{2}}}$$

$$S_E = \int_{E_2}^{E_3} S(E)dE$$

$$S_F = \int_{E_3}^{\infty} S(E)dE$$

In these expressions E_t is the thermal neutron energy, E_3 is roughly 300 Kev, and E_2 is the order of 1 ev.

For the calculations of the air effects h is assumed to be infinite, giving the geometry shown:

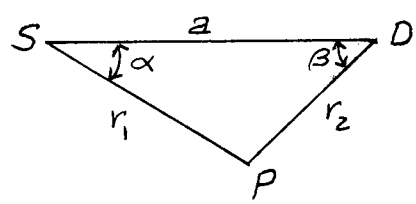

The contribution of virgin "thermal" captures is estimated by assuming that the flux at P is $S_T/4\pi r_1^2$ so that the number of radiative captures per unit volume about P is $\Sigma_c S_T/4\pi r_1^2$ where Σ_C is the macroscopic thermal radiative capture cross section in air. The gamma dose rate at D will thus be, approximately,

$$D(t.c.) = \int_V \frac{\nu \Sigma_c S_T}{16\pi^2 f_c} \frac{dV}{r_1^2 r_2^2}$$

where f_c is the appropriate flux to dose conversion factor, and ν is the number of photons per capture. The volume integral may be easily evaluated in the α, β coordinate system, thus:

[redacted]

ATOMIC ENERGY ACT - 1954

[redacted]

$$D(t.c.) = \int_0^{\pi}\int_0^{\infty} \frac{\nu S_T \Sigma_c}{16\pi^2 f_c} \frac{2\pi r_1^2 \sin\alpha \, d\alpha \, dr_1}{r_1^2 \, r_2^2} =$$

$$\frac{\nu \Sigma_c S_T}{8\pi a} \int_0^{\pi}\int_0^{\pi-\beta} d\alpha \, d\beta = \frac{\pi \nu \Sigma_c S_T}{16 a f_c}$$

These captures will occur predominantly in N^{14} whose radiative capture cross section we assume to be 0.10 barn with 1.7 photons (6 Mev) per capture.(1) For this energy f_c is approximately 1.5 X 10^5 photons/cm^2-sec per rem/hr. Using these values,

$$D(t.c.) = 8.8 \times 10^{-12} \frac{S_T}{a} \text{ rem/hr.}$$

with S_T in neutrons per sec and a in cm.

If the diffusion theory expression for the thermal flux $S_T e^{-Kr_1}/4\pi D r_1$, is used, the result is;

$$D(t.c.) = \frac{\nu \Sigma_c S_T}{8\pi a K D}\left[e^{Ka} E_1(Ka) + e^{-Ka} \overline{E_i}(Ka)\right],$$

where K is the reciprocal of the diffusion length, D is the diffusion coefficient,

$$E_1(x) = \int_x^{\infty} \frac{e^{-t}}{t} dt, \quad x > 0,$$

and $\overline{E_i}(x)$ is the negative of the principal value of $E_1(X)$ for $X < 0$. In the primary range of interest (25-200 feet) the two expressions for D(t.c.) differ by less than 25%, and the former expression has therefore been used for simplicity.

The effects of anisotropic source terms and gamma air attenuation have been investigated by R. L. French, D. L. Smith, J. E. Ward, et. al. In all cases considered these modifications have affected the results by less than a factor of two.

An estimate of the "fast" effects may also be made by using the above argument. We replace S_T by S_F, $\nu\Sigma_c$ by Σ_γ where Σ_γ is the average cross section for gamma production, and f_C by f_γ where f_γ is the appropriate flux to dose factor. The data on "fast" reactions in N^{14} and O^{16} indicates that the principal effect will be inelastic scattering in the former. From the measured(1) cross section at 14 Mev, 0.48

[redacted]

ATOMIC ENERGY ACT - 1954

[redacted]

barns, it would seem reasonable to take an average of the order of 0.2 barns with about 1.5 two Mev photons per reaction. These values are estimated on the basis of a water moderated ($\sim$ 20 cm) spectrum and represent only a rough guess. On this basis $f_C = 4.5 \times 10^5$ and,

$$D(F) = 5.2 \times 10^{-12} \frac{S_F}{a} \text{ rem/hr.}$$

For the contribution from degraded "fast" and "epithermal" neutrons, we consider the Fermi age expression for the slowing down density q, at a distance r_1 from a monoenergetic source of strength S,

$$q = \frac{S e^{-r_1^2/4\tau}}{(4\pi\tau)^{3/2}}$$

where τ is the neutron age. If the age to thermal is somewhat larger than the thermal diffusion length, then it is a fair approximation to assume that all neutrons are captured at the point of thermalization. Thus, the number of radiative captures per unit volume is approximately $(\Sigma_c/\Sigma_a)\, q_t$, where Σ_a is the total thermal capture cross section, q_t is the slowing down density evaluated at an energy just above the "thermal" range. This will give a gamma dose rate at the detector,

$$D(f.c.) = \frac{\Sigma_c S}{f_c \Sigma_a (4\pi\tau)^{3/2}} \int_0^\infty e^{-r_2^2/4\tau} dr_2 = \frac{\Sigma_c S}{\Sigma_c 8\pi\tau f_c}$$

The integral may be evaluated approximately by observing that, if $\tau^{1/2} \gg a, r_1^2$ may be replaced by r_2^2 in the exponential. This may be seen by noting that for small r_1 and r_2 the exponential is approximately unity, and in the region where it differs from unity (i.e., large r_1) $r_1 \cong r_2$. Using this approximation,

$$D(f.c.) = \frac{\Sigma_c S}{f_c \Sigma_a (4\pi\tau)^{3/2}} \int_0^\infty e^{-r_2^2/4\tau} dr_2$$

$$= \frac{\Sigma_c S}{\Sigma_a 8\pi\tau f_c}$$

[redacted]

[redacted]
ATOMIC ENERGY ACT - 1954

[redacted]

Applying this result separately to the "fast" and "epi-thermal" source neutrons with $\Sigma_c / \Sigma_a = 0.057$,

$$D(f.c.) = 1.5 \times 10^{-8} \left[\frac{S_F}{\tau_F} + \frac{S_E}{\tau_E} \right]$$

For τ_F and τ_E we use 4×10^8 and 4×10^7 cm^2, corresponding to initial source energies of the order of kev and ev, respectively. Therefore,

$$D \doteq 3.8 \times 10^{-16} \left(\frac{S_F}{10} + S_E \right)$$

In treating the contribution due to ground captures all neutrons incident on the ground are assumed to be "thermal." This is a fair approximation in cases where the "thermal" source term is somewhat larger than the "fast" and "epi-thermal" source terms since the greater penetration of the more energetic components will tend to compensate for the "fast" neutron effects (inelastic scattering, etc.).

Using the previous notation we consider the following geometry:

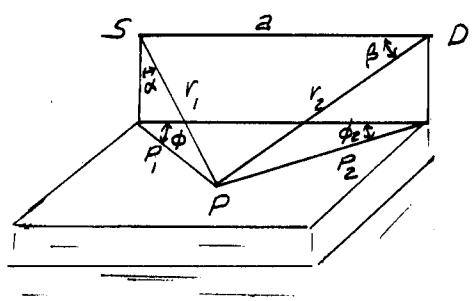

The incident neutron current into the area dA at the point P is assumed to be $J_0 = S \cos\alpha \, dA / 4\pi r_1^2$, where $S = S_T + S_E + S_F$. The diffusion theory expression for the neutron flux at a depth "z", $\phi(z) = 4 J_0 e^{-Kz} / 1 + 2KD$, is used to obtain the number of gammas produced per unit volume at (P, Z), $\nu \Sigma_c \phi(z)$. In these expressions K is the reciprocal of the thermal neutron diffusion length, D is the diffusion coefficient, Σ_c is the radiative capture cross section, and ν is the number of photons per capture, all corresponding

[redacted]

AEC-3314-CVAC
[redacted]
ATOMIC ENERGY ACT - 1954

[redacted]

to the ground material. If μ is the gamma absorption coefficient in the ground and f_g the flux to dose conversion factor, then the dose rate at D is approximately,

$$D(g.c.) = \int_A \int_{z=0}^{\infty} \frac{4\Sigma_c S \nu}{16\pi^2 f_g (1+2\kappa a)} \frac{e^{-\mu z/\cos\psi}}{r_2^2 r_1^2} \, dA \, dz$$

Evaluating the integral over z, defining $\beta = \mu/\kappa$, and noting $\cos\psi = h/r_2$:

$$D(g.c.) = \frac{\Sigma_c S \nu}{4\pi^2 f_g \kappa (1+2\kappa D)} \int \frac{1}{r_1^2 r_2^2} \frac{1}{1+\frac{\beta r_2}{h}} \, dA$$

Using $dS = \rho_2 \, d\rho_2 \, d\phi_2 = r_2 \, dr_2 \, d\phi_2$, and defining $x_1 h = r_1$, $x_2 h = r_2$, we have:

$$x_1^2 = x_2^2 + (a/h)^2 - (2a/h)(x_2^2 - 1)^{1/2} \cos\phi_2 ,$$

$$D(g.c.) = \frac{\nu \Sigma_c S}{4\pi^2 f_g \kappa (1+2\kappa D)} \int_1^{\infty} \int_0^{2\pi} \frac{dx_2 \, d\phi_2}{x_1^3 x_2 (1+\beta x_2)}$$

The integral over ϕ_2 is evaluated by using:

$$\int_0^{\pi} \frac{d\phi}{(a - b\cos\phi)^{3/2}} = \frac{2E\left[\left(\frac{2b}{a+b}\right)^{1/2}\right]}{(a-b)(a+b)^{1/2}}$$

$$E(k) = \int_0^{\pi/2} (1 - k^2 \sin^2 t)^{1/2} \, dt$$

The integral over x_2 may then be evaluated numerically.

For all calculations the ground material has been concrete for which we have used:

$\Sigma_c = 0.01$ cm^{-1}	$K = 0.1$ cm^{-1}
$\nu = 1.9$ gammas per capture (3.5 Mev)	$D = 1.0$ cm
$\mu = 0.1$ cm^{-1}	$f_g = 2.6 \times 10^5$ photons/cm^2-sec per rem/hr.

[redacted]

ATOMIC ENERGY ACT - 1954

[redacted]

Thus:

$$D(g.c.) = 1.5 \times 10^{-8} \frac{S}{h^2} \int_1^{\infty} \int_0^{2\pi} \frac{dx_2 \, d\phi_2}{x_1^3 x_2 (1 + x_2)}$$

A calculation of D(g.c.) using the "first collision source" diffusion theory expression for the neutron flux in the ground has also been performed for one case by D. L. Smith, et. al. The calculated dose rate was lower than given by the original expression by somewhat less than a factor of two.

To estimate the variation of the ground capture contribution with altitude, calculations have been made to determine the dose rate as a function of h for a = 66.5 feet. These results are shown in Figure 1. Due to the effect of multiple scattered neutrons, the ground capture expression (which predicts zero dose rate at h = 0) is probably not very accurate for small elevations, and rough calculations indicate that the variation with h is not large for h small. The results in Figure 1 are normalized to the predicted maximum which occurs at about 25 feet.

A crude estimate of the effect of captures in a crew shield may be made by assuming that $\pi r^2 S / 4\pi a^2$ neutrons per sec are captured in the crew shield whose average radius is R. If we denote by p the fraction of these which are radiative captures, by f_S the flux to dose conversion factor, and by A_S the average attenuation in the crew shield, the dose rate is, approximately,

$$D(c.s.) = \frac{pS}{16\pi a^2 f_s} (1 - A_s)$$

A detailed calculation of the crew shield contribution in one case has been made by B. T. Kimura using diffusion theory results for the thermal flux in the shield. The result of this calculation was in good agreement with the above expression using p = 1/12, $f_S = 4.5 \times 10^5$, and $A_S = 0.70$. The values for p and A_S were determined by considering only captures in hydrogen in the (borated) crew shield.

[redacted]

[redacted]
ATOMIC ENERGY ACT - 1954

[redacted]

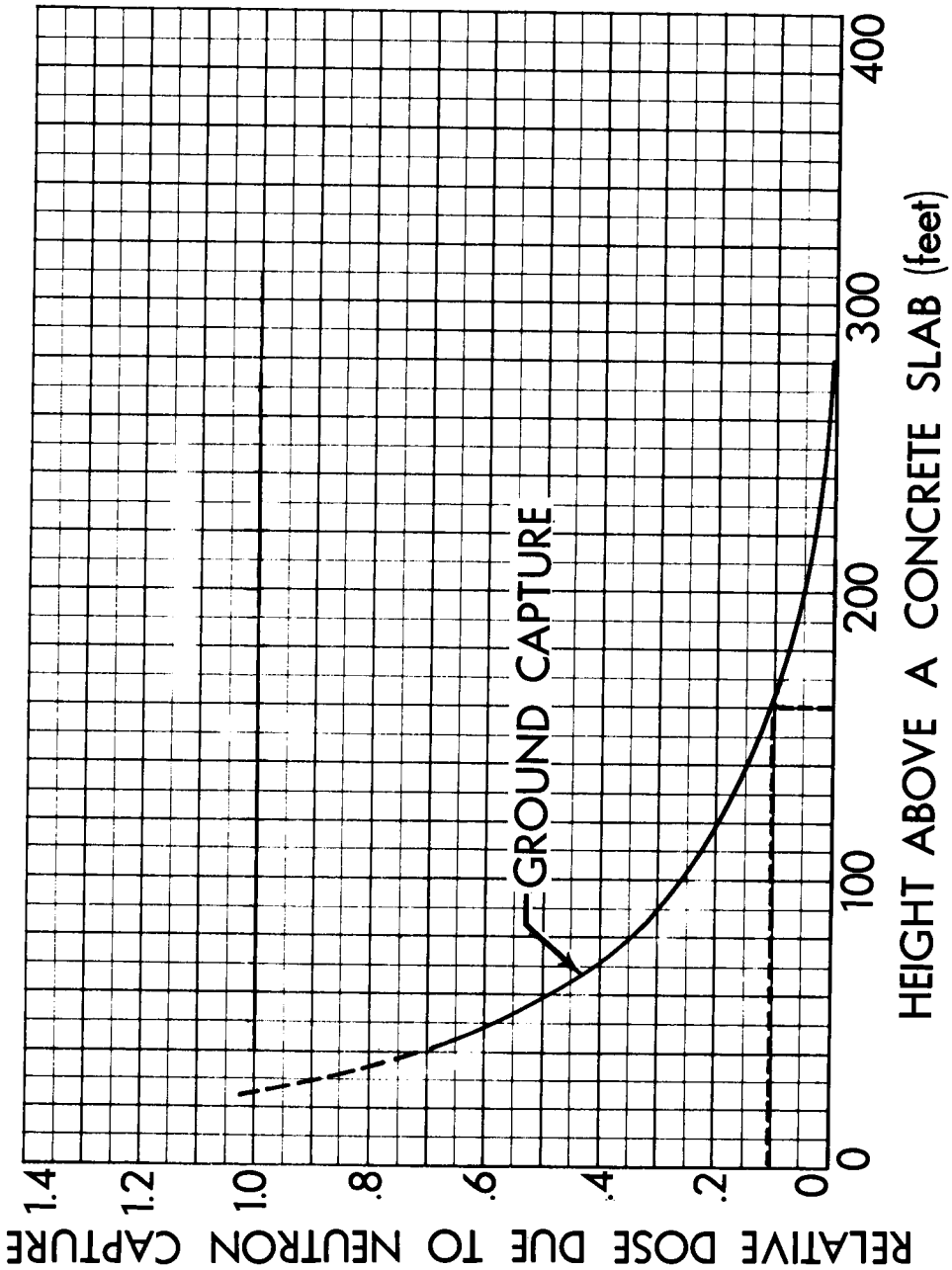

FIGURE 1. Relative Gamma Dose Rates Due to Neutron Capture

[redacted]

AEC-3314-CVAC
[redacted]
ATOMIC ENERGY ACT - 1954

[redacted]

COMPARISON WITH EXPERIMENTAL RESULTS

To illustrate the size of the various components considered above, values of the calculated dose rates for several Airborne Shield Test Reactor (ASTR) and Ground Test Reactor (GTR) experiments are given in Table I, together with measured values of the total gamma dose rates. Values calculated from ground and air single scattering theories are also given in several cases. For the dose rates inside the crew shield, attenuations have been estimated from single scattering calculations. The attenuation factors used were 0.60 for air capture gammas, 0.70 for ground capture gammas, and 0.80 for the inelastic gammas.

Source terms are given in the table for each configuration. The "fast" source terms were estimated from fast neutron dose measurements and the "thermal" from BF_3 measurements for the ASTR configurations and from BSF centerline data for the GTR. The "epi-thermal" source term is taken to be twice the "fast". The source-detector elevation (h) is 12.5 feet in all cases and the separation (a) is given for each situation. A description of the ASTR configurations is given in Reference 2.

DISCUSSION

The results given in Table I are typical of the agreement obtained in all situations examined with the exception of ASTR configuration 4. The results in this case are in poor agreement with experiment, and this is probably due to the large asymmetry of that configuration.

The general agreement would strongly indicate that the effect of neutrons is of considerable importance in many of the experimental situations. It is, of course, also true that the errors introduced by the approximations as well as the uncertainties in the cross sections and "source terms" do not allow us to exclude other contributing factors.

There are several obvious refinements which might be made in the above calculations. Among these are: (1) a more adequate treatment of the virgin thermal flux in the air either theoretically or by fitting to experimental measurements, (2) better treatment of the thermal flux in the ground, e.g., by using a first collision source, (3) improvement of the treatment of the "fast" and "epi-thermal" contributions which would involve more detailed spectral knowledge, and (4) more precise determination of crew shield attenuation. In addition to the calculational improvements there exist many uncertainties in the neutron cross sections involved and these, of course, can ultimately limit the accuracy of all calculations.

[redacted]

[redacted]
ATOMIC ENERGY ACT - 1954

TABLE 1

SUMMARY OF NEUTRON-INDUCED GAMMA ANALYSIS

Reactor	Crew Shield	a (ft)	S_T at 50' n's/sec	S_F at 50' n's/sec	Dose Rate (micro rep/hr-watt)							
					D_{gc}	D_{tc}	D_{fc}	D_f	D_{cs}	D_{ss}	D_{th}	D_{exp}
ASTR-3	Small Cyl.	66.5	3.0×10^7	3.3×10^6	0.054	0.052	0.0008	0.001	0.011	0.001	0.12	0.021
ASTR-5	Engineered	66.5	1.0×10^9	3.6×10^8	1.8	1.72	0.095	0.19	0.56	0.005	4.4	1.66
GTR	Engineered	66.5	3.0×10^9	2.9×10^8	5.4	5.2	0.075	0.15	1.04	3.0	15	13.2
ASTR-3	None	66.5	3.0×10^7	3.3×10^6	0.18	0.13	0.0024	0.008	----	0.64	0.96	1.02
ASTR-5	None	66.5	1.0×10^9	3.6×10^8	6.0	4.3	0.23	0.925	----	1.8	13.3	12.8
GTR	None	66.5	3.0×10^9	2.9×10^8	18	13	0.19	0.75	----	310	340	400
ASTR-3	None	30	3.0×10^7	3.3×10^6	0.90	0.29	0.0024	0.019	----	2.2	3.4	3.8
ASTR-5	None	30	1.0×10^9	3.6×10^8	30	9.6	0.23	2.05	----	6.1	48	40

AEC-3314-CVAC
ATOMIC ENERGY ACT -- 1954

[redacted]

REFERENCES

1. Ajzenberg and Lauritsen, Rev. Mod. Phys. pp. 27, 77 (1955).

2. C. E. Humphries, ASTR Mapping Prediction, Talk Presented at ANP Shielding Meeting, Oak Ridge, Tenn. (7-8 May 1956).

[redacted]

[redacted]
ATOMIC ENERGY ACT--1954

[redacted]

Paper II-F

MODIFICATION OF ALBERT-WELTON POINT KERNEL

F. A. Aschenbrenner
General Electric Company - ANP Dept.
Evendale

[redacted]

[redacted]

THIS DOCUMENT CONTAINS INFORMATION AFFECTING THE NATIONAL DEFENSE OF THE UNITED STATES WITHIN THE MEANING OF THE ESPIONAGE LAWS, TITLE 18 U. S. C., SECTIONS 793 AND 794. ITS TRANSMISSION OR THE REVELATION OF ITS CONTENTS IN ANY MANNER TO AN UNAUTHORIZED PERSON IS PROHIBITED BY LAW.

MODIFICATION OF ALBERT-WELTON POINT KERNEL

by

F. A. Aschenbrenner

General Electric Company - Aircraft Nuclear Propulsion Dept.
Evendale, Ohio

A modification of the Albert-Welton point kernel is described which gives good results for calculating fast neutron dose rates in water around the ORNL - Bulk Shielding Facility Reactor using an oxygen removal cross section of 0.99 barns. This modification is a result of assuming that 81% of the hydrogen collisions result in removal of the neutrons. Albert and Welton in their derivation of the point kernel assumed that all hydrogen collisions resulted in removal of the neutrons.

MODIFICATION OF ALBERT-WELTON POINT KERNEL

Fast neutron dose rates in hydrogenous media around reactor sources are presently calculated using what is called a point kernel technique.[1] This technique utilizes the assumption that the reactor consists of a volume distribution of point sources. The technique consists of summing up the calculated contribution of each of the point sources to obtain the total dose rate at each point. The function which describes the attenuation of the radiation from each of the point sources is called the point kernel.

Excellent results have been obtained using the Albert-Welton Point Kernel for calculating fast neutron dose rates in water around the ORNL-Bulk Shielding Facility Reactor (See Figure 2) To obtain these results it was necessary to use an oxygen removal cross section of 0.7 barns instead of the 0.99 barns which was measured at the ORNL-Liquid Tank Shielding Facility.[2] It is considered desirable to use a point kernel which will not only give good results for calculating the dose rates around the BSF reactor but will also utilize the 0.99 barns for the oxygen removal cross section. This point kernel should also give good results for calculating dose rates around other sources, as for example the ORNL-Liquid Tank Source Plate.

A point kernel has been obtained which gives even better results for calculating dose rates around the BSF reactor, using the 0.99 barns for the oxygen removal cross section, than was obtained with the original Albert-Welton Point Kernel.[3] This point kernel was obtained by modifying one of the assumptions used in deriving the original Albert-Welton Point Kernel. This modification will be discussed here. The Albert-Welton point kernel can be written as,

$D(r)=N(r)/4\pi r^2$ where $D(r)$ is the dose rate at a distance r and $N(r)$ has the form shown in Figure 1. The symbols in Figure 1 are defined as follows:

θ - volume fraction of water
Σ_0 - macroscopic oxygen removal cross section
a_1, a_2, a_3, a_4 - constants derived from theory and comparison to experimental data.

Albert and Welton derived the function $N(x)$ by integrating over neutron energy the product of the probability of emission from the source (the fission spectrum) times the probability of penetration in the hydrogenous shielding medium.[4] Several

[redacted]

[redacted]

$$N(x) = \alpha_1 (\theta x)^{\alpha_2} \, \varepsilon^{-\alpha_3 (\theta x)^{\alpha_4}} \, \varepsilon^{-\Sigma_0 (\theta x)}$$

OLD CONSTANTS	NEW CONSTANTS
$\alpha_1 = 1.013 \times 10^{10}$	$\alpha_1 = 7.29 \times 10^{9}$
$\alpha_2 = 0.29$	$\alpha_2 = 0.29$
$\alpha_3 = 0.928$	$\alpha_3 = 0.830$
$\alpha_4 = 0.58$	$\alpha_4 = 0.58$
$\Sigma_0 = 0.0234$	$\Sigma_0 = 0.0331$

FIGURE 1

[redacted]

[redacted]

simplifying assumptions were made in the derivation. These are:

1. The fission spectrum can be represented by $AE^{-0.72E}$ which is a good approximation only in the energy range of 2 to 12 mev. A more exact expression is $B \sinh \sqrt{2E}\, e^{-E}$.

2. Every neutron collision with a hydrogen nucleus results in removal of the neutron. Therefore, the total hydrogen cross section is used for calculating the probability of penetration. This cross section was approximated by $\sigma_H = 5.13\ E^{-0.725}$ barns.

3. The probability of neutron removal due to a collision with a non-hydrogen nucleus is independent of energy, i.e. the effect of non-hydrogen nuclei can be represented by constants called effective neutron removal cross sections.

A good fit with BSF centerline water data was obtained, as published in the Reactor Handbook, by using an oxygen removal cross section of 0.7 barns. However, to obtain an equally good fit with the Lid Tank Centerline water data it was necessary to assume an oxygen removal cross section of 0.91 barns. The fitting was done in both cases by a geometry transformation which transformed the data to the case of a plane - collimated fission source. As was previously pointed out, a later measurement at the Lid Tank indicated that the oxygen removal cross section should be 0.99 barns.

The constants listed in Figure 1 as old constants were those used in calculating the curve shown in Figure 2. The constants a_2, a_3 and a_4 were evaluated by Albert and Welton directly from the theoretical calculations. However, a_1 and Σ_o were determined by fitting the data. The value of Σ_o shown corresponds to an oxygen removal cross section of 0.7 barns. The calculations used for determining the curve in Figure 2 consisted of an actual integration over the source volume and included the effect of the reactor materials.

It is obvious that if a good fit to the BSF data is obtained with an oxygen removal cross section of .99 barns, then it is necessary to modify the assumption that every hydrogen collision results in removal. By a trial and error process it was determined that if it is assumed that only 81% of the hydrogen collisions result in removal of the neutrons then a good fit can be obtained using an oxygen removal cross section of .99 barns. The constants listed in Figure 1 as new constants were derived with the new assumption. The constant a_1, was again derived by fitting the dat , however, a_2, a_3 and a_4 were evaluated directly from the theoretical calculations. The value of Σ_o shown corresponds to an oxygen removal cross section of 0.99 barns.

Calculations with the modified point kernel are compared with BSF Centerline water data in Figure 3. No deviation from the data is observed for distances greater than 10 cm from the reactor surface. The deviation for distances less than 10 cm is believed to be due to the calculational procedure which consisted of dividing the reactor into a finite number of point sources.

The differential scattering cross section and energy change for neutron and proton scattering in the laboratory system was examined to determine the validity of assuming that only 81% of the hydrogen collisions result in removal of the neutrons. The ratio of the differential scattering cross section in the laboratory system to that in the center mass system was calculated to be proportional to $\cos\theta$ where θ is the scattering angle in the laboratory system (See Figure 4).

[redacted]

[redacted]

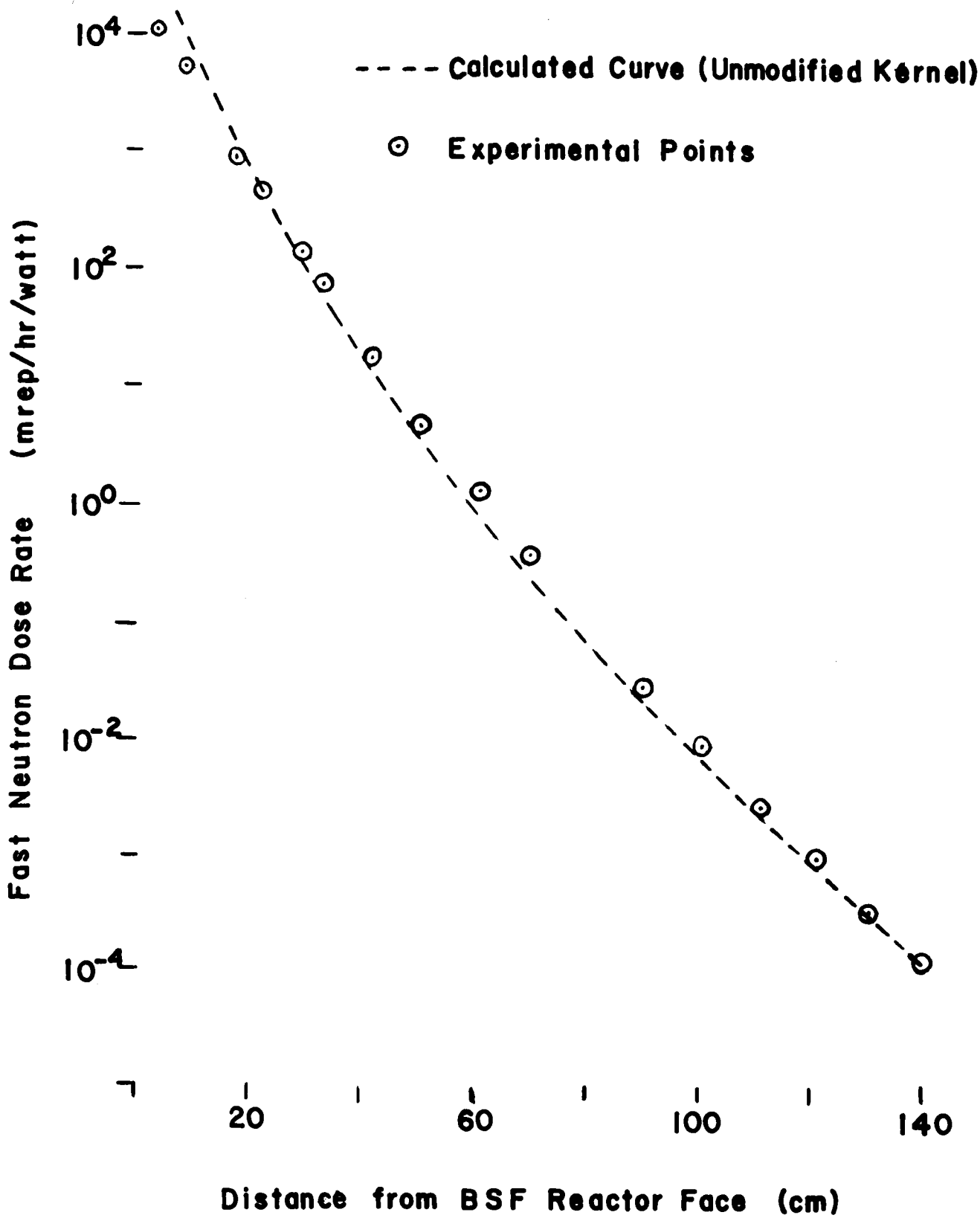

[redacted]

FIGURE 2

[redacted]

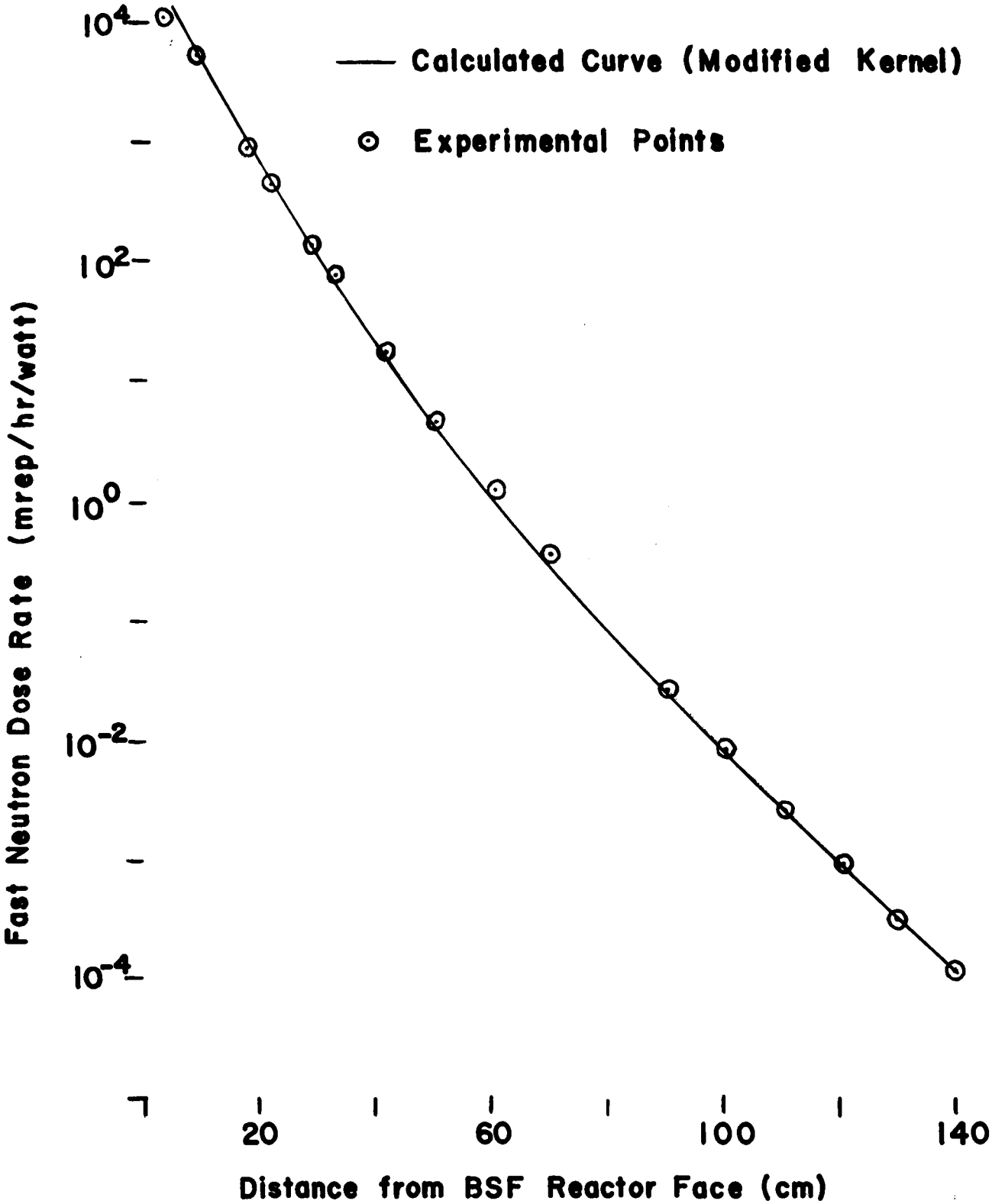

[redacted]

FIGURE 3

[redacted]

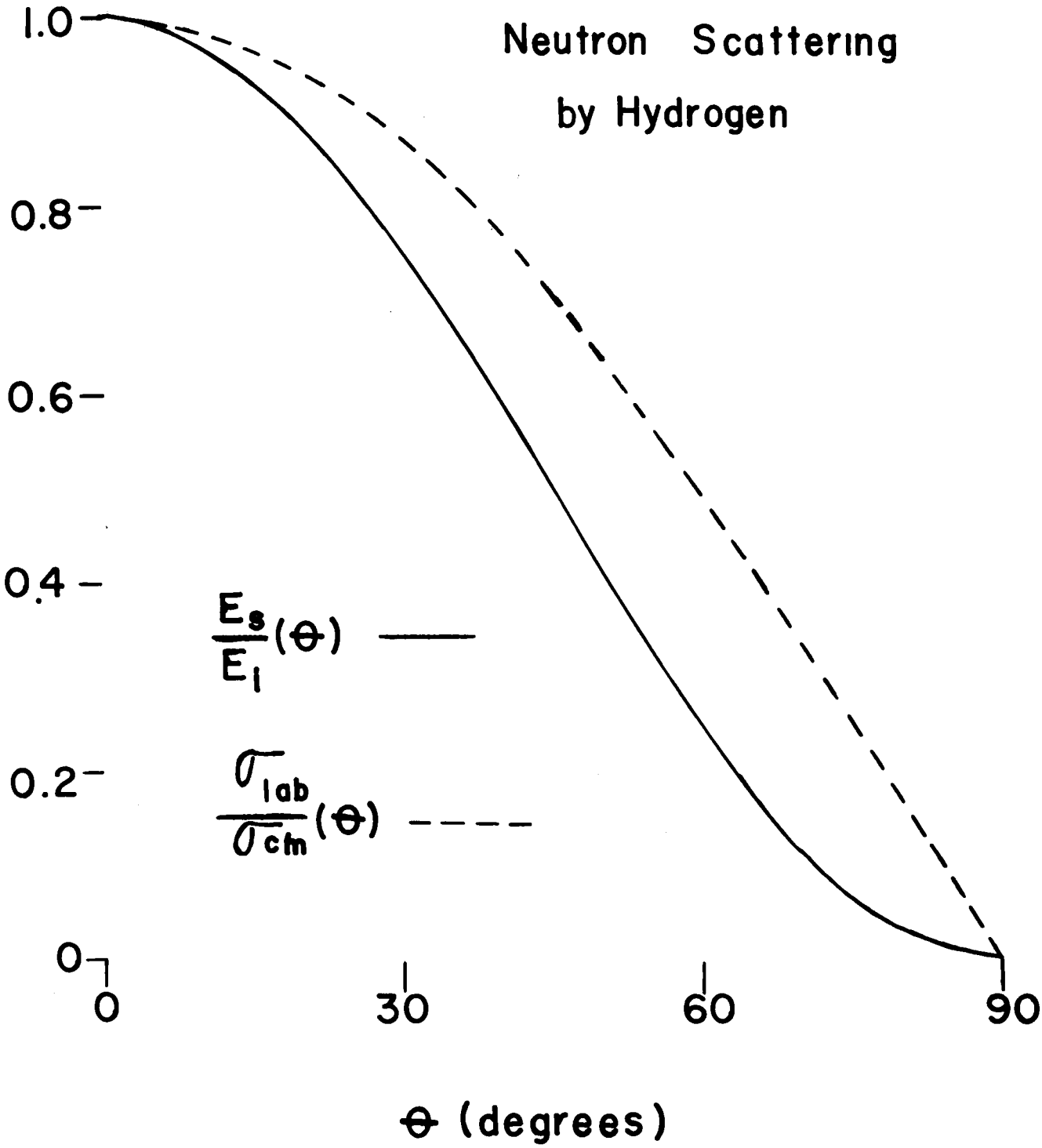

FIGURE 4

[redacted]

[redacted]

Since the angular distribution in the center of mass system is isotropic to well within 10% the ratio σ_{lab}/σ_{cm} shown in Figure 4 can be considered as the angular distribution in the laboratory system. If it is assumed that the angular distribution in thelaboratory system is proportional to $\cos\theta$ then it is found that 81% of the collisions result in scattering the neutrons into angles greater than 25° and 19% of the collisions result in scattering the neutrons in angles less than 25°. Since the ratio of the scattered energy to the incident energy (E_s/E_i) is proportional $\cos^2\theta$ it is found that 19% of the collisions result in an energy change of less than 20%. This makes it seem reasonable to assume that only 81% of the hydrogen collisions result in removal of the neutrons.

[redacted]

[redacted]

REFERENCES

1. MacDonald, J. E., and Edwards, W. E., Programming Nuclear Aircraft Shields Analysis, Methods on IBM-701, XDC 55-6-109, June 9, 1955.

2. Chapman, G. T., and Storrs, C. L., Effective Neutron Removal Cross Sections for Shielding, ORNL-1843, September 19, 1955.

3. Haffner, J. W., and Van Valkenburg, H. M., Modification of Albert-Welten Point Attenuation Kernel, XDC 55-9-150, September 20, 1955.

4. Albert, R. D., and Welton, T. A., A Simplified Theory of Neutron Attenuation and its Application to Reactor Shield Design, WAPD-15, November 30, 1950.

[redacted]

SECRET

Paper II-G

A NEUTRON AIR SCATTERING MODEL

J. W. Haffner
General Electric Company - ANP Dept.
Cincinnati

SECRET

[redacted]

[redacted]

A NEUTRON AIR SCATTERING MODEL

by

J. W. Haffner

General Electric Company
Aircraft Nuclear Propulsion Department
Cincinnati, Ohio

The problem of computing the dose rates inside shielded crew compartments due to nuclear power plants involves consideration of the various mechanisms by which radiation can reach the crew compartment. For the case of neutrons, the dose rate is generally considered to consist of two components — direct and air scattered. This paper is concerned with the air scattered fast neutron dose rate inside the crew compartment.

GENERAL CONSIDERATIONS

The geometry considered is shown in Figure 1. The nuclear power plant is replaced by a point source with a polar angular distribution $F(\alpha)$. The R-1 experiments carried out at the TSF indicate that for values of r_1 greater than about 18 feet, the dose rates decrease as $1/r_1^2$. Thus the point source approximation is believed to be a reasonable one. The cylindrical crew compartment is considered to be coaxial with the line joining it to the point source. The walls of the crew compartment are composed of some hydrogenous material.

For the case of a crew compartment with walls of 0 thickness (i.e. no crew shield at all) the air scattered dose rate can be easily computed, provided only first order scattering is considered. The derivation proceeds by considering the dose rate due to fast neutrons which are scattered in a unit of volume dV. The total singly air scattered dose rate is obtained by integrating over all space. The result is:

$$\text{Dose Rate} = \frac{2\pi n}{a K(E')} \int_{\alpha=0}^{\alpha=\pi} \int_{\beta=0}^{\beta=\pi-\alpha} E'(\theta) F(\alpha) \left(\frac{d\sigma}{d\Omega}\right)_{\theta} d\alpha \, d\beta$$

[redacted]

[redacted]

In this formula

n = number of scattering centers per unit volume in air

= 5.1×10^{19} nuclei/cm^3

$K(E')$ = energy flux to dose rate conversion factor in $\frac{\text{mrep/hr}}{\text{Mev/cm}^2\text{/sec}}$

$F(\alpha)$ = angular distribution of the equivalent point source

$\left(\frac{d\sigma}{d\Omega}\right)_\theta$ = differential scattering cross-section

(For fast neutrons the scattering is considered to be isotropic in the center of mass system)

$E'(\theta)$ = energy of the fast neutrons after having been scattered.

The rigorous evaluation of the preceeding equation appears to be a rather formidable job. However, it can be modified in such a way that it can be easily handled without appreciably imparing the accuracy of the calculation.

The ratio of energies of a particle of mass M_1 after and before being scattered elastically through an angle by a particle of mass M_2 is:

$$\frac{E'}{E}(\theta) = \left(\frac{M_1}{M_1+M_2}\right)^2 \left[1+\left(\frac{M_2}{M_1}\right)^2 - 2\sin^2\theta \pm 2\cos\theta\sqrt{\left(\frac{M_2}{M_1}\right)^2-\sin^2\theta}\right]$$

For the case of neutrons elastically scattered by nitrogen and oxygen nuclei in the air ($M_2 = 14.4$) this can be reduced to

$$\frac{E'}{E_0}(\theta) = 0.88 + 0.12\cos\theta$$

[redacted]

[redacted]

The error introduced by this approximation is less than 1%. The interesting thing about this relationship is that the ratio of final to initial energies depends only upon masses of the particles involved and angle of scattering and not upon the initial energy. The neutrons arriving at the crew compartment have been scattered through many different angles θ. Therefore, the average energy of singly air scattered neutrons can be computed by evaluating the ratio

$$\overline{\left(\frac{E'}{E_o}\right)} = \frac{\int_0^{\pi} \frac{E'}{E_o}(\theta)\, P(\theta)\, d\theta}{\int_0^{\pi} P(\theta)\, d\theta}$$

where $P(\theta)$ = differential probability of a neutron being scattered from source to receive through an angle θ

$= \theta$

Substituting; the result is:

$$\overline{\left(\frac{E'}{E_o}\right)} = \frac{\int_0^{\pi} (0.88 + 0.12 \cos\theta)\, \theta\, d\theta}{\int_0^{\pi} \theta\, d\theta} = 0.833$$

This means that the average neutron loses only ~17% of its energy upon being air scattered once. This will reduce the energy-flux-to-dose-rate conversion correspondingly. It is noted that the only effect of loss of energy upon the air scattered dose rate at an unshielded receiver point is through the conversion factor $K(E')$.

METHOD OF CALCULATION

The calculation of fast neutron dose rates inside the cylindrical crew shield (Figure 1) proceeds through the following 4 steps:

1. Calculation of the energy and angular distribution of the fast neutrons arriving at the outside of the crew shield.

2. Calculation of the air scattered fast neutron dose rates outside the crew shield.

3. Calculation of the attenuation in the crew compartment walls.

4. Calculation of the air-scattered dose rates at a point on the axis inside the crew compartment.

[redacted]

[redacted]

The calculation of the energy distribution for the unscattered neutrons is obtained from knowledge of the reactor and shield assembly which is represented by the equivalent point source, and the Albert-Welton point attenuation kernel. The energy distributions obtained from this theory, which is based upon line-of-sight attenuation, are gaussion in shape and depend only upon the equivalent water shielding of the source. The energy distribution of the singly air scattered fast neutrons is considered to be the same except that the entire spectrum has been shifted lower by about 17% while retaining its shape.

The calculation of the angular distribution of the singly air scattered fast neutron is straightforward, involving evaluation of the integral

$$F(\beta) = \frac{n\sigma}{2K(E')a}\int_0^{\pi-\beta} F(\alpha)\,d\alpha$$

Where σ = 1.28 barns/atom for air

The calculation of the air scattered fast neutron dose rate outside the crew compartment shield has already been discussed. It involves evaluation of the expression

$$D.R. = \frac{n\sigma}{2K(E')a}\int_0^{\pi}\int_0^{\pi-\alpha} E'(\theta)F(\alpha)\,d\alpha\,d\beta$$

The various factors entering this expression have been previously identified.

The calculation of the attenuation of the air scattered fast neutrons in the walls of the crew compartment employs the Albert-Welton attenuation kernel. In addition to being based upon line-of-sight-attenuation, it shows that nearly all of the attenuation ($\sim$90%) of fast neutrons in hydrogenous media like water is due to scattering from the hydrogen nuclei. Thus, the relaxation lengths of the air scattered fast neutrons in the crew compartment walls can be estimated from the ratio

$$\frac{\lambda'}{\lambda} = \frac{\int \sigma_H(E_0)\,dE_0}{\int \sigma_H(\overline{E'})\,dE'}$$

[redacted]

[redacted]

where E_o = unscattered neutron energy

E^1 = const. E_o

= $0.833E_o$ for single scattering

λ', λ = relaxation lengths in the equivalent hydrogenous shield of the crew compartment after and before scattering respectively

σ_H = hydrogen scattering cross-section for neutrons

The expression is evaluated by integrating over the energy spectra. The attenuation in the crew compartment walls involves evaluation of the ratio:

$$\frac{\int_0^{\beta_1} F(\beta)\, \varepsilon^{-t_r/\lambda' \cos\beta} d\beta + \int_{\beta_1}^{\beta_2} F(\beta) \varepsilon^{-t_s/\lambda' \sin\beta} d\beta + \int_{\beta_2}^{\pi} F(\beta) \varepsilon^{-t_f/\lambda' \cos\beta} d\beta}{\int_0^{\pi} F(\beta) d\beta}$$

In this ratio:

t_r = water equivalent thickness of hydrogenous shielding at the rear (source side) of the crew compartment.

t_s = water equivalent thickness of hydrogenous shielding at the side of the crew compartment

t_f = equivalent thickness of hydrogenous shielding at the front of the crew compartment.

The angles β_1 and β_2 are shown in Figure 1.

The calculation of the fast neutron dose rate at a point on the axis inside the crew compartment is simple — just a multiplication of the air scattered fast neutron dose rate outside the crew compartment and the attenuation of the equivalent hydrogenous shielding of the crew compartment walls.

As an example, this sort of calculation was carried out to obtain the expected air scattered fast neutron dose rate inside a cylincrical crew shield mockup due to the R-1 reactor shield mockup. Below are tabulated the calculated quantities and tht actual dose rates measured at the TSF.

[redacted]

[redacted]

	Calculated	Measured
Fast neutron Dose Rate outside the crew shield mockup	2.4×10^{-5} mrep/hr/watt	1.8×10^{-5} mrep/hr/watt
Attenuation due to crew shield mockup walls	3.5×10^{-3} ($\lambda' = 8.88$ cm) 1.3×10^{-3} ($\lambda' = 7.50$ cm)	
Fast neutron Dose Rate inside the Crew Shield Mockup	3.1×10^{-8}	2.5×10^{-8} mrep/hr/watt

The values of λ were estimated to be

$\lambda' =$ 8.88 cm in H_2O for singly air scattered fast neutrons

$\lambda' =$ 7.50 cm in H_2O for multiple air scattered fast neutrons

CONCLUSIONS

This comparison indicates that multiple air scattering may be an important process even for cases where the source and detector are only separated by a relaxation length (for these experiments a = 64 feet, λ in air is $\sim$ 500 feet).

In addition, it can be pointed out, it is possible to work the calculation backwards in order to obtain the optimum reactor shield configuration for a given crew shield configuration. The effect of multiplying scattered radiation introduces some error, but this is not believed to be prohibitive. Within these limits the method of calculating air scattered fast neutron dose rates appears to be a reasonable one.

[redacted]

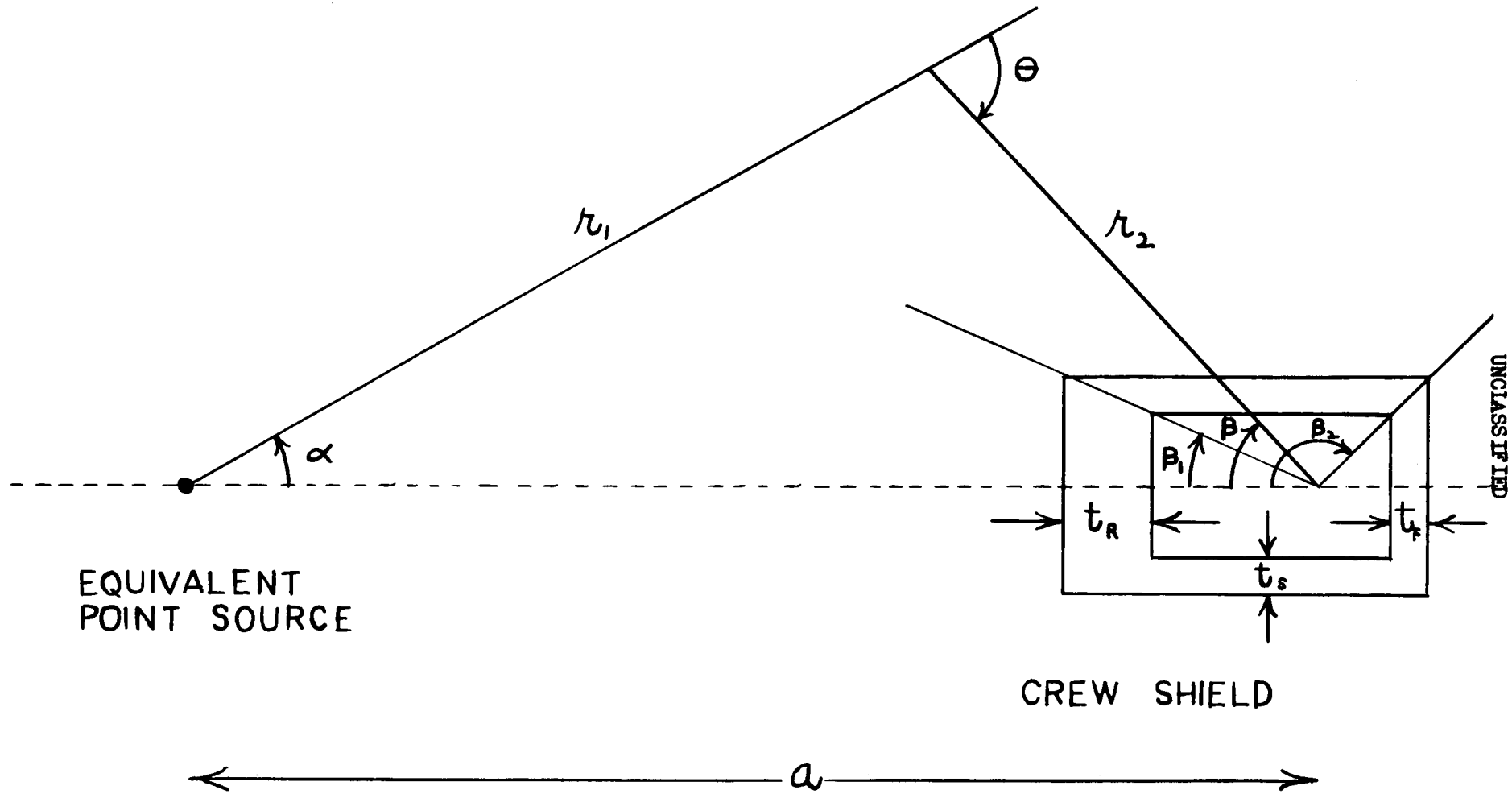
θ
r_1
r_2
α
β
β_1
β_2
t_R
t_F
t_s
EQUIVALENT
POINT SOURCE
CREW SHIELD
a

FIGURE 1

Paper II-H

ENERGY ABSORPTION RESULTING FROM GAMMA RADIATION INCIDENT ON A MULTIREGION SHIELD WITH SLAB GEOMETRY

S. Auslender*
Oak Ridge National Laboratory

*Loan employee from Pratt and Whitney Aircraft Company

ENERGY ABSORPTION RESULTING FROM GAMMA RADIATION INCIDENT ON A MULTIREGION SHIELD WITH SLAB GEOMETRY

by

S. Auslender*
Oak Ridge National Laboratory
Oak Ridge, Tennessee

Preliminary results are presented on a Monte Carlo calculation of heating and penetration of gamma rays in a two-region, lead and water shield.

The code of a Monte Carlo calculation of energy penetration and deposition resulting from transport gamma radiation in a shield of slab geometry[1] has been used in a parametric study of a two-region lead-water shield. The code utilizes straightforward sampling techniques except for a doubling technique operating on the unscattered flux.

In the calculation only three processes were used. The first is the photoelectric process. It and the second, pair production, were treated as purely absorptive. The third, scattering, was treated using the Klein-Nishima differential scattering formula.

The heating in shields other than the one shown in Figs. 1, 2, 3, and 4 have been calculated. The shields are made up of eight different combinations of lead and water. For each shield and for each of four angles of incidence, results were obtained for the following three cases:

	E(Mev)	$\mu_o r$(mfp)
a	1	2
b	1	1
c	3	1

The angles of incidence are such that the secant of the angles are 1, 2, 3, and 4. Table I contains the results for the fractions of the total energy absorbed, reflected, and transmitted for the cases a, b, and c and for the four angles of incidence listed above, all for the combination of lead and water described in Fig. 1.

For the parametric study the radiation was 1-Mev gamma rays incident on the slab at 0 deg, 60 deg, 70 deg 32 min, and 75 deg 31 min. The first region

*Loan employee from Pratt and Whitney Aircraft Company.

Table I. Fractional Absorption, Reflection, and Transmission of the Total Energy Incident upon a Shield

	Cases	sec θ			
		1	2	3	4
Absorption	a	.724	.858	.841	.838
	b	.460	.675	.733	.765
	c	.497	.740	.840	.883
Reflection	a	.0345	.0910	.1338	.1448
	b	.0292	.0769	.1215	.1497
	c	.0066	.0250	.0459	.0583
Transmission	a	.242	.0512	.0249	.0177
	b	.511	.248	.145	.0858
	c	.496	.235	.114	.0589

UNCLASSIFIED
2-01-059-47

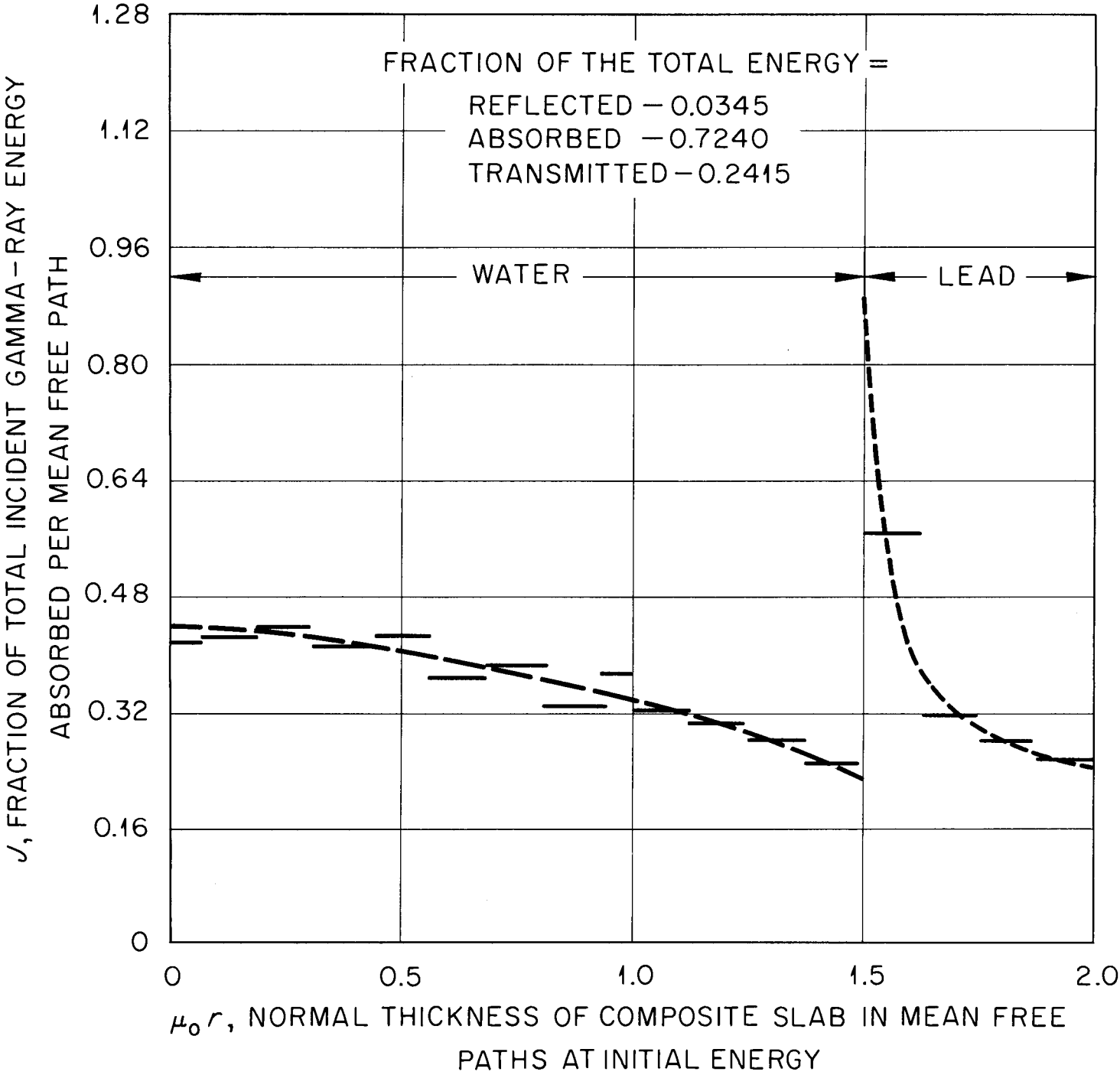

Fig. 1. Fraction of Energy from 0-deg Incident, 1-Mev Gamma Rays Absorbed in a Water-Lead Slab.

UNCLASSIFIED
2-01-059-48

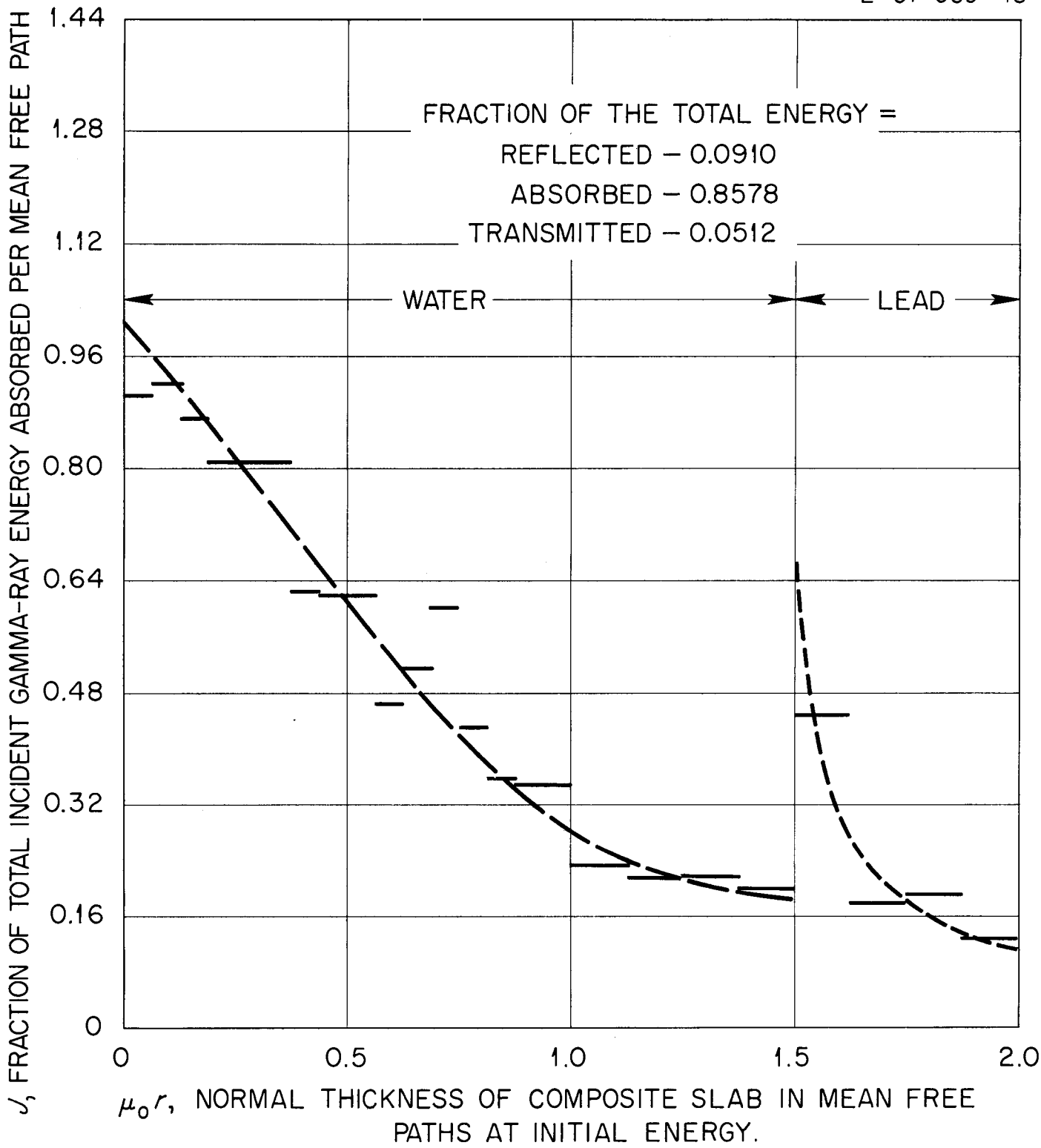

Fig. 2. Fraction of Energy from 60-deg Incident, 1-Mev Gamma Rays Absorbed in a Water-Lead Slab.

UNCLASSIFIED
2-01-059-49

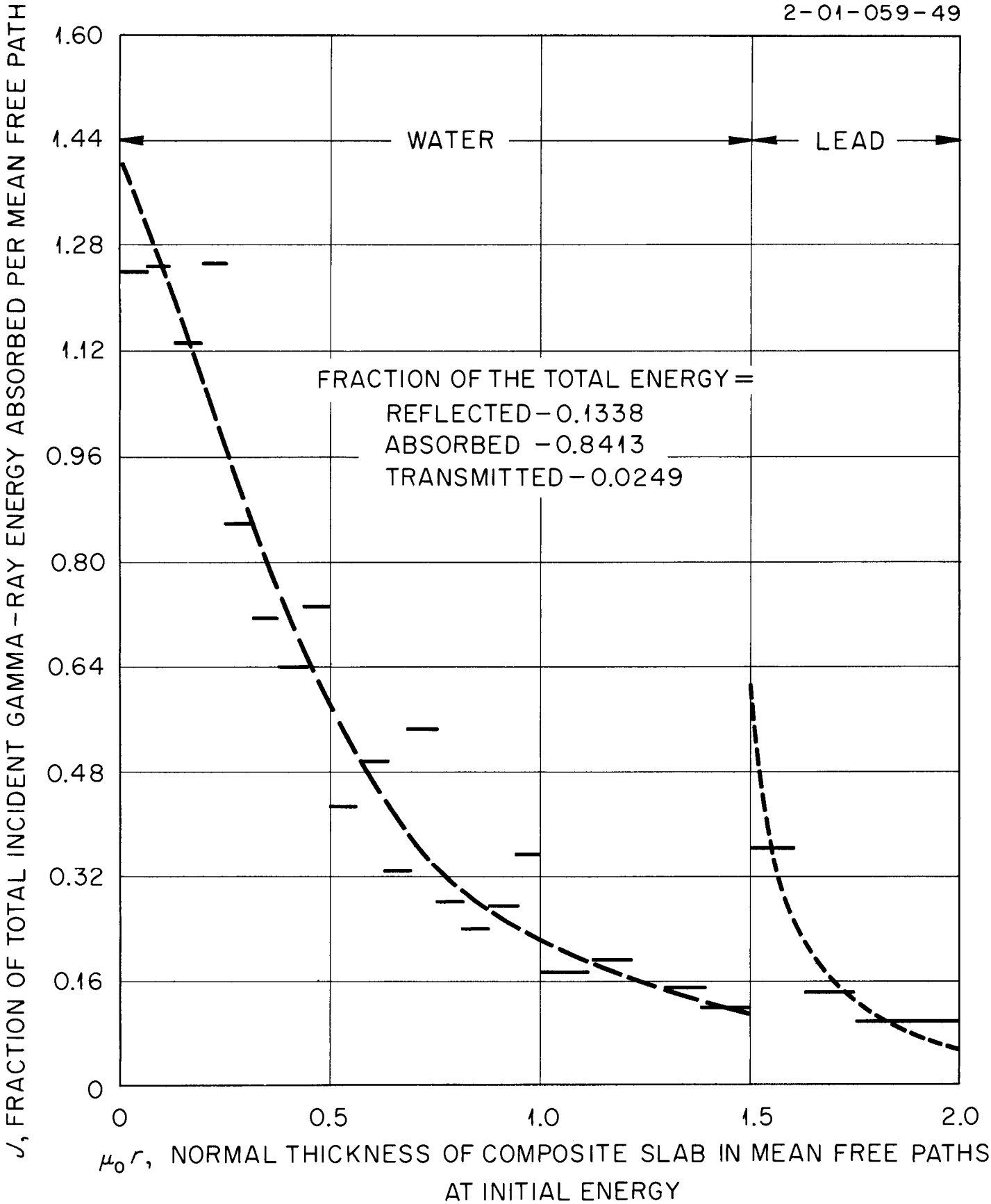

Fig. 3. Fraction of Energy from 70-deg, 32-min Incident, 1-Mev Gamma Rays Absorbed in a Water-Lead Slab.

UNCLASSIFIED
2-01-059-50

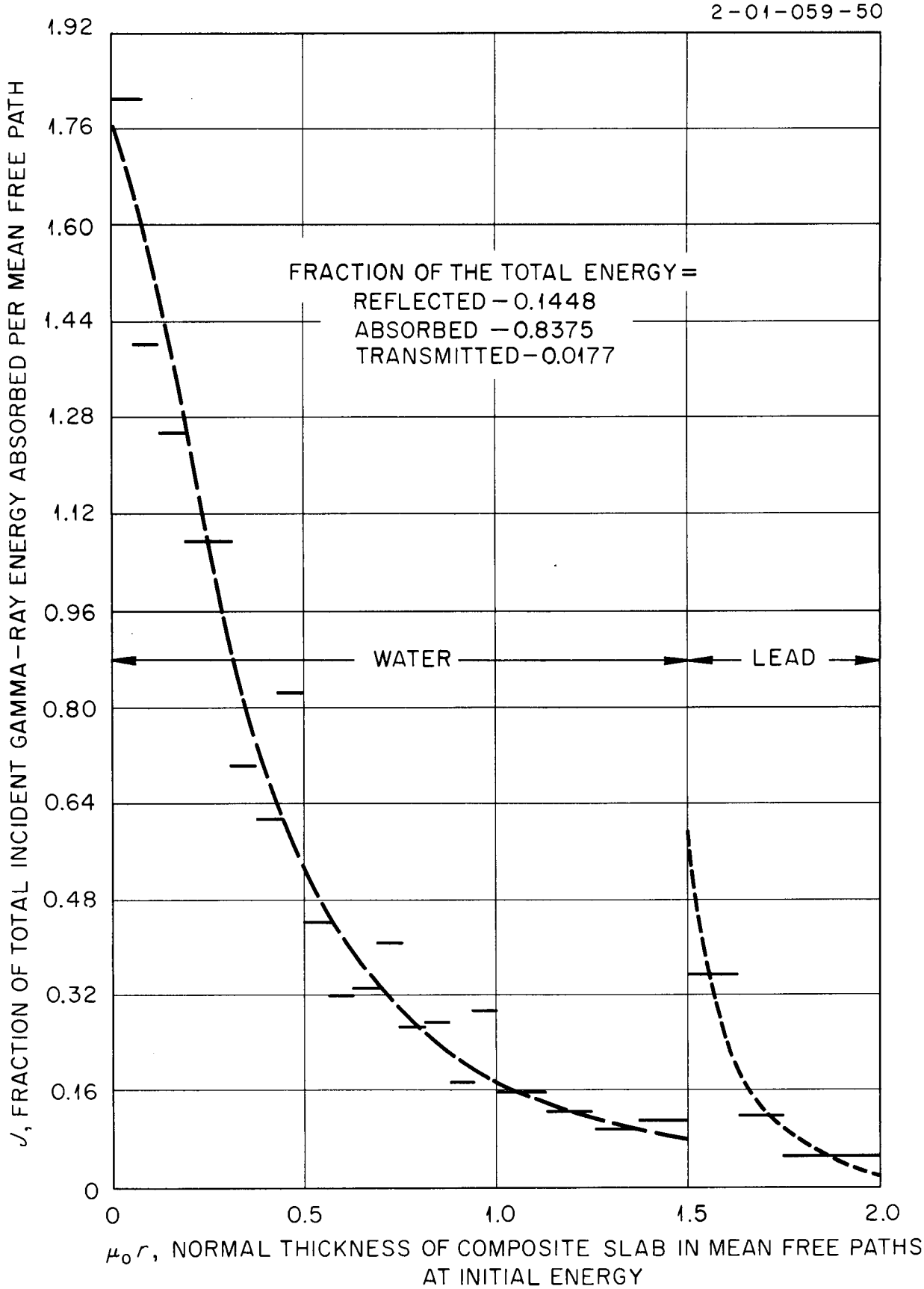

Fig. 4. Fraction of Energy from 75-deg, 31-min Incident, 1-Mev Gamma Rays Absorbed in a Water-Lead Slab.

of the slab was composed of water 1.5 mfp thick at the initial gamma-ray energy, and the second region was composed of lead 0.5 mfp thick. Preliminary results of the calculation are shown in Figs. 1 through 4. The dashed lines are a fit by eye to the data. The large rate of change of heat deposition near the front surface of the lead can be explained by the rapid absorption in the lead of the low energy.

The coding has been extended to calculate energy flux and tissue dose rate as well as energy deposition. Figures 5 through 9 are plots of the buildup factor for the dose rate, due to the gamma rays that have penetrated the slab, as a function of the composition of the slab. The buildup factor is defined as:

$$B_r \equiv \frac{D}{D_o e^{-\mu_o r \sec \theta}}$$

where

D = calculated dose rate (mr/hr),

D_o = dose rate with the source unchanged but with the slab missing,

$\mu_o r \sec \theta$ = oblique thickness of the slab in mean free paths at the source energy.

The composition of the slab is denoted by P and defined as

$$P \equiv \frac{\text{thickness of lead (mfp)}}{\text{thickness of entire slab (mfp)}}, \text{ at the source energy}$$

$$= \frac{(\mu_o r)_{Pb}}{\mu_o r}$$

where

$$\mu_o r \equiv (\mu_o r)_{Pb} + (\mu_o r)_{H_2O}$$

Figures 5, 7, and 9 are for shields with the lead in front of the water, and Figs. 6 and 8 are for water in front of lead. The sources for Figs. 5 through 8 are plane monodirectional. The source for Fig. 9 is a surface

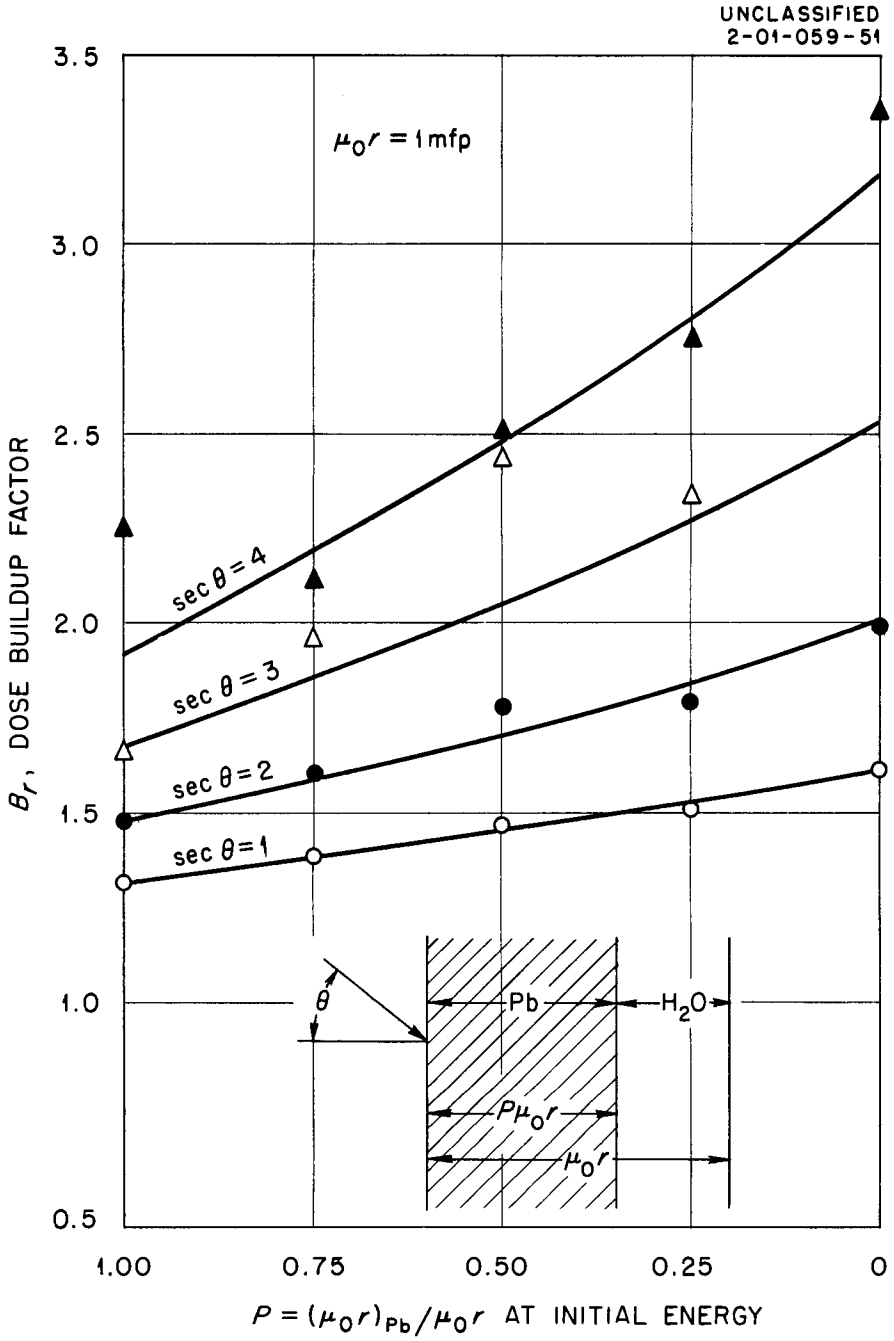

Fig. 5. Buildup Factor for Dose Rate in a Lead-Water Shield Resulting from 3-Mev Incident Photons from a Plane, Monodirectional Source.

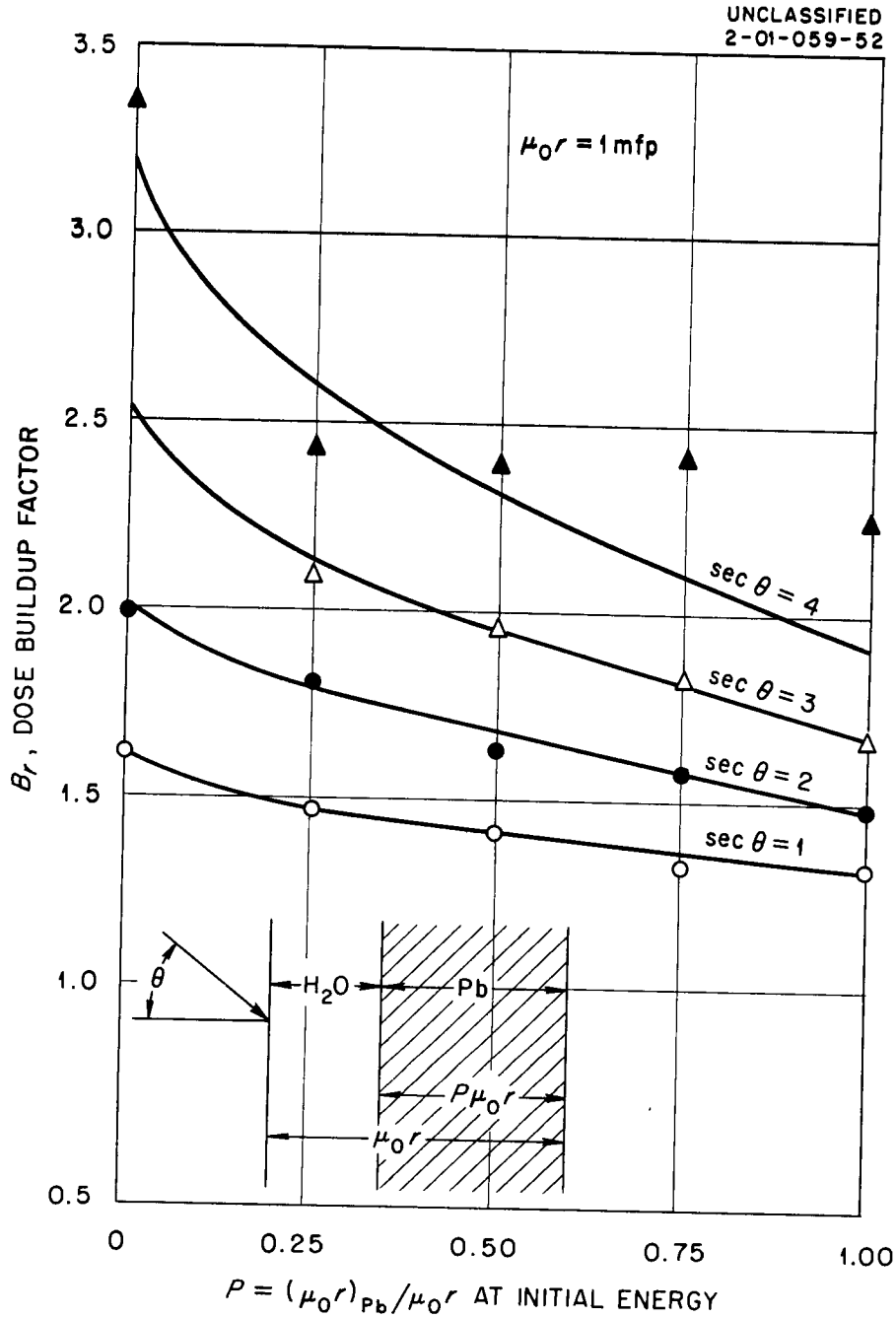

Fig. 6. Buildup Factor for Dose Rate in a Water-Lead Shield Resulting from 3-Mev Incident Photons from a Plane, Monodirectional Source.

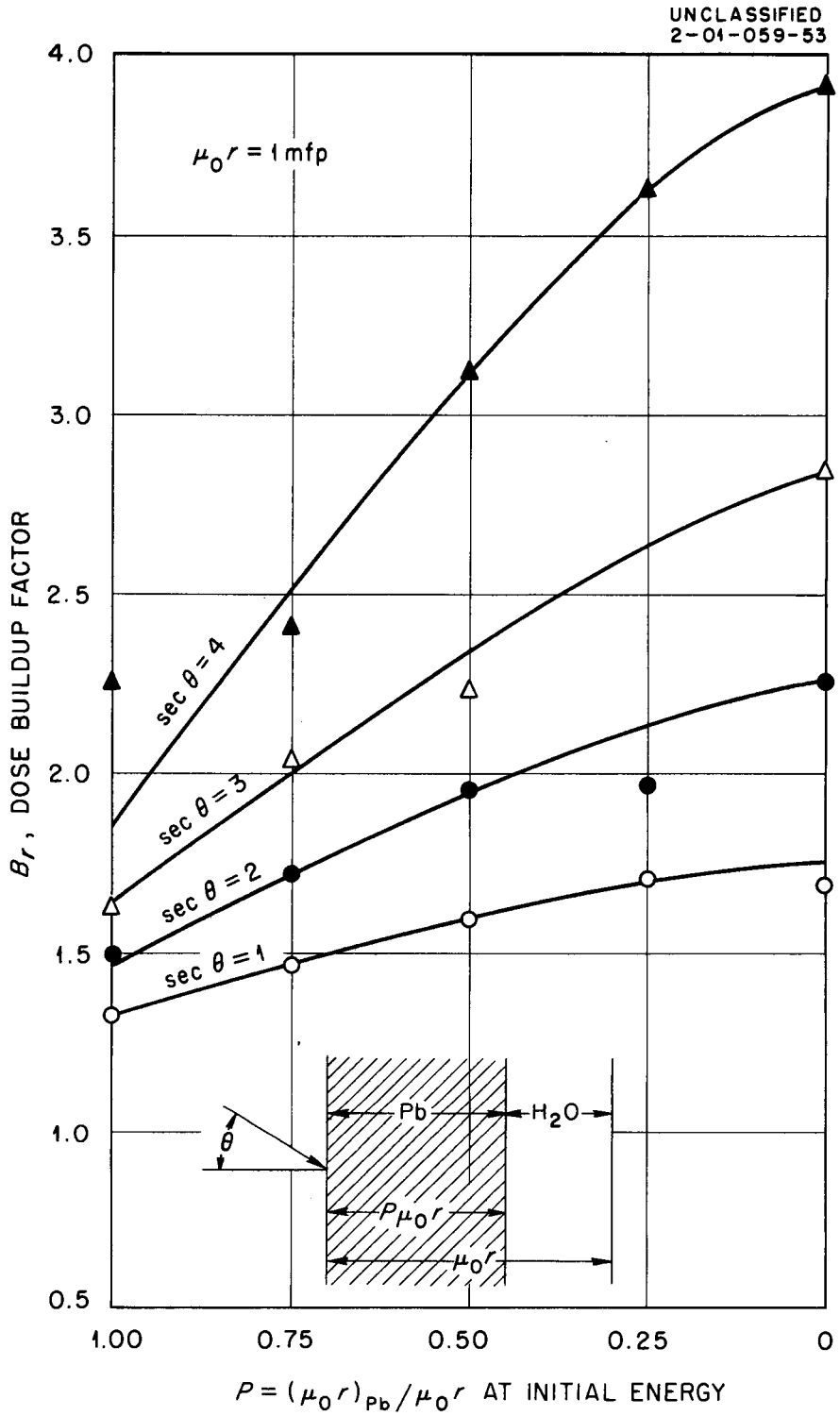

Fig. 7. Buildup Factor for Dose Rate in a Lead-Water Shield Resulting from 1-Mev Incident Photons from a Plane, Monodirectional Source.

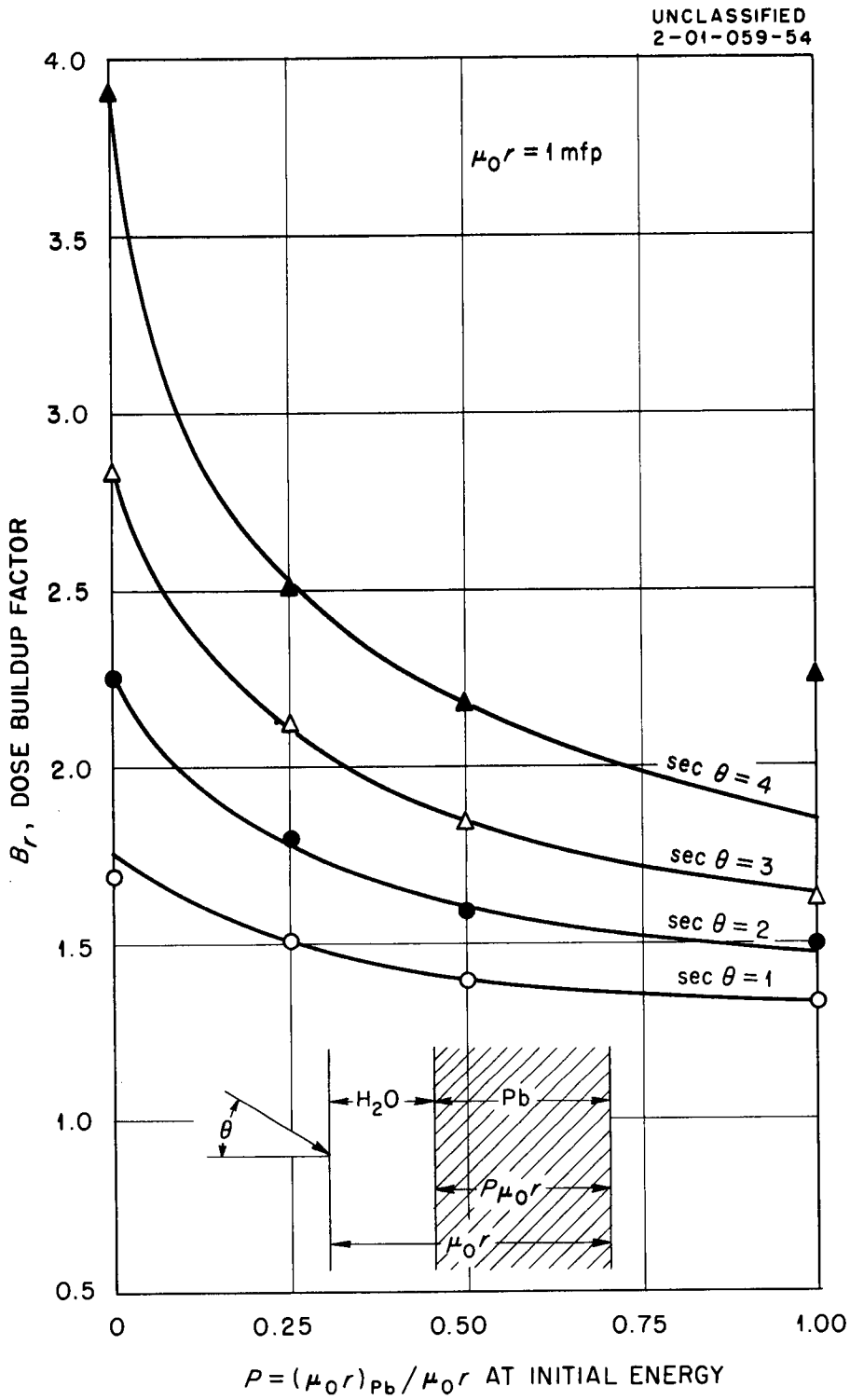

Fig. 8. Buildup Factor for Dose Rate in a Water-Lead Shield Resulting from 1-Mev Incident Photons from a Plane, Monodirectional Source.

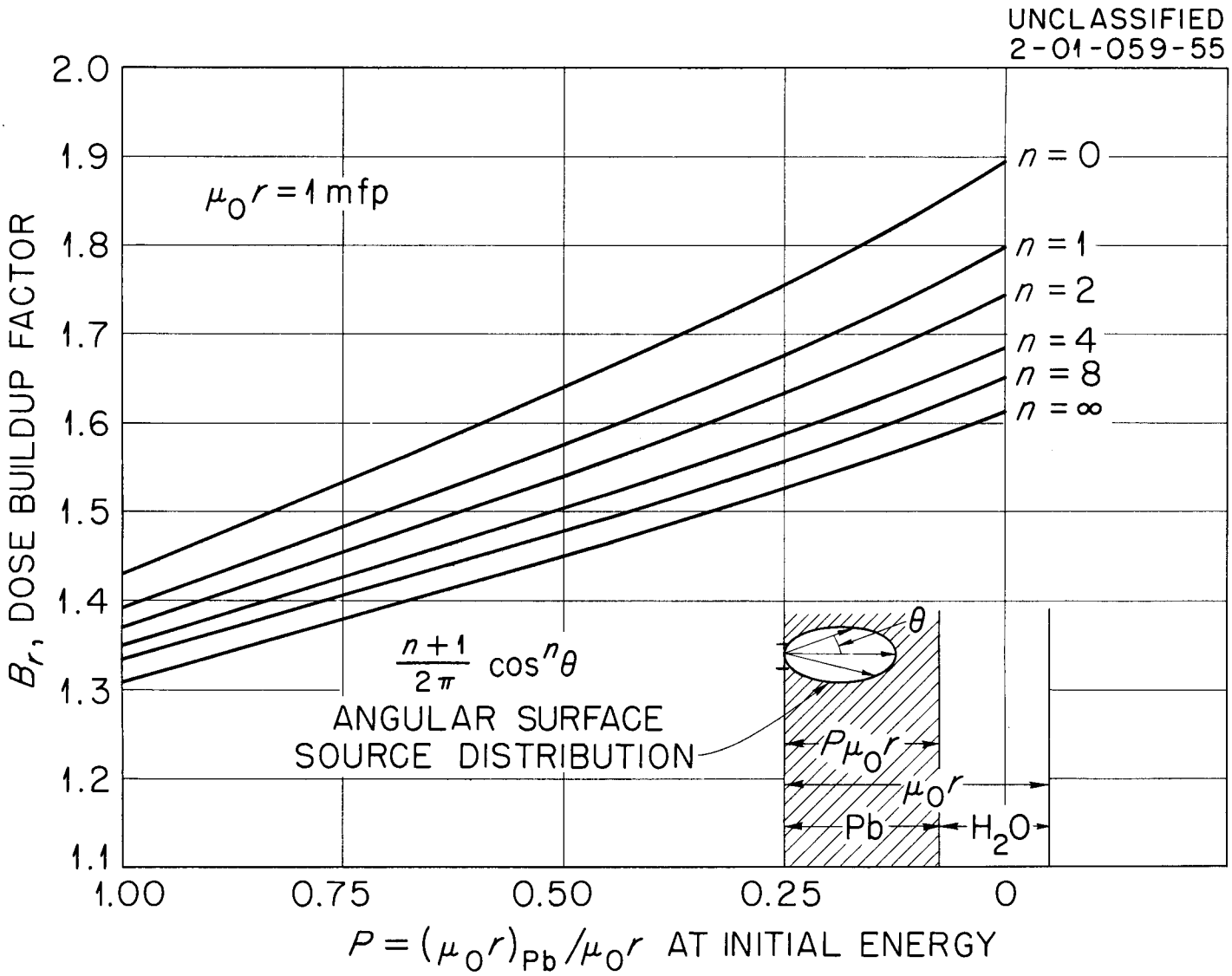

Fig. 9. Buildup Factor for Dose Rate in a Lead–Water Shield Resulting from 3-Mev Incident Photons from a Plane $\cos^n \theta$ Surface Source.

source having a $\cos^n\theta$ angular distribution where θ is measured from the normal to the surface. This source is normalized to one gamma ray per unit area of surface per 2π steradians (in the forward direction):

$$1 = \int_{2\pi} S(\Omega)\, d\Omega$$

$$S(\Omega) = \frac{n+1}{2\pi} \cos^n\theta$$

When $n = 0$, the source is isotropic. For $n = \infty$, the source is plane monodirectional and normal to the surface.

It is obvious from the figures that lead is more effective in stratified slab shields when it is placed behind a good scatterer such as water. This is especially true for the lower source energies. The explanation for this is fundamentally the same as for the large energy deposition rate in the front edge of the lead when it is behind water. The scatter in the answers is, of course, due to the method of solution. Since the answers are estimates of the correct answer, any one problem may be calculated several times, each time with a new set of random numbers. If this is done, the average of the several estimates can be accepted as the answer and a standard deviation can be calculated for it.

REFERENCES

1. C. D. Zerby and S. Auslender, ANP Quar. Prog. Rep. Dec. 10, 1955, ORNL-2012, p. 203.

Paper II-I

THE EFFECT OF ANGULAR DISTRIBUTION AT THE SHIELD SURFACE ON THE GAMMA-RAY AIR SCATTERING PROBABILITIES

D. R. Otis* and H. C. Woodsum**
Oak Ridge National Laboratory

*Loan employee from Convair, San Diego, California.
**Loan employee from Pratt and Whitney Aircraft Company, E. Hartford, Conn.

[redacted]

THE EFFECT OF ANGULAR DISTRIBUTION AT THE SHIELD SURFACE ON THE GAMMA RAY AIR SCATTERING PROBABILITIES

by
D. R. Otis* and H. C. Woodsum**
Oak Ridge National Laboratory
Oak Ridge, Tennessee

This memorandum presents gamma ray air scattering probabilities for a reactor emitting radiation from the shield surface with an angular distribution other than radial emission. The scattering probabilities for a point source[1] are modified for use with shielding calculations where the gamma ray angular distribution at the shield surface can be represented by $\cos^n \alpha$ where α is the angle between the radiation path and a line normal to the reactor shield surface. The results of these calculations are presented in Table I.

INTRODUCTION

The gamma ray scattering probabilities obtained by Goldstein[1] for a point source have been used extensively for calculating the scattered gamma ray dose in the crew compartments of proposed nuclear powered aircraft. Since these probabilities are for a point source emitting radiation radially, it is necessary to correct for the fact that the radiation from the surface of a reactor does not necessarily follow radial lines. The concept of the "disadvantage angle" was introduced[2] to account partially for the effect of the angular distribution at the reactor shield surface. However, this was found to be inadequate.

If the reactor shield possessed spherical symmetry, the surface angular distribution would be of little importance since the crew compartment scattered dose would be unaffected. However, it has become standard practice to shape the gamma ray shield so as to obtain a dose contribution in the crew compartment from each point on the reactor shield surface. Hence the angular distribution does become important in determining the optimum shield shape. Unfortunately, there is little

*Convair, San Diego, California.
**Pratt and Whitney Aircraft Corp., E. Hartford, Connecticut.

[redacted]

[redacted]

data on angular distributions, and it is certain that the shape of the distribution depends upon the energy of the radiation and upon reactor geometry. Nevertheless, it is instructive to study the effects of non-radial emission for some simple types of distributions even though they do not correspond exactly to the real situation.

For this study, it was assumed that the angular emission from the shield surface could be represented by $\cos^n\alpha$ where α is the angle between the radiation path and a line normal to the shield surface. The cosine function was chosen for several reasons: (a) it is easy to handle analytically, (b) it has become common practice at the ORNL Tower Shielding Facility to speak in terms of cosine distributions and (c) it is a fair approximation to some data taken at the Bulk Shielding Facility.[3]

The calculation of the results presented in this report made use of the scattering probabilities available for a point source. For several points on the shield a mean probability is calculated by integrating over the 2π solid angle of emission. The details are presented in the next section. For better understanding of the work to follow, it is recommended that the reader become acquainted with the work done for the point source.[1]

ANALYSIS

Figures 1 and 2 show a differential element dA on the surface of a reactor shield. The area dA is separated from the detector by the distance D, and the radius of the reactor is assumed to be quite small compared with D. The detector is located in the center of a cylindrical crew compartment which is not shown in the figure. The crew compartment model is the same as that used by Goldstein[1]. Photons are being emitted from dA in all directions in the half hemisphere away from the reactor ($0 \leq \alpha \leq \pi/2$) and this distribution can be represented by

$p(E_o, \alpha)$ = fraction of radiation at E_o which is emitted at angle α per unit solid angle.

where

$$2\pi \int_0^{\pi/2} p(E_o, \alpha) \sin\alpha \, d\alpha = 1 \qquad (1)$$

The scattering probability as given in Ref. 1 is:

[redacted]

UNCLASSIFIED
2-01-059-72

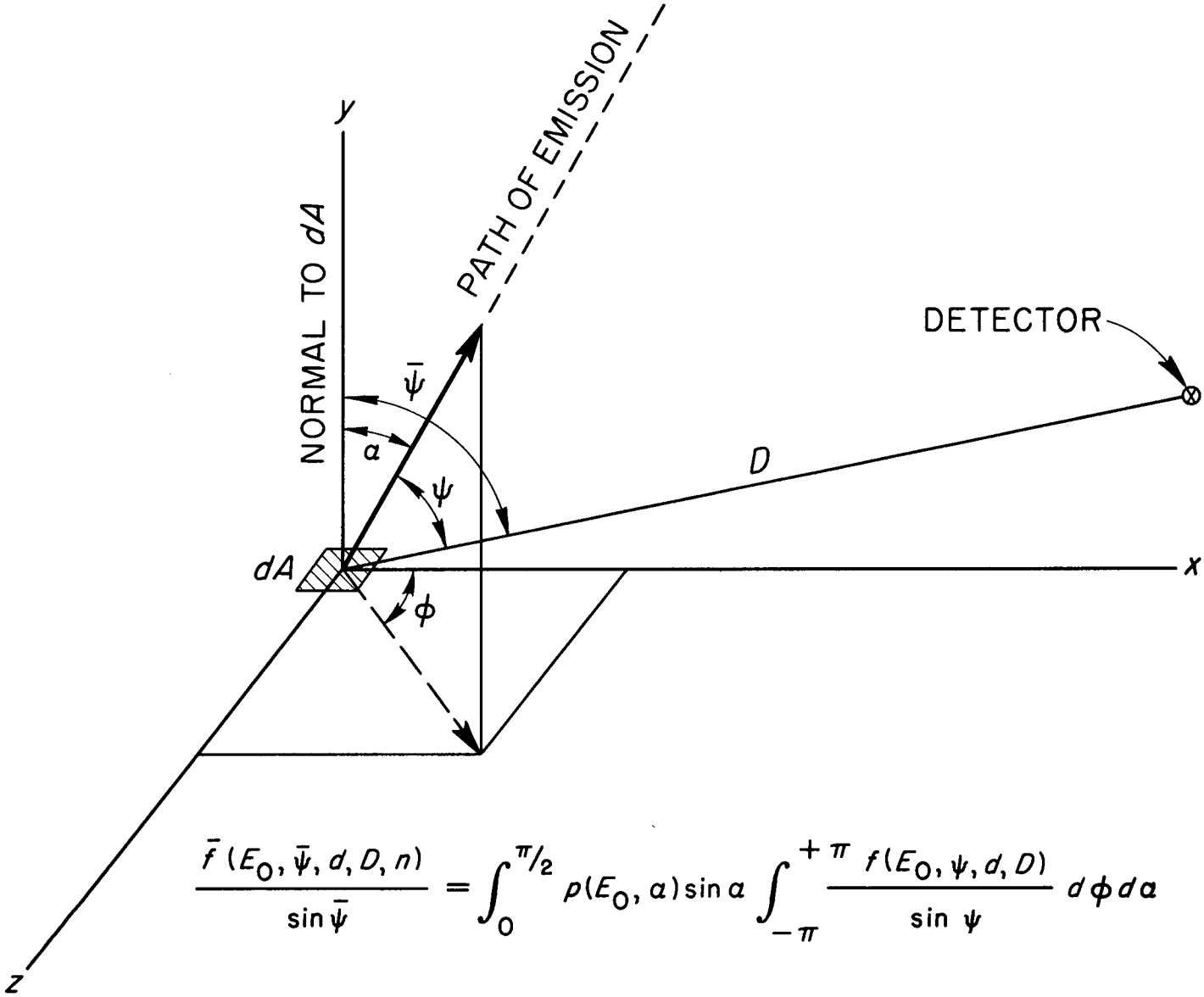

$$\frac{\bar{f}(E_0, \bar{\psi}, d, D, n)}{\sin\bar{\psi}} = \int_0^{\pi/2} p(E_0, \alpha)\sin\alpha \int_{-\pi}^{+\pi} \frac{f(E_0, \psi, d, D)}{\sin\psi}\, d\phi\, d\alpha$$

Fig. 1. The (α, ϕ) Coordinate System.

UNCLASSIFIED
2-01-059-73

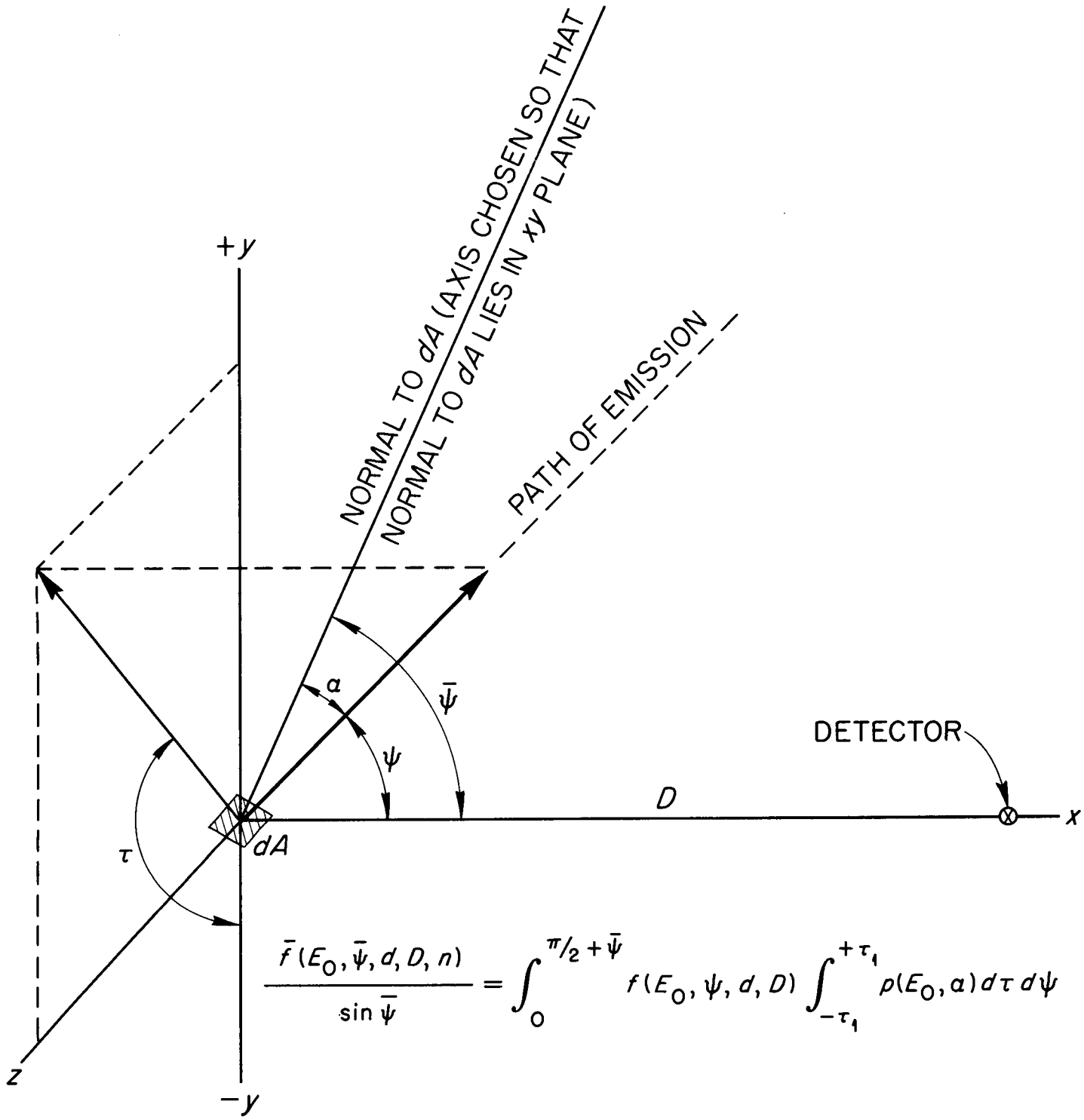

$$\frac{\bar{f}(E_0, \bar{\psi}, d, D, n)}{\sin \bar{\psi}} = \int_0^{\pi/2 + \bar{\psi}} f(E_0, \psi, d, D) \int_{-\tau_1}^{+\tau_1} \rho(E_0, \alpha)\, d\tau\, d\psi$$

Fig. 2. The (ψ, τ) Coordinate System.

[redacted]

$$\frac{2}{\sin\psi} f(E_o, \psi, d, D) = \text{single scattered dose at a distance D with a crew shield d due to a unit source emitting photons of energy } E_o \text{ at angle } \psi \text{ only.} \quad (2)$$

We wish to obtain a scattering probability that is averaged over the angular distribution and it will be defined as follows:

$$\frac{2}{\sin\bar{\psi}} \bar{f}(E_o, \bar{\psi}, d, D, n) = \text{single scattered dose at a distance D with a crew shield d due to a unit source emitting photons of energy } E_o \text{ with an angular distribution defined by n whose axis of symmetry is in the direction } \bar{\psi}. \quad (3)$$

These two probabilities are related by:

$$\frac{\bar{f}(E_o, \bar{\psi}, d, D, n)}{\sin\bar{\psi}} = \int_0^{2/\pi} p(E_o, \alpha) \frac{f(E_o, \psi, d, D)}{\sin\psi} d\Omega \quad (4)$$

It is this integral that was solved for several angular distributions and it is actually a double integral since $d\Omega$ represents a differential element of solid angle. There are two convenient co-ordinate systems that could be used to evaluate the integral, and each will be considered in turn.

(1) The (α, ϕ) co-ordinate system (see Fig. 1):

The differential element of solid angle is:

$$d\Omega = \sin\alpha \, d\alpha \, d\phi$$

Equation (4) can now be written:

$$\frac{\bar{f}(E_o, \bar{\psi}, d, D, n)}{\sin\psi} = \int_0^{\pi/2} p(E_o, \alpha) \sin\alpha \int_{-\pi}^{+\pi} \frac{f(E_o, \psi, d, D)}{\sin\psi} d\phi d\alpha \quad (5)$$

(2) The (ψ, η) co-ordinate system (see Fig. 2):

The differential element of solid angle is:

$$d\Omega = \sin\psi \, d\psi \, d\eta$$

[redacted]

[redacted]

Equation (4) can now be written

$$\frac{\bar{f}(E_o, \bar{\Psi}, d, D, n)}{\sin\bar{\Psi}} = \int_o^{\pi/2 + \bar{\Psi}} f(E_o, \Psi, d, D) \int_{-\Upsilon_1}^{+\Upsilon_1} p(E_o, \alpha)\, d\Upsilon\, d\Psi \quad (6)$$

Where

$$\cos\alpha = \cos\bar{\Psi} \cos\Psi + \sin\bar{\Psi} \sin\Psi \cos\Upsilon$$

$$\Upsilon_1 = \pi \qquad \text{for } 0 \leq \Psi \leq \frac{\pi}{2} - \bar{\Psi}$$

$$= \text{arccosine}\left[-\cot\bar{\Psi} \cot\Psi\right] \qquad \text{for } \frac{\pi}{2} - \bar{\Psi} \leq \Psi \leq \frac{\pi}{2} + \bar{\Psi}$$

The unusual limits on the integrals are necessary to confine the path of integration within the region defined by $0 \leq \alpha \leq \frac{\pi}{2}$.

RESULTS

The cosine angular distributions are defined by:

$$p(E_o, \alpha) = \frac{n + 1}{2\pi} \cos^n\alpha \quad (7)$$

The power of the cosine, n, is a parameter in the study. The energy dependence of $p(E_o, \alpha)$ is not considered as all calculations are for $E_o = 6\ mc^2$.

The (Ψ, Υ) co-ordinates were used, and substituting for $p(E_o, \alpha)$ in Eq. 6 one obtains

$$\frac{\bar{f}(E_o, \bar{\Psi}, d, D, n)}{\sin\bar{\Psi}} = \frac{n + 1}{2\pi} \int_o^{\pi/2 + \bar{\Psi}} f(E_o, \Psi, d, D) \int_{-\Upsilon_1}^{\Upsilon_1} \cos^n \alpha\, d\Upsilon\, d\Psi \quad (8)$$

This integral was numerically evaluated by hand computation for $\bar{\Psi} = 0^\circ, 20^\circ, 45^\circ, 90^\circ, 160^\circ$, and 180° using several crew compartment configurations and several values of n.

Since point source scattering probabilities were not available for Ψ greater than 80°, it was necessary to extrapolate to 180° the curves of $f(E_o, \Psi, d, D)$ presented in Ref. 1. This was done using a straight line tangent to the curves at $\Psi = 80^\circ$. Originally it was felt that

[redacted]

[redacted]

this would not introduce too great an error. However, upon more careful study it was realized that the extrapolation was not a good one and that it accounted for some puzzling discrepancies in the results. A straight line extrapolation yields a finite value for $f(E_o, \psi, d, D)$ at $\psi = 180^\circ$ whereas it should be zero. Therefore, $f(E_o, \psi, d, D)/\sin\psi$ goes to infinity for $\psi = 180^\circ$ as is shown in Fig. 3. The extrapolation error is quite apparent in Fig. 3 for n = 20 for large values of $\bar{\psi}$. An inspection of the calculations indicates that the extrapolation error is significant for

$$n = 5, 20 \text{ at } \bar{\psi} = 160^\circ$$

$$n = 1, 5, 20 \text{ at } \bar{\psi} = 180^\circ$$

The integrations were done by Simpson's rule, and intervals of 2° to 10° were used for $\Delta\Upsilon$ and $\Delta\psi$ depending upon the behavior of the integrand. The calculation error should not exceed 10% unless otherwise noted.

CONCLUSIONS

It is evident by inspection of the tabulated results that the value of $\bar{f}(E_o, \bar{\psi}, d, D, n)/\sin\bar{\psi}$ is strongly dependent upon n, therefore, the assumption of radial emission could lead to a considerable error in the calculation of the scattered gamma ray dose.

ACKNOWLEDGEMENT

Mr. S. Auslender was responsible for the derivation of Eq. 6 and was helpful in clearing the cloud of confusion surrounding this problem. Mr. W. H. Phillips completed all of the hand calculations.

[redacted]

[redacted]

2-01-059-74

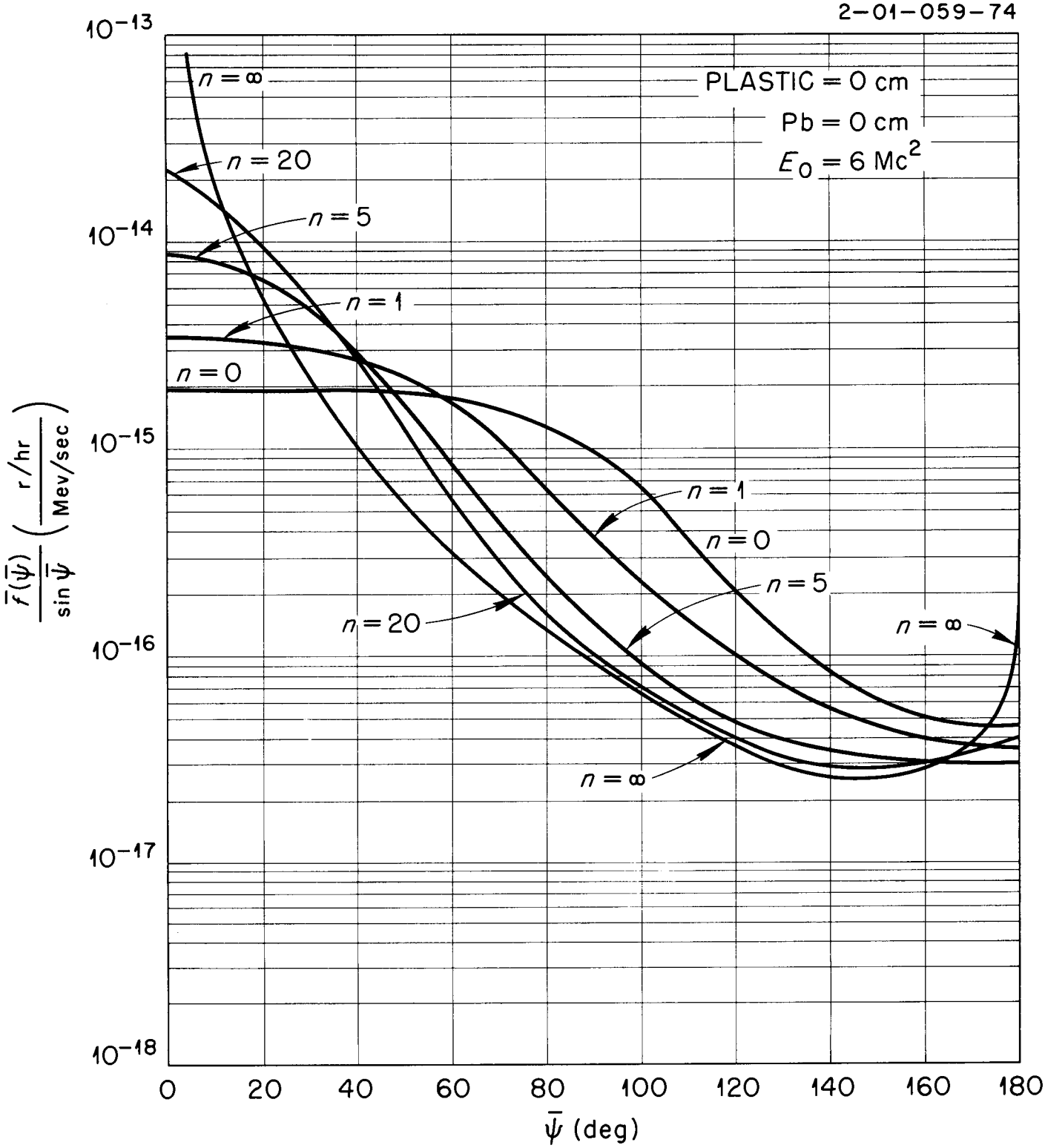

Fig. 3. Gamma Ray Scattering Probabilities with $\cos^n\alpha$ Angular Distribution.

TABLE I. TABULATED RESULTS

$E_o = 6\ mc^2$

$D = 15$ meters

	Crew Compartment Configuration, d		$\frac{\bar{f}(E_o, \bar{\psi}, d, D, n)}{\sin\bar{\psi}}$					
n	Lead Thickness (cm)	Plastic Thickness (cm)	$\bar{\psi} = 0^\circ$	$\bar{\psi} = 20^\circ$	$\bar{\psi} = 45^\circ$	$\bar{\psi} = 90^\circ$	$\bar{\psi} = 160^\circ$	$\bar{\psi} = 180^\circ$
0	0	0	1.94 (-15)[a]	1.91 (-15)	1.91 (-15)	9.95 (-16)	5.09 (-17)	4.57 (-17)
		17.5	2.16 (-16)	2.12 (-16)	2.15 (-16)	1.09 (-16)	3.32 (-18)	2.66 (-18)
		35	4.83 (-17)	4.76 (-17)	4.79 (-17)	2.43 (-17)	3.89 (-19)	3.06 (-19)
	.635	0	3.73 (-16)	3.69 (-16)	3.72 (-16)	1.61 (-16)	2.62 (-19)	1.45 (-19)
		17.5	7.06 (-17)	6.96 (-17)	7.02 (-17)	3.53 (-17)	2.52 (-20)	1.16 (-20)
		35	1.52 (-17)	1.48 (-17)	1.52 (-17)	7.50 (-18)	1.81 (-21)	6.47 (-22)
	1.27	0	1.65 (-16)	1.63 (-16)	1.70 (-16)	5.24 (-17)	5.72 (-21)	1.49 (-21)
		17.5	2.71 (-17)	2.69 (-17)	2.74 (-17)	1.36 (-17)	3.33 (-22)	3.37 (-23)
		35	6.88 (-18)	6.79 (-18)	7.00 (-18)	3.44 (-18)	2.90 (-23)	3.61 (-24)
1	0	0	3.53 (-15)	3.32 (-15)	2.52 (-15)	3.85 (-16)	4.02 (-17)	3.58 (-17)
		17.5	3.99 (-16)	3.75 (-16)	2.87 (-16)	3.72 (-17)	2.21 (-18)	1.84 (-18)
		35	9.04 (-17)	8.49 (-17)	6.46 (-17)	7.42 (-18)	2.41 (-19)	1.84 (-19)

TABLE I. CONTINUED

$E_o = 6\ mc^2$

$D = 15$ meters

	Crew Compartment Configuration, d		$\frac{f(E_o, \bar{\psi}, d, D, n)}{\sin\bar{\psi}}$					
n	Lead Thickness (cm)	Plastic Thickness (cm)	$\bar{\psi} = 0^\circ$	$\bar{\psi} = 20^\circ$	$\bar{\psi} = 45^\circ$	$\bar{\psi} = 90^\circ$	$\bar{\psi} = 160^\circ$	$\bar{\psi} = 180^\circ$
1	.635	0	7.19 (-16)	6.75 (-16)	5.10 (-16)	4.62 (-17)	9.35 (-20)	4.06 (-20)
		17.5	1.37 (-16)	1.28 (-16)	9.65 (-17)	7.92 (-18)	1.01 (-20)	4.00 (-21)
		35	2.92 (-17)	2.74 (-17)	2.10 (-17)	1.57 (-18)	6.61 (-22)	1.89 (-22)
	1.27	0	3.24 (-16)	3.04 (-16)	2.36 (-16)	1.46 (-17)	1.93 (-21)	3.63 (-22)
		17.5	5.00 (-17)	4.99 (-17)	3.80 (-17)	2.61 (-18)	3.85 (-23)	5.74 (-24)
		35	1.35 (-17)	1.27 (-17)	9.75 (-18)	5.65 (-19)	8.81 (-24)	6.71 (-25)
5	1.27	0	8.70 (-15)	6.68 (-15)	2.27 (-15)	1.45 (-16)	3.15 (-17)	3.11 (-17)
		17.5	1.02 (-15)	7.73 (-16)	2.52 (-16)	1.18 (-17)	1.41 (-18)	1.30 (-18)
		35	2.34 (-16)	1.77 (-16)	5.59 (-17)	1.95 (-18)	1.22 (-19)	9.64 (-20)
	.635	0	1.93 (-15)	1.45 (-15)	4.29 (-16)	4.64 (-18)	1.69 (-20)	7.55 (-21)
		17.5	3.72 (-16)	2.79 (-16)	8.01 (-17)	6.77 (-19)	1.61 (-21)	6.22 (-22)
		35	8.04 (-17)	6.01 (-17)	1.72 (-17)	9.70 (-20)	1.09 (-22)	2.91 (-23)

TABLE I. CONTINUED

$E_o = 6\ mc^2$

$D = 15$ meters

	Crew Compartment Configuration, d		$\frac{f(E_o, \overline{\psi}, d, D, n)}{\sin\overline{\psi}}$					
n	Lead Thickness (cm)	Plastic Thickness (cm)	$\overline{\psi} = 0^\circ$	$\overline{\psi} = 20^\circ$	$\overline{\psi} = 45^\circ$	$\overline{\psi} = 90^\circ$	$\overline{\psi} = 160^\circ$	$\overline{\psi} = 180^\circ$
5	1.27	0	8.99 (-16)	6.70 (-16)	1.92 (-16)	7.11 (-19)	1.67 (-22)	2.29 (-23)
		17.5	1.44 (-16)	1.11 (-16)	3.08 (-17)	1.17 (-19)	7.11 (-24)	3.49 (-25)
		35	3.80 (-17)	2.82 (-17)	7.82 (-18)	1.81 (-20)	5.52 (-25)	1.54 (-26)
20	0	0	2.23 (-14)	9.65 (-15)	5.67 (-16)[b]	1.03 (-16)	3.14 (-17)	3.91 (-17)
		17.5	2.71 (-15)	1.12 (-15)	5.46 (-17)[b]	7.81 (-18)	1.29 (-18)	1.45 (-18)
		35	6.38 (-16)	2.58 (-16)	1.09 (-17)[b]	1.13 (-18)	9.77 (-20)	9.51 (-20)
	.635	0	5.35 (-15)	2.14 (-15)	6.15 (-17)[b]	1.13 (-18)	5.29 (-21)	2.75 (-21)
		17.5	1.06 (-15)	4.11 (-16)	1.01 (-17)[b]	1.37 (-19)	4.15 (-22)	2.13 (-22)
		35	2.32 (-16)	8.87 (-17)	1.87 (-18)[b]	1.22 (-20)	1.01 (-23)	3.69 (-24)
	1.27	0	2.59 (-15)	9.91 (-16)	1.78 (-17)[b]	4.84 (-20)	3.80 (-23)	2.49 (-24)
		17.5	4.29 (-16)	1.63 (-16)	8.29 (-18)[b]	4.70 (-21)	2.90 (-26)	8.24 (-27)
		35	1.20 (-16)	4.17 (-17)	3.76 (-18)[b]	4.33 (-22)	3.21 (-27)	3.56 (-28)

a 1.94 (-15) means 1.94×10^{-15}.

b These values appear incorrect and have not been checked.

[redacted]

REFERENCES

1. Goldstein, H., The Reactor Handbook, Vol. I., Chapt. 2.9 (1953).

2. ANP Quarterly, September 10, 1955, p. 190.

3. Maienschein, F. C., Bly, F. T., Love, T. A., "Gamma Radiation in a Divided Aircraft Shield", ORNL-1714 (Aug. 20, 1954).

[redacted]

Paper II-J

MONTE CARLO STUDY OF MULTIPLE SCATTERING OF GAMMA RAYS IN AIR*

G. K. Abel
Convair, Ft. Worth

*Published at Convair, Ft. Worth, as Report No. FZM-432.

MONTE CARLO STUDY OF MULTIPLE SCATTERING OF GAMMA RAYS IN AIR
(Title Unclassified)

by

G. K. Abel

Convair, A Division of General Dynamics Corporation, Fort Worth, Texas

The flux and dose rates of gamma rays multiply scattered in air are being computed on an IBM-701 by a semi-deterministic Monte Carlo Method. Energy spectra for each of the first three scattered components, from an isotropic source are being obtained at two source-detector separations, and five initial energies.

The flux and dose rates of gamma rays multiply scattered in air are being calculated by a semi-deterministic Monte Carlo method. These calculations are being made for an isotropic point source emitting gamma rays at several energies between 0.5 and 8 Mev. The gamma rays are assumed to undergo single, double, or triple scattering before entering a nondirectional point detector. Fluxes and dose rates are being obtained separately for each scattered component as a function of the energy at the detector.

The calculations are being performed with the aid of the IBM-701 computer at Convair-Fort Worth. The program is being run for two different source-detector separation distances: 40 and 60 feet, 5 different initial gamma energies: 0.5, 1.25, 2, 4, and 8 Mev, and standard temperature and pressure. At the source and at each collision point, polar and azimuthal scattering angles and distance to the next collision are selected at random from the proper distributions. At each collision, the probability per steradian of the photon being scattered into the proper direction and reaching the detector without further interaction is computed. This probability, divided by the square of the distance from the collision point to the detector, is proportional to the flux.

The program for these computations took approximately two days to write and one day to code. Twenty-five hundred histories, requiring one hour of machine time, are being run for each combination of parameters. Cumulative results are being printed out after each group of 200 histories, so that tests of statistical significance can be made simply.

The method used is a relatively simple one, requiring only small amounts of computation. This work was done primarily to obtain data quickly for immediate use. More extensive and detailed computations along the same lines are being performed at present by Lt. R. Lynch at Wright Air Development Center. For this reason, little further work on this problem is contemplated at Convair-Fort Worth.

Results of the computation were not yet available as this paper was being prepared for printing.